505

METHODS TO ESTIMATE DISPLACEMENTS OF PG&E STRUCTURES

G. A. MacRae and H. Tagawa
University of Washington
Seattle, Washington

Gregory MacRae, Principal Investigator

A Final Report on Research Conducted Under
PG&E/PEER Research Program
PG&E/PEER Task No: 505

August 2002

ABSTRACT

Dynamic inelastic time-history analyses of single-degree-of-freedom (SDOF) bilinear oscillators were undertaken to determine the ability of the Coefficient Method (FEMA273/FEMA356) and the Capacity Spectrum Method (ATC-40) to predict the total displacement demands of simple structures. Both the Coefficient Method (CM) and the Capacity Spectrum Method (CSM) were calibrated to obtain the exact inelastic response displacements for near-fault (NF) and far-fault (FF) shaking.

When the CM was calibrated to predict the exact response, it was found that a bilinear relationship between lateral force reduction factor (or response modification factor), R, and period, T, was reasonable for a specific target ductility. When the CSM method was calibrated, the effective period, T_{eff}, of the oscillator was assumed to be based on the secant stiffness of the oscillator at the peak displacement. Both the effective damping, ζ_{eff}, and spectral reduction, SR, for a specific target ductility were shown to be dependent on period.

Oscillators with demands estimated by the CM, and with fundamental periods less than about 0.8s, were not affected significantly by near-fault shaking effects. For longer period oscillators, oscillator strengths may need to be increased by more than 60% to account for inelastic shaking effects from NF sites in the region of positive directivity compared to that for shaking from FF or NF near-epicenter sites for the same target displacement ductility. NF shaking did not cause significant trends in the displacement demands of oscillators evaluated by the CSM method.

When both the CM and CSM were calibrated to predict the exact response, it was found that the scatter in displacement from both methods was similar for oscillators with effective (secant) periods up to about 3s. For oscillators with longer effective periods, the CSM had significantly more scatter.

The ATC-40 calibration of the CSM non-conservatively estimated median peak inelastic demands over most of the period range from 0-3s. For some periods, ATC-40 estimated displacements which were on average only 60% of the actual median displacements. The FEMA356 calibration of the CM conservatively estimated peak inelastic demands over most of the period range from 0-3s. For some periods, FEMA356 estimated displacements more than 30% greater than the actual median displacements.

It was determined in conjunction with PG&E/PEER that the FEMA356 CM Linear Dynamic Procedure (LDP) should be used to evaluate the demands of PG&E mill-type structures. The estimation of inelastic response should be made using the C_1 factor from the FEMA356 Nonlinear Static Procedure (NSP). While the C_1 factor may be modified for NF shaking effects, this is only required for structures with fundamental periods greater than 0.8s. Since most PG&E mill-type structures have shorter periods than 0.8s, C_1 does not need to be modified for NF shaking effects. Specific consideration of the difference between member and system ductility demands should also be considered. A design procedure and example for assessing NF shaking inelastic displacement demands on a mill type structure using the CM was provided.

ACKNOWLEDGEMENTS

This work was sponsored by Pacific Gas and Electricity through the Pacific Earthquake Engineering Research Program as PG&E/PEER Task No. 505. Kent Ferre of PG&E oversaw the project. Ronald Hamburger acted as the consultant on the project and made numerous constructive criticisms regarding design. Maryanne Phipps was involved with the quarterly meetings and provided valuable input. Reviews by Kent Ferre, Ron Hamburger and Maryann Phipps increased the quality of the work. Also, Norm Abrahamson and Nancy Smith (of URS) and Ellen Raithe (of the University of Texas) provided earthquake records and information about the locations of these records relative to the fault. Others who participated in the progress meetings and whose comments contributed to this report are Ed Matsuda, Chris Poland, V. V. Bertero, James Anderson and Allin Cornell. The input of the sponsors and all others involved was gratefully appreciated. All opinions expressed in this document are those of the authors which are not necessarily those of the sponsor.

TABLE OF CONTENTS

ACRONYMS

AIJ	Architectural Institute of Japan
ARS	Acceleration Response Spectrum
APE	Annual Probability of Exceedance
ATC	Applied Technology Center
CDMG	California Division of Mines and Geology
CM	Coefficient Method (FEMA356)
CSM	Capacity Spectra Method (ATC-40)
CSMIP	California Strong Motion Instrumentation Program
DDR	Displacement Demand Ratio
DOF	Degree of Freedom
DCSM	Direct Capacity Spectra Method (ATC-40)
EAM	Equal Acceleration Method
EDM	Equal Displacement Method
EEM	Equal Energy Method
EPP	Elastic Perfectly Plastic
FEMA	Federal Emergency Management Agency
FF	Far-Fault
ITHA	Inelastic Time History Analysis
IRC	Inelastic Response Curve
JMA	Japan Meteorological Agency
JR	Japan Railway Company
LDP	Linear Dynamic Procedure
LPP	Locus of Performance Points
LSP	Linear Static Procedure
MDOF	Multi Degree of Freedom
NDP	Nonlinear Dynamic Procedure
NF	Near Fault
NGDC SMCAT	National Geophysical Data Center Strong Motion Catalog
NSP	Nonlinear Static Procedure
P&GE	Pacific Gas and Electricity
PEER	Pacific Earthquake Engineering Center
RC	Reinforced Concrete
SDOF	Single Degree of Freedom
SDOFO	Single Degree of Freedom Oscillator
SN	Strike Normal
SP	Strike Parallel
SR	Spectral Reduction (factor)
SSM	Substitute Structure Method
UBC	Uniform Building Code
USGS	United States Geological Society

CHAPTER 1. INTRODUCTION

In order to prevent a large impact on society, PG&E structures should not collapse during severe near-fault (NF) earthquake shaking. Displacement demands on structures from NF shaking should therefore be smaller than the displacements which the structure can sustain. A large number of PG&E structures are short period substations or rigid wall/flexible diaphragm structures. Short structures, with short fundamental periods, are not expected to be subject to large displacement demands. However, the damage of more than 100,000 short structures in Kobe indicates that short structures may be susceptible to failure.

PG&E/PEER initiated the research described in this report to resolve two issues related to assessing the likely peak displacements of short-period structures during an earthquake. These issues are described below.

1) Research was recently carried out for PG&E/PEER to evaluate the likely effect of near-fault (NF) shaking on short period structures. However, while Bill Iwan at Caltech claimed that the inelastic demands of short-period structures due to NF shaking are more severe than that due to far-fault (FF) shaking, Gregory MacRae at the University of Washington has claimed that they are not necessarily any more severe.

2) Two different methods are commonly used to assess the peak demands in structures. The first is the Coefficient Method (CM) as described by FEMA273 (1997) or FEMA356 (2001). Here the displacement of the structure, if the structure remained elastic, is scaled by a number of coefficients to obtain the inelastic displacement. The second method is referred to as the Capacity Spectra Method (CSM) (e.g. ATC-40, 1997). Here, the yielding structure is modeled as a substitute elastic structure with an increased period and damping. Using current design recommendations, displacements predicted by the CM and CSM for the same earthquake record may differ significantly. Some eminent engineers and researchers state that the CSM should be used in performance based design in the US. At the same time, others believe that the CM is better, and that the CSM approach is not appropriate for design, and is overly complex especially for MDOF structures. It is also recognized that both CM and CSM may require special modifications to account for near-fault shaking effects.

The objectives of this applied research are to answer the following questions:

- Why do different recommendations come from researchers regarding the response of short-period structures to near-fault shaking?
- What are the advantages, disadvantages and relative reliability of the CM and CSM methods for design?
- What modifications are required to the CM and CSM approaches to allow them to accurately predict the response of structures of different periods to near-fault shaking?
- How should PG&E structures be designed using the findings above?

Chapter 2 describes relevant previous work that has been carried out and amplifies the issues outlined above. It describes the advantages and disadvantages of the CM and CSM approaches. Chapter 3 describes the records, modeling and analysis techniques used. Chapter 4 describes the response of oscillators to NF shaking and describes modifications needed to more accurately calibrate the CM and CSM methods. Chapter 5 describes reasons for the behavior observed and

shows how the findings can be applied to the design of PG&E structures and Chapter 6 summarizes the major findings.

CHAPTER 2. BACKGROUND AND LITERATURE SUMMARY

A detailed literature summary of studies undertaken to assess demands on structures due to near fault shaking have been described by MacRae and Roeder (1999). This chapter summarizes the FEMA273/FEMA356 Coefficient Method (CM) as well as the ATC-40 Capacity Spectra Method (CSM) to estimate inelastic displacement demands on structures, the relative advantages of these methods, the assessment of near-fault structure inelastic demands, and the behavior and assessment methods for mill-type structures.

2.1 METHODS FOR ESTIMATING DISPLACEMENTS OF STRUCTURES

A summary of the different relationships needed to assess the inelastic demands of SDOF structures is given in **Figure 2.1**. The symbols will be described in the appropriate section below.

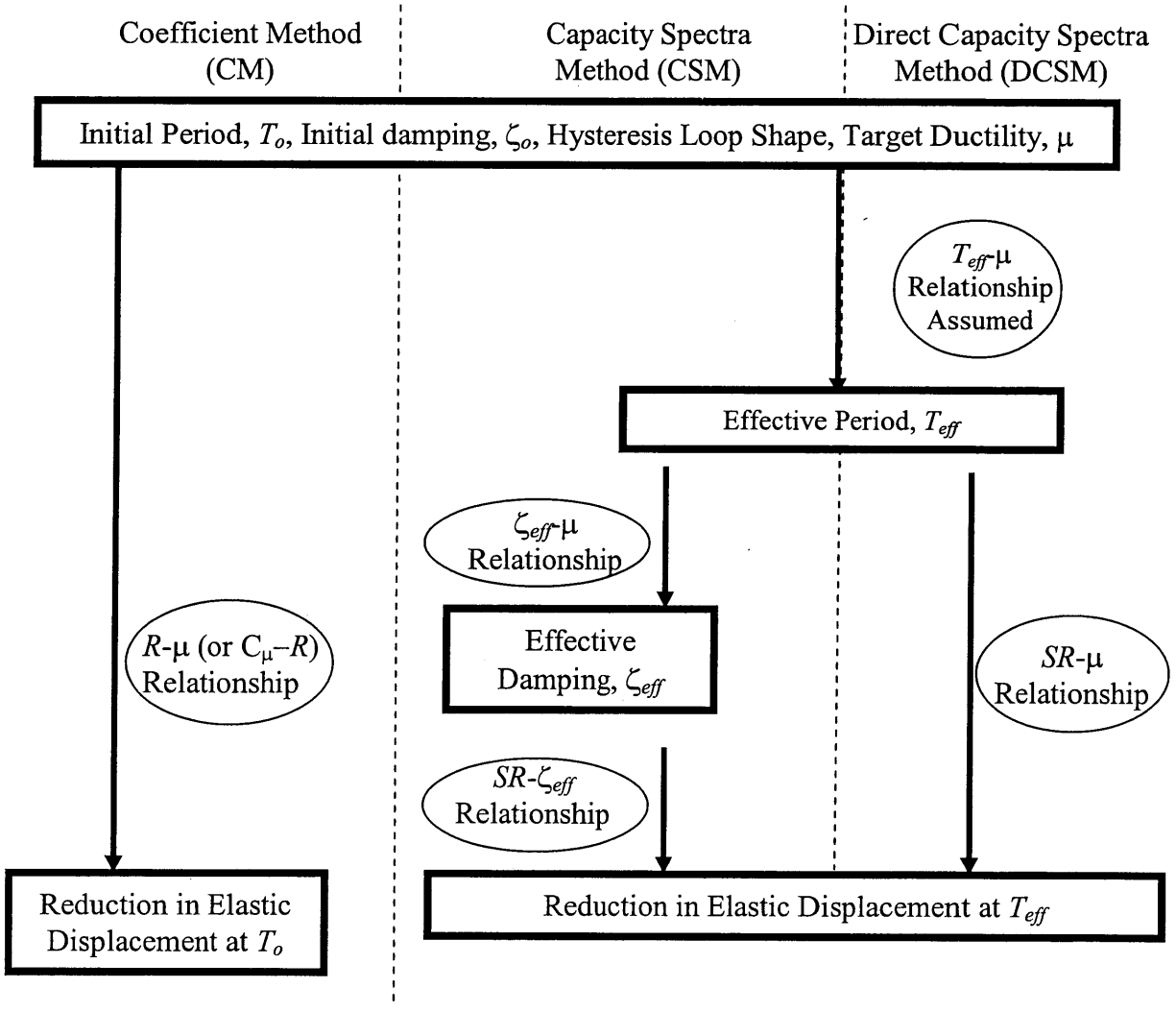

Figure 2.1. Summary of Relationships Needed for Different Procedures

2.1.1 FEMA273/FEMA356 Coefficient Method (CM) – LSP & LDP

FEMA273 (1997) and FEMA356 (2001) Linear Static Procedure (LSP) and Linear Dynamic Procedure (LDP) estimate inelastic displacements, d_u, as $C_1C_2C_3$ times the elastic displacement, d_e as shown in **Equation 2.1**. Here C_1 is a factor representing the likely increase in demand for inelastically responding structures with short periods. When the period of the structure, T_s, is less than the period of the peak amplitude of the acceleration response spectrum (ARS), T_p, then C_1 is greater than unity and the maximum value that it can have is 1.5. For structures with fundamental periods greater than the period of the peak amplitude of the ARS, then C_1 is unity. The factors C_2 and C_3 account for degrading hysteretic characteristics and P-delta effects respectively. The ratio of inelastic to elastic displacement, d_u/d_e, may also be written as C_μ.

$$d_u \quad = C_1C_2C_3 . d_e \quad = C_\mu . d_e \tag{2.1}$$

Although numerous researchers have demonstrated that displacement ductility demand for short period structures, μ, is dependent on the ratio of the force on the elastically responding oscillator to the actual strength, R, the C_1 coefficient ignores this effect. Also, Roeder and MacRae (1999) have shown that the demand estimated for a short period structure which is strong enough to remain elastic using the $C_1C_2C_3$ coefficients above may be twice actual demand of an elastically responding structure. In addition, the FEMA356 upper bound on C_1 of 1.5 is arbitrary and it may be non-conservative.

While the FEMA356 Linear Static Procedure (LSP) and Linear Dynamic Procedure (LDP) methods for estimating C_1 have the major disadvantages listed above for accurately predicting demands, there is a practical advantage in using such a method. It is that the ductility and yield displacement of the structure do not need to be found explicitly. While this simplifies design it may be very conservative or non-conservative depending on the strength of the structure.

2.1.2 FEMA273/FEMA356 Coefficient Method (CM) – Nonlinear Static Procedure (NSP)

FEMA273/FEMA356 nonlinear static procedure uses:

$$d_u \quad = C_0C_1C_2C_3\, d_e \quad = C_\mu . d_e \tag{2.2}$$

Here C_0 describes the roof displacement of a structure in terms of the response of a SDOF structure displacement. The C_1 value is different from that in the LSP method as shown in **Equation 2.3**. Here, C_1 depends on the lateral force reduction factor, R, which is computed according to **Equation 2.4**, where d_y is the yield displacement for a SDOF structure, H_y is the structure yield force and H_e is the force if the structure were to remain elastic. C_1 is also dependent on the structural period, T, and $T_o = T_s$ which is the characteristic period of the response spectrum. The values of S_{X1} and S_{XS} relate to the design spectral response spectrum at the site considered. For the PG&E Berkeley F substation site specific spectra indicate that S_{X1}/S_{XS} is approximately equal to 0.7 indicating that T_o would be about 0.7s for this particular case.

$$C_1 = \begin{cases} 1.0 & \text{for } T \geq T_o \\ \dfrac{\left(1.0 + (R-1)\dfrac{T_o}{T}\right)}{R} & \text{for } T < T_o \end{cases} \quad \text{(a)} \qquad (2.3)$$

$$T_o = \frac{S_{X1} B_S}{S_{XS} B_1} \quad \text{(b)}$$

where B_S and B_1 are damping coefficients from FEMA356 Table 1-6. For a structure with 2% or 5% initial viscous damping, $B_S/B_1 = 1$.

$$R = d_e/d_y = H_e/H_y \qquad (2.4)$$

Again, C_2 depends on the type of hysteretic strength degradation expected, and C_3 depends on the *P*-delta effect.

2.1.2.1 FEMA356 (or FEMA273) CM NSP C_1 Equation

The NSP C_1 equation is much more rational than the LSP and LDP equation since it considers the strength of the structure. Structures with a strength sufficient for them to remain elastic, $R = 1$, will have a C_1 value of unity.

The C_1 equation follows the equal displacement assumption for longer period structures. That is, the inelastic displacement, d_u, is equal to the elastic displacement, d_e. **Equation 2.3** follows the methodology developed by Berrill et al. (1980). The equation of Berrill et al. is given in **Equation 2.5**. Here μ is the ductility computed for a SDOF oscillator as the inelastic displacement, d_u, divided by the yield displacement, d_y according to **Equation 2.4**. Berrill et al. used $T_o = 0.7$s. For FEMA356, $T_o = T_s$ which is the characteristic period of the response spectrum.

$$R = 1 + (\mu - 1)\left(\frac{T}{T_o}\right) \leq \mu \qquad (2.5)$$

$$\mu = d_u/d_y \qquad (2.6)$$

The relationship of **Equation 2.5** is plotted in the schematic of **Figure 2.2** for a specified target ductility, μ.

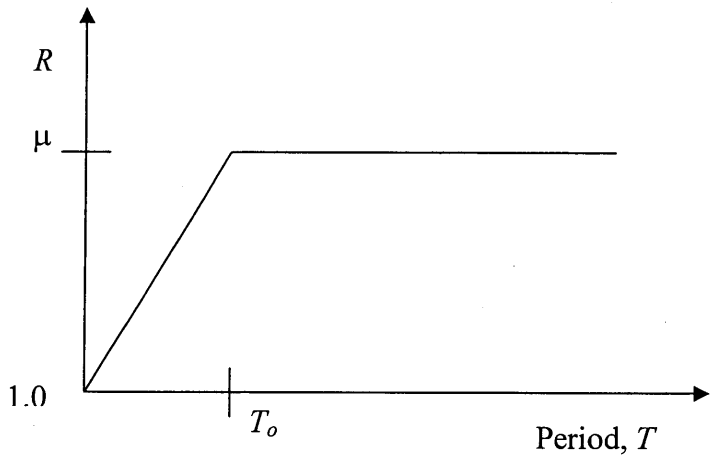

Figure 2.2. *R-T* Curve After Berrill et al. (1980)

From **Equations 2.6** and **2.4**

$$d_u = \mu d_y = \frac{\mu d_e}{R} \tag{2.7}$$

From **Equation 2.5**

$$C_1 = d_u/d_e = \mu/R = \frac{1+(R-1)\left(\frac{T_o}{T}\right)}{R} = \frac{\mu}{1+(\mu-1)\left(\frac{T}{T_o}\right)} \geq 1 \tag{2.8}$$

Equation 2.3 is identical to **Equation 2.8**. A schematic of the C_1-T relationship is given in **Figure 2.3**.

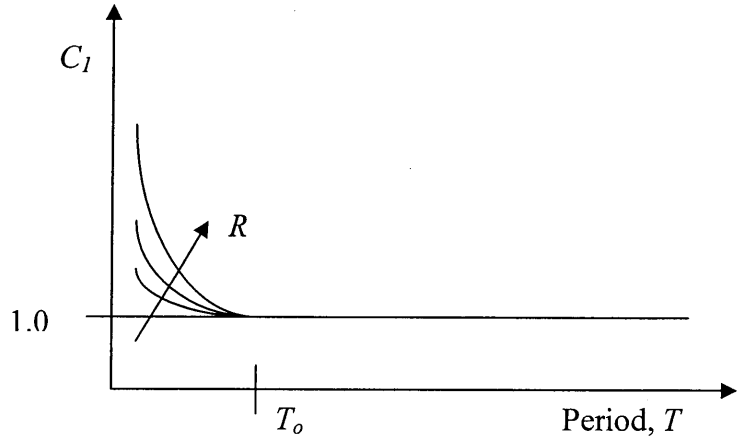

Figure 2.3. FEMA356 C_1-T Curve

2.1.2.2 C_2 Coefficient

The coefficient C_2 is used to increase the displacements of structures when the hysteresis loop shape is degrading. While this should only affect yielding structures, the value of C_2 is not dependent on the strength or on the lateral force reduction factor, R. It is therefore possible for a structure with sufficient strength to remain elastic to have a predicted displacement which is greater than that of an elastically responding structure.

2.1.2.3 Other R-T or C_μ-T Relationships for Standard Records

A number of other methods of this type have been summarized by Miranda and Bertero (1985). Vidic, Fajfar and Fischinger (1994) made an improvement to the estimation of the behavior of short period structures by considering that T_o is dependent on the target ductility. **Equation 2.3** is used where:

$$T_o = 0.65 T_c \mu_c^{0.3} \quad \text{(a)} \qquad (2.9)$$

$$T_c = 2\pi \frac{S_v}{S_a} \approx 2\pi \frac{c_v}{c_a} \frac{(\dot{x}_g)_{\max}}{(\ddot{x}_g)_{\max}} \quad \text{(b)}$$

where S_v and S_a are the maximum spectral velocity and acceleration respectively and c_a and c_v are coefficients which may be obtained from the acceleration and velocity response spectral plots as well as from the ground accelerations. Suggested values for these parameters are 2.5 and 2.0 respectively (Chai, Fajfar and Romstad, 1998).

Krawinkler proposed a parabolic-linear relationship, rather than a bilinear R-T relationship as shown in **Figure 2.4** since this more closely fitted the experimental results.

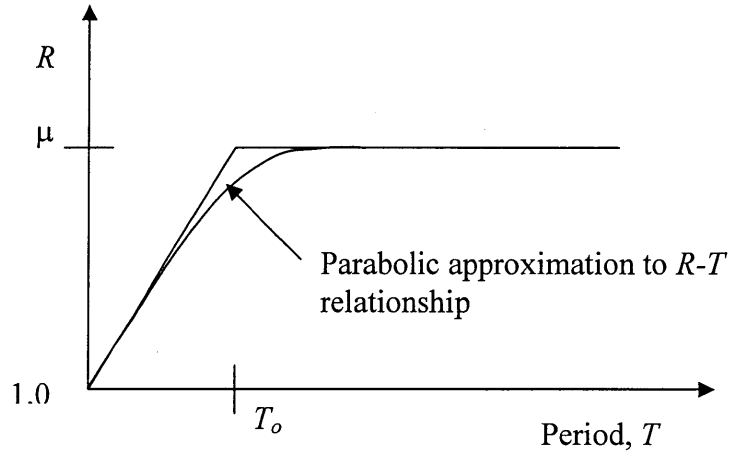

Figure 2.4. R-T Curve With Parabolic Approximation

Miranda (2001) has shown that the methods by which many researchers (Reinhorn 1997, Fajfar 1999, 2000 and Chopra & Goel, 1999) found the R-μ relationships for a number of records

may be incorrect, and even non-conservative when applied to design. These researchers were really interested in $C_\mu = d_u/d_e = \mu/R$. Therefore, they should have obtained the average value of $[\mu/R] = \mu$ times [the average value of $1/R$] for a constant value of μ. However, they found the [average value of R] for constant value of μ. Then they approximated the average value of d_u/d_e as μ/[average value of R]. Miranda showed that the average value of $d_u/d_e = \mu$ times [the average value of $1/R$] is always greater than μ/[average value of R], so that the values obtained for these researchers were non-conservative.

The CM may be expressed in terms of an acceleration-displacement plot for design. This form of plot is similar to the CSM described below, except lines of constant ductility are used instead of lines of constant damping. These plots can be based on either the structural yield point (Ascheim 1999), or on the point of ultimate displacement (Fajfar 2000, Chopra and Goel 1999, MacRae, Morrow and Roeder, 2000). If the ultimate displacement point is used, then a capacity curve can be compared with the demand curve in exactly the same way as it is for the CSM. Also, if damping is actually related directly to ductility, as assumed in the CSM, then a line of constant ductility in the CM will be identical to a line of constant damping in the CSM.

Miranda (2000) suggested that C_μ be taken as that in **Equation 2.10** for EPP oscillators. Miranda's equation satisfies all boundary conditions since C_μ tends to unity for very long period structures or as μ tends to unity, and C_μ tends to μ as T tends to zero. However, C_μ is limited to be between the limits of unity and μ. For actual earthquake records, C_μ is often less than unity and this behavior is unable to be captured by this equation.

$$C_\mu = \frac{1}{[1+(1/\mu-1)e^{\{-12T\mu^{0.8}\}}]} \tag{2.10}$$

Baez and Miranda (2000) analyzed oscillators using 82 NF records. These records were defined as being within 15 km of the fault plane. They found that for oscillators with periods between about 0.1s and 1.3s, NF records on average increased the displacement response to 1.3 times greater than that from the FF records for target ductilities of 4 or 6. Stronger components of shaking had greater inelastic demands than the weaker components of shaking.

2.1.3 ATC-40 Capacity Spectra Method (CSM)

The Capacity Spectra Method is based on the Substitute Structure Method (SSM) (Gulkan and Sozen, 1974, 1977) and it is used in its present form following developments by Freeman (1978). The concepts describing this method are given below.

2.1.3.1 Substitute Structure Method (SSM)

Gulkan and Sozen (1974, 1977) idealized the behavior of an inelastic structure as an elastic substitute structure with a lower effective stiffness causing a longer effective period, T_{eff}, and higher effective damping, ζ_{eff}, due to hysteretic energy dissipation and initial viscous damping. This is referred to as a "substitute structure". A relationship between the ductility, μ, or hysteretic energy dissipated in one cycle, and the effective damping, ζ_{eff}, is required. Three relationships must be known to be able to use the SSM. They are:

(1) a relationship to establish the effective period, T_{eff}, of the structure

A large range of definitions of effective period, T_{eff}, are possible. However, T_{eff} is often assumed to be based on the secant (or effective) stiffness, k_{eff}, to the point of peak displacement, d_{max}, as shown in **Figure 2.5**. In this case, for an oscillator with a bilinear loading curve, T_{eff} is:

$$T_{eff} = T\sqrt{\frac{\mu}{(1+\mu r - r)}} \tag{2.11}$$

(2) a relationship between ductility, μ, and effective damping, ζ_{eff}

Gulkan and Sozen suggested a method for determining this damping based on the following assumptions. They are;

- both inelastic structure and substitute structure move to same maximum displacement in each cycle.
- the energy dissipated by the elastic and inelastic structures and its substitute structures are the same in each cycle.
- the substitute structure is oscillating in a sinusoidal motion at its natural period when it reaches its peak displacement.

According to these assumptions, the effective damping may be found as follows.

$$\zeta_{hyst} = \frac{2R}{\pi} \quad \text{(a)}$$

$$\zeta_{eff} = \zeta_o + \zeta_{hyst} \quad \text{(b)} \tag{2.12}$$

where R is ratio of the area of the hysteresis loop during one cycle to that of a rectangle surrounding the loop as shown in **Figure 2.6** (Chopra, 1995), ζ_o is the initial viscous damping, and the hysteretic damping is ζ_{hyst}. For a bilinear oscillator with post-elastic stiffness ratio, r,

$$R = \frac{(1-r)(\mu-1)}{(1+\mu r - r)\mu} \tag{2.13}$$

An alternative method to obtain the effective damping was proposed by Tagawa from the response of bilinear oscillators based on their response to impulse loading as shown in the **Appendix**. The equation below is an approximation to the actual impulse response and it's error is less than 20%. It considers only the shape of the loading curve.

$$\zeta_{eff} = \frac{2}{\pi}\cdot\ln\sqrt{1-\frac{1}{\mu}+\frac{1}{1+\mu r - r}} + \zeta_o \tag{2.14}$$

(3) A relationship between effective damping, ζ_{eff}, and reduction in displacement, SR. The displacement is expected to decrease with greater damping. This relationship tends to be empirical.

Using the information obtained from steps (1) to (3), T_{eff}, ζ_{eff} and SR, the peak displacement may be found as illustrated in **Figure 2.7**.

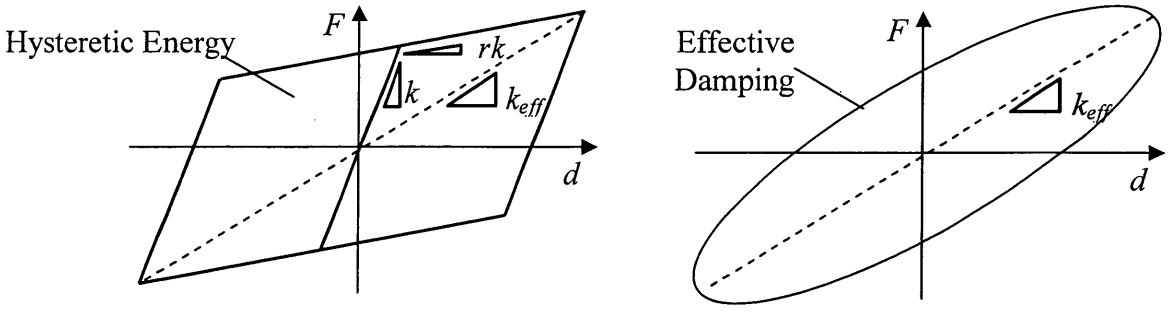

a) Actual Yielding Structure b) Substitute Elastic Structure

Figure 2.5. Yielding and Substitute Elastic Structure

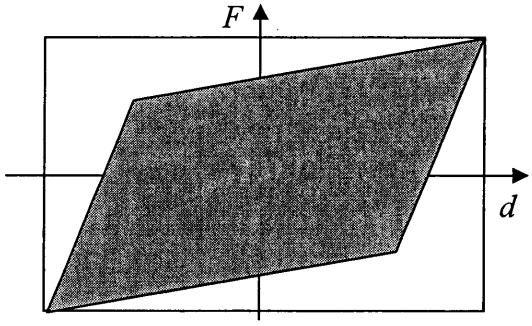

Figure 2.6. Hysteretic Area and Rectangular Area used to Compute *R*

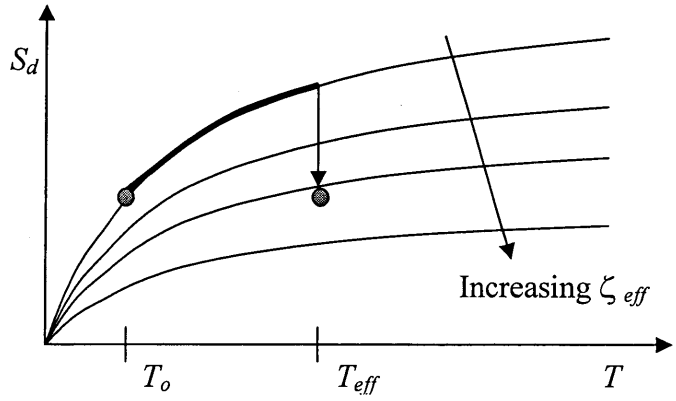

Figure 2.7. Yielding and Substitute Elastic Structure

In the SSM, iteration is generally performed to determine the likely displacement demand, since T_{eff} and ζ_{eff} are based on the estimate of displacement. The SSM has been used for many years for the design of base-isolated structures.

2.1.3.2 Development of the CSM

The CSM was developed initially in 1978 (Freeman, 1978). It has increasingly become associated with performance based design. While performance based design may be used with any analysis method, some engineers have come to think of the CSM as being the *performance-based design* method. Actually, it is simply another approximate procedure to estimate the likely displacement response of a structure.

The CSM (ATC-40) is simply the SSM expressed in terms which give a nice visual interpretation of the dynamic response.

The background, as well as steps to apply this method, are described in detail in ATC-40 (1996). The elastic response spectra is plotted using axes of spectral acceleration, S_a, and spectral displacement, S_d, as shown in **Figure 2.8**. This is called a *demand plot*. Structures with constant period lie on lines extending radially from the origin. The *capacity plot* is simply the lateral force vs. displacement plot obtained from a push analysis of the structure converted to S_a–S_d format. **Figure 2.9** shows the lateral force-displacement (H-Δ) of the structure plotted in terms of acceleration (= H/m) and displacement (Δ) on the same plot as the demand spectra. The displacement at the peak force on the capacity curve represents the "effective stiffness" and "effective period". If a point on the capacity curve associated with some performance level is outside the demand line for a damping related to the ductility, then the structure satisfies that particular performance criteria. Iteration is not required in this method if the check is simply to compare the capacity with the demand. However, if the likely displacement is to be estimated, iteration is required in the same way as for the SSM, and the same answer as that obtained in the SSM will be obtained.

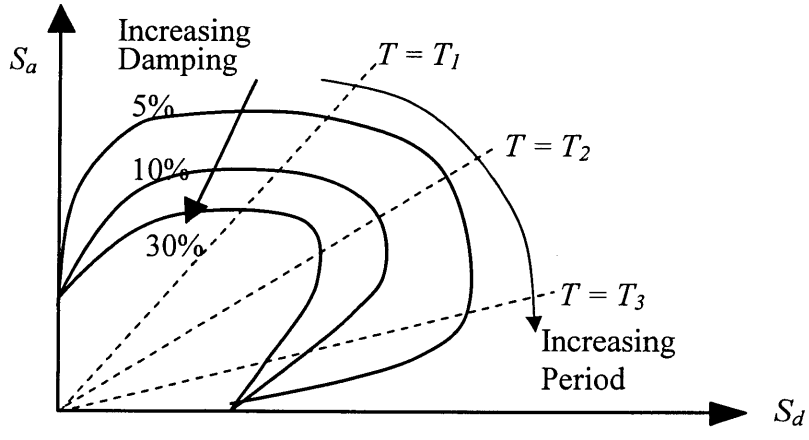

Figure 2.8. Demand Curves

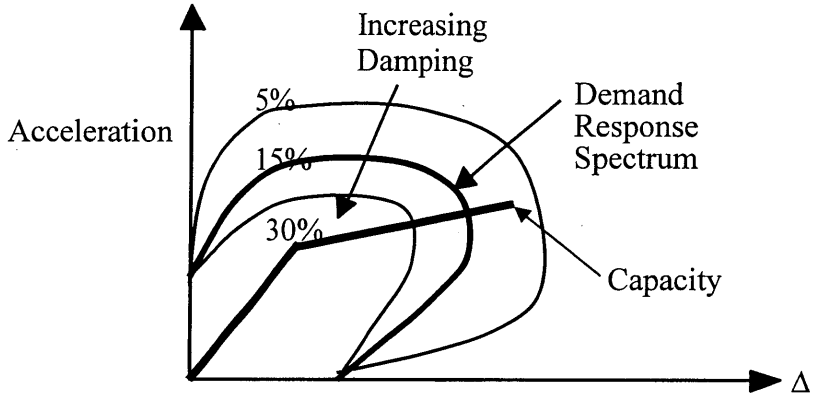

Figure 2.9. Capacity-Demand Curves

MDOF structures with periods greater than about 1s are problematic for the CSM method since higher modes become more significant, nevertheless an approach has been developed in ATC40. The approach is relatively complex and it may be argued that since a nonlinear model must be developed for the static pushover analysis to obtain the demand curves, it may be easier, and far more accurate to go the next step and carry out a number of inelastic dynamic time-history analyses rather than to pretend that useful information is coming from an approximate analysis based on the elastic structure mode shapes when the structure is actually yielding.

Some authors, such as Priestley (2000), have argued that the CSM method using the first mode approximation and inelastic push analysis is sufficient to assess the demands of multistory structures. However since the member forces are not estimated well by this method (MacRae, Carr and Walpole, 1990) capacity design (SANZ, 1984) should be used to assess member forces.

2.1.3.3 Expressions to Assess Effective Damping

(a) ATC-40 has an expression to compute effective damping for structures which have a bilinear hysteresis loop based on the behavior of an oscillator undergoing sinusoidal response (Chopra, 1995, Gulkan and Sozen, 1974) which is slightly modified for high damping values. The hysteretic damping, ζ_{hyst}, is given by **Equation 2.15**. This is identical to that from **Equation 2.12** and **Equation 2.13** for bilinear structures. In ATC-40, the total effective damping, ζ_{eff}, is equal to the hysteretic damping, ζ_{hyst}, multiplied by an empirical modification factor, κ, plus the initial elastic damping assumed, ζ_o, as given in **Equation 2.14**. The κ value used here is for ATC-40 Type A construction which implies hysteretic loops without degradation. Type A construction was assumed because the hysteresis loops used in the analyses had no degradation.

$$\zeta_{hyst} = 0.637(a_y/a_{pi} - d_y/d_{pi}) \tag{2.15}$$

$$\zeta_{eff} = \zeta_o + \kappa\zeta_{hyst} \tag{2.16}$$

$$\kappa = \begin{cases} 1.0 & \text{for } \zeta_{hyst} \le 16.25 \\ = 1.13 - 0.008\zeta_{hyst} & \text{for } \zeta_{hyst} > 16.25 \end{cases} \tag{2.17}$$

For example, for an elastic-perfectly plastic oscillator with $\mu = 4$ and $\zeta_o = 2\%$, the effective damping should be given as:

$$\zeta_{hyst} = 0.637(a_y/a_{pi} - d_y/d_{pi}) \quad (2.15)$$
$$= 0.637(1.0 - 1/4)$$
$$= 47.75\%$$

$$\kappa = 1.13 - 0.008\zeta_{hyst} \text{ since } \zeta_{hyst} > 16.75\% = 0.748 \quad (2.17)$$

$$\zeta_{eff} = \zeta_o + \kappa\zeta_{hyst} \quad (2.16)$$
$$= 2\% + 0.748 \times 47.75\%$$
$$= 37.72\%$$

ATC-40 (1997) states that this damping is also appropriate for reinforced concrete (RC) structures. MacRae, Priestley and Tao (1993) found that the hysteresis loop area is generally significantly less for reinforced concrete (RC) structures than it is for bilinear structures and calculated lower damping values leading to a less conservative design.

(b) According to Gulkan and Sozen (1974), the hysteretic damping, ζ_{hyst}, for an elastic-perfectly plastic oscillator ($r = 0.0$) with $\mu = 4$ and $\zeta_o = 2\%$ should be given according to **Equations 2.12 and 2.13.** The expressions are equivalent to **Equation 2.16** where $\kappa = 1$.

$$\zeta_{hyst} = 2/\pi.R_{epp} = 2/\pi.(\mu\text{-}1)/\mu = 2/\pi \times 0.75 = 47.75\%$$

$$\zeta_{eff} = \zeta_o + \zeta_{hyst} = 2\% + 47.75\% = 49.75\%$$

(c) Based on impulse loading, **Equation 2.14** gives:

$$\zeta_{eff} = \frac{2}{\pi} \cdot \ln \sqrt{1 - \frac{1}{\mu} + \frac{1}{1 + \mu r - r}} + \zeta_o = \frac{2}{\pi} \cdot \ln \sqrt{1 - \frac{1}{4} + 1} + 2\% = 19.8\%$$

2.1.3.4 Expressions to Assess Spectral Reduction, *SR*

A number of methods are presented in different design guidelines to determine the reduction in strength, *SR*, for a specified damping, ζ_{eff} (Nishiyama 2000). However, even though this relationship is dependent on structural period as described above, all of the methods assume it to be independent. A couple of methods are described below.

(a) ATC-40 uses **Equation 2.19** to determine a displacement reduction factor, SR, when $\zeta_o = 5\%$. SR_A applies to structures that have a period less than the transition period, T_T, while the second factor, SR_V, applies to longer period structures.

$$SR_A = (3.21-0.68 \ln(\zeta_{eff}))/2.12 > 0.33 \quad (2.18)$$

$$SR_V = (2.31-0.41 \ln(\zeta_{eff}))/1.65 > 0.50 \quad (2.19)$$

The maximum damping, ζ_{eff}, affecting SR_A and SR_V are 40% and 37.4% respectively. When $\zeta_{eff} =$ 5% then $SR_A = SR_V = 1.0$.

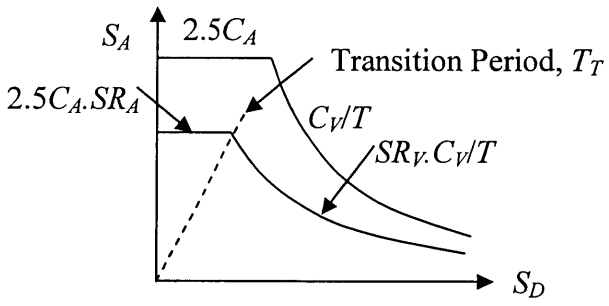

Figure 2.10. CSM Reduced Response Curves due to Damping (ATC40)

Using these ATC-40 SR equations values, and considering the ATC-40 damping value of $\zeta_{eff} =$ 37.72% from the example above, the reduction for a ($\zeta_o =$) 5% damped spectra is given below.

$SR_A = (3.21-0.68 \ln(37.72\%))/2.12 > 0.33$
$= 0.349$ which is greater than 0.33
$SR_V = (2.31-0.41 \ln(37.72\%))/1.65 > 0.50$
$= 0.498$ which is not greater than 0.50
so $SR_A = 0.349$ (for short period structures) and $SR_V = 0.50$ (for longer period structures).

While the reduction method was not meant to be used in this way, the increase in demand due to 2% damping ($\zeta_o = 2\%$) from $\zeta_o = 5\%$ is 1.29 and 1.23 for SR_A and SR_V respectively. The SR value needed for a reduction from 2% to 37.72% is given below. This reduction is used in conjunction with the response of oscillators with 2% elastic damping and elastic-perfectly plastic oscillators with a target ductility, μ, of 4. For periods greater than the transition period, T_T, SR_V is used and for shorter periods, SR_A is used. The transition period, T_T, is given in **Equation 2.20**. For type D soil (which is the site condition on which most of the records described in this report were obtained) assuming a shaking intensity of greater than or equal to 0.4, the ratio of $C_V/C_A =$ 1.45 (ATC-40 Table 4.7 & 4.8). In the example above, $T_T = 0.874$s. This transition period is an "effective" rather than a "fundamental" period since the effective period is the one at which we are considering the elastic response. The structures fundamental period, T, at this transition is therefore given from **Equation 2.11** as $T =$ 0.874s/2 = 0.437s for EPP oscillators with $\zeta_o = 2\%$ and $\mu = 4$.

$SR_A = 0.349/1.29 = 0.270$

$$SR_V = 0.50/1.23 = 0.407$$

$$T_T = \frac{0.4\, C_V SR_V}{C_A SR_A} = \frac{0.58\, SR_V}{SR_A} = 0.874\text{s} \qquad (2.20)$$

(b) The Architecture Institute of Japan (AIJ, 1993) ratio of displacements, d_2/d_1, due to different damping ratios, ζ_1 and ζ_2, for all periods is:

$$d_2/d_1 = SR = \frac{(1+10\zeta_1)}{(1+10\zeta_2)} \qquad (2.21)$$

To increase the damping from 5% to 47.75% gives a *SR* value of:

$$d_2/d_1 = SR = \frac{(1+10\text{x}5\%)}{(1+10 \text{ x } 49.75\%)} = 1.5/5.975 = 0.251$$

Similarly, to increase the damping from 2% to 49.75%, $SR = 0.201$.

To increase the damping from 2% to 37.72% gives a *SR* value of 0.251. This is lower than the ATC40 SR_A and SR_V values of 0.270 and 0.407 respectively. The AIJ method therefore predicts lower *SR* values than does the ATC-40 method.

(c) For a response to an *impulse*, *SR* may be computed directly, independently of ζ_o as:

$$SR = e^{\left(-\zeta_{hyst} \cdot \frac{\pi}{2}\right)} \qquad (2.22)$$

For a hysteretic damping of 17.8%, *SR* is 0.756. For $\zeta_{hyst} = 37.72\%$, *SR* is 0.552.

2.1.3.5 Theoretical Assessment and Understanding of Spectral Reduction, *SR*

The effect of damping is to decrease the displacement of a structure. However for very long or very short period structures, the displacement response is almost independent of damping. This is shown in the schematics below:

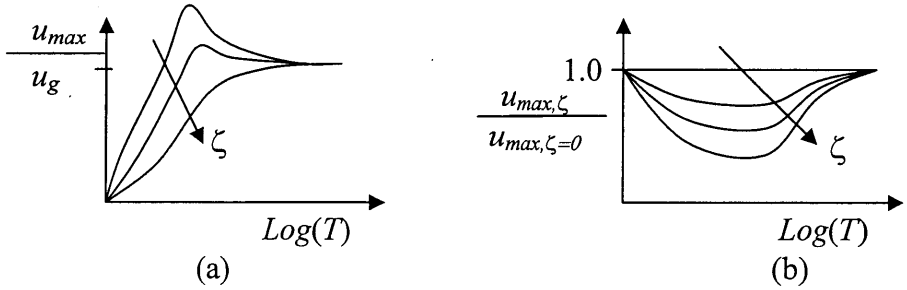

Figure 2.11. Schematic of Theoretical Effect of Damping, ζ, on Relative Displacement, d_{max}, for Different Periods, T

(a) Very Short Period Structures

These figures indicate that for structures of very short period, the displacement tends to zero and the ratio of $u_{max,\zeta}/u_{max,\zeta=0}$ tends to unity. This can be shown from the equation of motion, EOM, given in **Equation 2.23**, as follows where u is the relative displacement, u_t is the total displacement, and u_g is the ground displacement.

$$m\ddot{u}_t + c\dot{u} + ku = 0 \tag{2.23}$$

$$\ddot{u}_t + 2\zeta\omega\dot{u} + \omega^2 u = 0$$

$$u = \frac{\left(-\ddot{u}_t - 2\zeta\omega\dot{u}\right)}{\omega^2}$$

$$= \frac{\left(-\ddot{u}_g - \ddot{u} - 2\zeta\omega\dot{u}\right)}{\omega^2}$$

At u_{max}, the velocity term is zero so

$$u_{max} = -\frac{\ddot{u}_t}{\omega^2} \tag{2.24}$$

$$= -\frac{\ddot{u}_g}{\omega^2} - \frac{\ddot{u}}{\omega^2}$$

As T tends to zero, the relative response terms tend to zero since the structure tends to move with the ground. This means that the right hand term in the equation above, which is a function of damping, ζ, will tend to zero faster than the left-hand term, which is a function only of the ground motion characteristics. Therefore the displacement term, u_{max}, is given by **Equation 2.25** and becomes a function only of the peak ground acceleration and not a function of the damping. The response for different damping ratios becomes similar. As T tends to zero, ω tends to infinity and the displacement tends to zero as shown in **Figure 2.11a**. Since the response becomes independent of damping, the displacement of all oscillators have the same peak displacement as this displacement tends to zero as shown in **Figure 2.11b**.

$$u_{max} = -\frac{\ddot{u}_g}{\omega^2} \tag{2.25}$$

(b) Very Long Period Structures

For long period structures the displacement as the period of the structure becomes long may be found from the EOM given in **Equation 2.26**:

$$\ddot{u}_t + 2\zeta\omega\dot{u} + \omega^2 u = 0 \tag{2.26}$$

As the period tends to infinity, the circular frequency tends to zero. The absolute acceleration therefore tends to zero throughout the complete earthquake record.

$$\ddot{u}_t \rightarrow 0 \tag{2.27}$$

Therefore the relative acceleration is related only to the ground motion.

$$\ddot{u} = -\ddot{u}_g \tag{2.28}$$

For this to be true throughout the whole earthquake record, and if the oscillator starts from rest, integrating both sides twice results in

$$u = -u_g \tag{2.29}$$

So, as the ground moves, the oscillator remains in the same place. The absolute displacement will be zero and the relative displacement will therefore be that of the ground. The displacement as the period increases becomes independent of damping and the ratio of $u_{max,\zeta}/u_{max,\zeta=0}$ tends to unity as shown in **Figure 2.11**.

For intermediate period structures, which are those of real interest, the effect of damping reduces the response. The amount of the reduction depends on the earthquake record considered.

It should be noted that most code expressions to obtain SR_A, including those described above, are generally not considered to be dependent on period.

(c) Intermediate Period Structures

Imagine an elastic displacement response spectra that increases linearly with period, and $SR_V = 0.5$ for a particular EPP oscillator with a target ductility μ of 4. If the spectral displacement at the fundamental period, T, is S_D, then the effective period will be $T_{eff} = 2T$ according to **Equation 2.11** and the displacement at this period is $2S_D$ since the spectra is increasing linearly with period. The predicted peak displacement is then SR_V x $2S_D$ = 0.5 x $2S_D$ = S_D . That is, the prediction of the demand is the elastic demand at the initial period. A value less than 0.5, such as ATC-40 value of $SR_V = 0.407$ obtained above indicates that the estimated demand would be less than the elastic demand. ATC-40 will give lower estimates of displacement demand if the slope of the elastic response spectra decreases with period at large periods.

2.1.4. Direct Capacity Spectra Method

The CSM approach may be carried out without explicitly computing damping as shown in **Figure 2.1**. Instead a factor (*SR*) is computed which is the ratio of the actual displacement to the elastic displacement at the effective period of the structure. This will be referred to as the Direct Capacity Spectrum Method (DCSM).

According to the DCSM, the theoretical relationship between spectral reduction, *SR*, and ductility, μ, at the effective period of the structure, T_{eff}, is required. Usually the effective period is based on the secant stiffness at the peak displacement.

2.1.4.1 Theoretical Assessment of Behavior

The schematic below indicates that *SR* tends to unity for structures with both long period and short period. For intermediate period structures, it is expected that *SR* will generally be less than unity. If it is greater than unity, then a negative damping is implied. The figure is similar to **Figure 2.11b** because ductility has an effect which can be regarded as a type of damping.

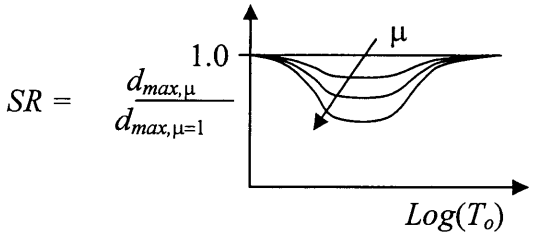

Figure 2-12. Schematic of Theoretical Effect of Damping, μ, on Relative Displacement, d_{max}, for Different Periods, *T*

2.1.4.2 ATC-40 *SR* Values

ATC-40 and other procedures may be used to obtain SR for a certain ductility and hysteresis loop shape. The estimates for an EPP oscillator with $\mu = 4$ and $\zeta_o = 2\%$ are identical to that given in **Section 2.1.3.4**. For example, ATC-40 predicts $SR_A = 0.270$ and $SR_V = 0.407$.

2.1.5. Inelastic Time History Analysis (ITHA) or Nonlinear Dynamic Procedure (NDP)

The FEMA356 NDP is often used by researchers to assess the likely inelastic demands on a structure during a particular earthquake. It is sometimes used to confirm the behavior of structures designed by simplified methods. In general, a number of earthquake records should be used to analyze a structure in order to give confidence regarding the structural performance.

While US practitioners generally consider that the NDP is presently too complex for routine design, the use of the NDP has been incorporated by the Specification for Highway Bridges (1996) in Japan as a routine procedure for structures which are not simple. Records are given in the Japanese bridge code (JRA1996) and procedures for modeling and applying damping to different elements are laid out.

It is the opinion of the authors that the increased complexity of simplified analysis methods, the rapid increase in the number of earthquake records available, and the increase in computational power, will cause the NDP to play a much greater role in routine design in the next few years.

2.2. COMPARISON CSM & CM

The Coefficient Method (CM), and the Capacity Spectra Method (CSM) are compared below:

Advantages of the CM are that:

- It is very simple to use and does not require an inelastic push analysis.
- For longer period structures the inelastic displacement is often assumed to be identical to the elastic displacement so yield displacement does not need to be computed.

Disadvantages of the CM are that:

- The ultimate displacement predicted for a short period structure is sensitive to the structural elastic stiffness and to the yield displacement. The lateral force-displacement relationship for actual structures is often non-linear so "elastic" stiffness is difficult to define. Also, many structures exhibit no clear yield displacement so methods are required to define yield displacement which will allow consistent demand assessment. While consensus has been reached by some schools of researchers regarding the definition of elastic stiffness and yield displacement for certain classes of structure, other schools of researchers have different methods. No study had been carried out to evaluate which set of definitions provides the best estimate of seismic demands.
- The relationship between R and μ will depend slightly on the assumed initial viscous damping. This in not usually taken into account in design.
- There is disagreement about the R-T-μ relationship in the short period range.

Advantages of the CSM are that:

- Response predictions are less sensitive to the elastic stiffness and yield displacement than the CM
- For multistory structures an indication of the frame mechanism and "feeling" for structural behavior may be obtained from a push analysis
- It is easy to consider the effect of different hysteretic characteristics
- Different amounts of viscous damping can easily be considered in design

Disadvantages of the CSM are that:

- It is more complex to use than the CM procedures.
- Three empirical relations are required. They are μ-T_{eff}, μ -ζ_{eff} and ζ_{eff}-SR.
- Iteration is required to estimate the likely structural displacements.
- The CSM relies on the elastic demand estimated at the effective period of the structure, T_{eff}. This period, T_{eff}, is often significantly greater than that at the fundamental period, T_o. For long period structures subject to high ductilities, T_{eff} may be greater than 6s. Since devices for measuring ground accelerations have been calibrated to give the best accuracy over shorter period ranges, the ability for recorded ground motions to reasonably estimate the demands at T_{eff} is questionable.
- For a strength degrading hysteresis loop, the peak strength at the maximum displacement (and hence the peak displacement secant stiffness) is dependent on the load history of the oscillator. It is therefore not clear what T_{eff} should be used.
- There is a large amount of disagreement regarding the value for effective damping to be used to produce the response (e.g. Iwan and Gates 1979, Freeman, 1998), the sensitivity of effective damping to hysteretic energy dissipated, and the CSM calibrated according to the method given in ATC-40 is often unsafe. Tsopelas et al. (1997) find that the CSM

either accurately estimates or overestimates the mean displacements obtained from nonlinear time history analysis. Chopra and Goel (1999, 2000) conducted a study and state that the CSM using the ATC-40 empirical equations for effective period, effective damping and spectral reduction, is less accurate than the CM procedures and it often underestimates displacements by more than 50%. While other methods to estimate effective damping are available, agreement has not been reached amongst engineers as to what equation may be most appropriate for any particular case. Also, Fenwick and Bull (2002) and Judi et al. (2002) reference a number of studies by different researchers using a wide range of oscillators. Oscillators with the same initial stiffness and strength with fat bilinear loops (representing steel structures), with pinched stiffness degrading loops (representing reinforced concrete structures), or with very pinched loops (representing timber structures) had similar displacements. Loops with greater hysteretic energy dissipation did not show smaller displacements indicating that the relationship between hysteretic energy dissipation and effective damping may not be as strong as that often expected. Non-linear elastic oscillators and those in which progressive yielding tends to occur in the same direction were not considered in the comparison by Fenwick and Bull (2002) and Judi et al. (2002).

- For structures in which oscillation does not occur about the initial at-rest position, as a result of the structural form or the earthquake record, effective damping values may be very low. In some cases effective damping may be negative (MacRae, Morrow and Roeder, 2001). Physical understanding of the oscillator behavior is easily lost.
- The design procedure for multi-story structures uses a monotonic push analysis. This requires more complex software than that needed for the CM.
- Monotonic push analysis may give designers a feeling that they are getting a good idea of the likely inelastic behavior of a frame in an earthquake. In this way the CSM may be more dangerous than the CM. It has been shown that cyclic loading to the same displacement may give significantly larger member demands and different mechanisms than that found from push analysis (MacRae, Carr, Walpole, 1990). Statistical variation in material properties as well as dynamic effects can also effect behavior.

The DCSM has the same advantages and disadvantages as the CSM except that the damping is not considered explicitly so different equations for SR will have to be developed for different hysteretic loops. Also, only two empirical relations are required which are μ-T_{eff} and μ-SR relationships. The scatter in this method is less than in the CSM because the number of steps is less.

2.3 NEAR-FAULT EFFECTS ON SDOF STRUCTURES

A summary of how NF shaking effects are likely to influence structures is given by MacRae and Roeder (1999). It is well known that the inelastic demand of NF records may be significantly greater than that of FF records as shown in **Figure 2.13**. A summary of some recent and relevant research is given below.

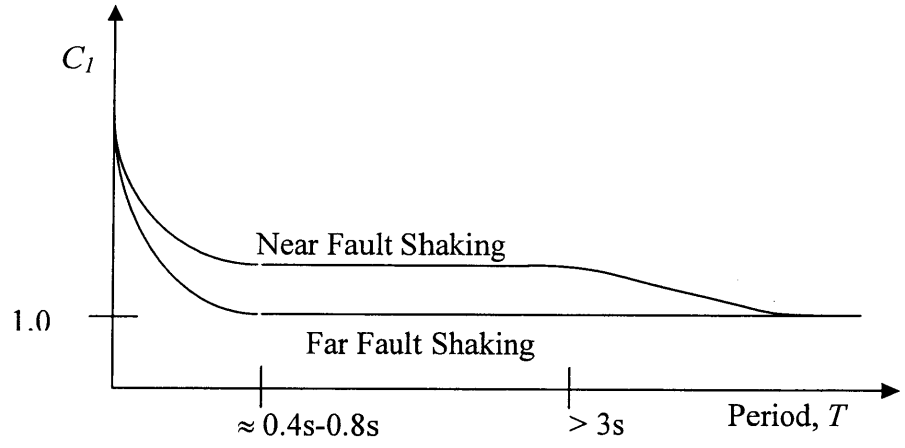

Figure 2.13. Schematic of Increased Demand (C_1) due to NF Shaking

Iwan, Huang and Guyader (1998) described the behavior of SDOF structures to NF shaking using 7 earthquake records which he had identified as containing significant near-fault pulse type characteristics. Pulses in these records were considered to have durations ranging from 1.2s to 5s. They showed that over some period ranges some of the records had elastic acceleration response spectra which were significantly greater than the 1997 UBC design elastic spectra considering near-fault shaking effects.

They conducted analyses of SDOF oscillators with a post-elastic stiffness ratio of 10% and found that some records have large inelastic demands over a wide range of periods as shown by R-T-μ plots. It was shown that short period structures generally have a greater inelastic demand, d_u/d_e, than do longer period structures. It was also stated that when the structure period is less than the period of peak pulse excitation, that the inelastic demand was generally greater than for longer period structures. The difference in demand due to NF and FF records was not discussed because FF records were never analyzed.

They evaluated the ability of the CSM (ATC40) to estimate SDOFO total displacement demands using a plot of the locus of performance points (LPP) on a S_a-S_d plot for various earthquake records. This LPP is simply the predicted peak displacement for structures of a certain period, T_o, with different values of lateral force reduction factor R, according to the CSM. The actual inelastic response, found by determining the peak demands for structures with the same period, T_o, and different R values, was plotted as an inelastic response curve (IRC) as shown in **Figure 2.14**. For some of the NF records, the IRC gave greater displacements than the LPP method indicating that the inelastic response of these records could be greater than the elastic displacements.

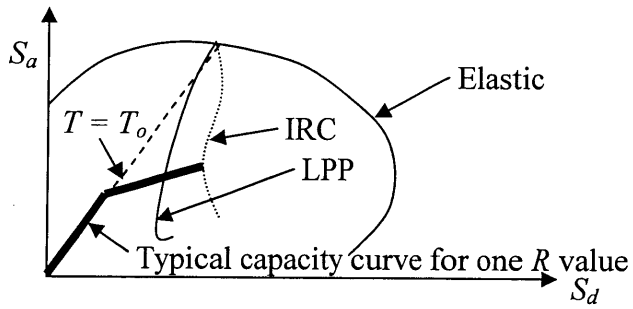

Figure 2.14. Schematic of Loci of Performance Points (LPP) and Inelastic Response Curve (IRC) for a Structure with Period, T_o

A displacement demand ratio, DDR, was defined as the ratio of the displacement of the actual inelastic displacement of a structure with a specified lateral force reduction factor, R, and period, T, to that predicted from the CSM. The CSM was conservative for some period ranges in some records but it was never conservative for all period ranges. In some records, the inelastic demand implied by the CSM was non-conservative by a factor as high as five. The DDR was especially high for shorter period structures. It was not possible to check the accuracy of the DDR plots from the LPP-IRC plots because the LPP-IRC plots were based on a target ductility, μ, of 8, while the DDR plots used target ductilities, μ, of 2, 4 and 6.

They used a shear building to model the response of MDOF structures and found that the CSM was good at estimating the peak roof drift for all structures and the story drift distribution for structures with a fundamental period less than 0.7s. For taller structures, story drifts were underestimated by a factor as high as four due to higher mode contributions.

Krawinkler (1999) has also studied the effect of near fault shaking on structural response. Following the methodology of previous researchers he used pulses to describe the near-fault shaking response. In his work:

- pulse magnitude was related to earthquake magnitude for assessment of the demand and there is a lot of scatter in these plots. Such an approach is only suitable for strike-normal records from sites near the end of the faulted region since a significant pulse may not have developed at any other location (MacRae and Roeder, 1999). The method described by Krawinkler may be very conservative for structures near the epicenter.
- the shape of Krawinkler's pulse does not give a good indication of pulses seen in actual earthquake records.

MacRae and Roeder (1999) conducted a number of studies to look at the effects of near-fault type shaking on PG&E type structures. They defined the record inelastic demand in terms of a bilinear R-T curve for EPP oscillators with a target ductility, μ. This was carried out for artificial records, for measured NF records at different locations relative to the epicenter and fault, as well as for FF records as described below.

- Using a pure pulse record it was found that the demand of oscillators with a fundamental period less than the pulse period, Δ_u/Δ_e, was generally greater than that for oscillators with a fundamental period greater than the pulse period. This indicates that structures with shorter periods, at least with periods less than the pulse period, have greater ductility

demands than longer period oscillators. Similar studies have been conducted by many researchers in the past.

- In actual earthquake records, the high short period demands may not be as high as that obtained from pulses only, since there is a lot of high frequency shaking which affects the design force and inelastic response of inelastic structures. To investigate whether pulses have a big effect on the behavior of short structures, artificial records were manufactured by superimposing a pulse record on a white noise record. Neither pulse or the white noise were particularly realistic however, by comparing the *R-T* response of the short period structures before and after the pulse was imposed, it was possible to see if there was a change in response due to the presence of the pulse. It was found that the pulse actually increased the demand slightly. However, there were questions about what size and period of pulse is suitable for this type of analysis.
- "Correcting" the record displacement offset had little effect on oscillator elastic or inelastic demands.

MacRae and Roeder (1999) evaluated the severity of inelastic shaking from records obtained at different locations relative to the fault. This approach has the advantage that no arbitrary NF record definition is required. Records from sites at known locations relative to the epicenter and fault plane were used.

The means of expressing the data was to plot parameters representing the inelastic displacements for records at their location relative to the epicenter and fault plane as shown in **Figure 2.15a**. The distance along the fault from the epicenter, *s*, and the distance perpendicular to the fault plane, r_{rup}, was used. The severity of the shaking varied along the fault as shown in the schematic of **Figure 2.15b**. Since there was expected to be significant scatter amongst records, the sites were placed in sectors as shown in **Figure 2.16** so that the may be able to be plotted.

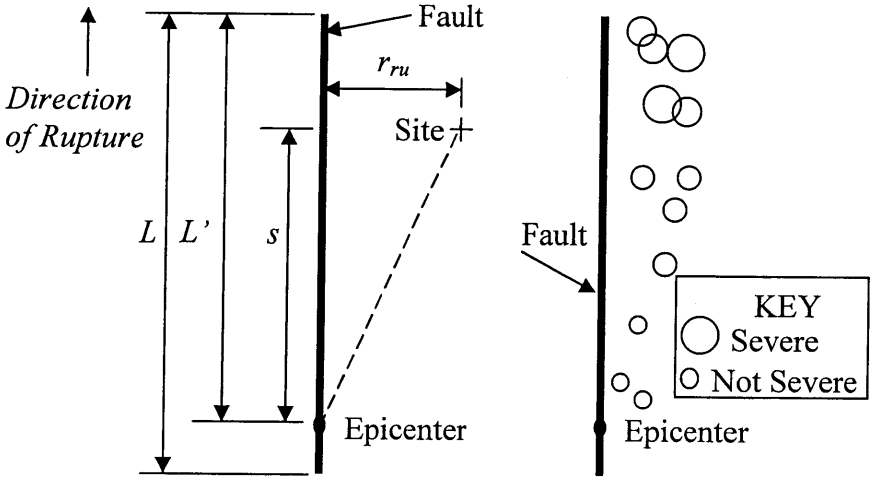

(a) Location of Site (b) Severity Plot

Figure 2.15. Plan of Faults and Patterns

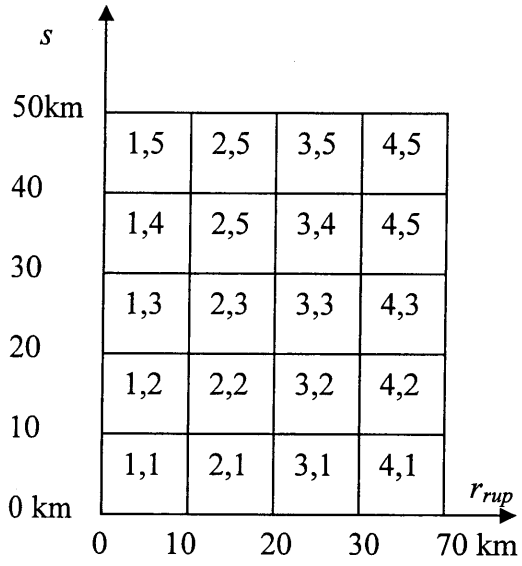

Figure 2.16. Notation and Position of Each Sector
Used to Describe Site Location Relative to the Fault

MacRae and Roeder (1999) compared the *inelastic severity* of oscillators by approximating the *R-T* relationship by a bilinear curve. Different approaches were used for long period and short period oscillators. The exact procedure for computing the demands (MacRae and Roeder 1999) and MacRae, Morrow and Roeder 2001) is described below.

(a) Long Period Oscillators

Long and short period structures are defined in order to obtain a simplified bilinear *R-T* curve. The longer period oscillators are defined as those with a period between 1s and 3s for the purpose of this study. The period of 1s was selected because this is usually on the flattish portion of the *R-T* plot. R_L is defined as the average lateral force reduction factor, *R*, over this longer period range for a specified target ductility, μ, as shown in **Figure 2.17**. Severe shaking corresponds to low R_L as shown in **Figure 2.18**.

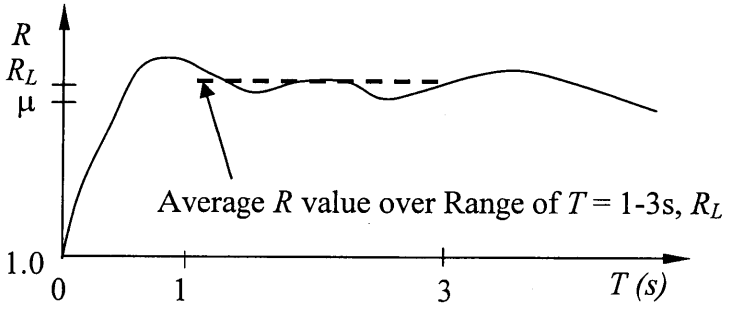

Figure 2.17. Elastic and Inelastic Peak Displacements

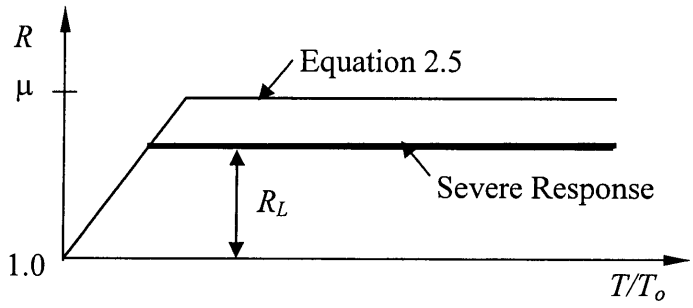

Figure 2.18. Idealized *R-T* relationship given target μ for "Normal" and Severe Records

(b) Short Period Oscillators

Severe shaking may cause a low slope, $\delta R/\delta T$, of the *R-T* curve in the short period range as shown in **Figure 2.19**. Since different soil categories may also affect this slope care must be taken to correctly attribute any change in slope to the correct source.

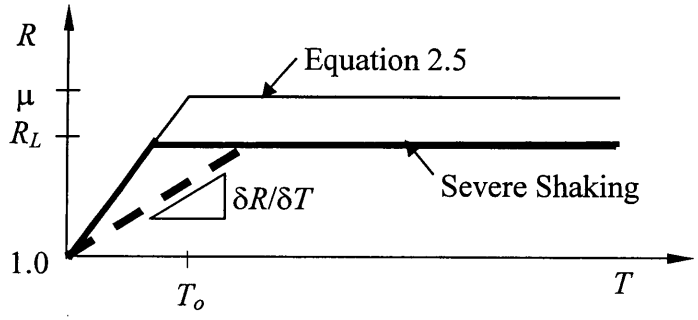

Figure 2.19. Idealized *R-T* Relationship for Structures Subject to Severe Loading

The steps taken to determine this slope are:

i) Firstly, R for long period structures (T = 1.0 – 3.0s), R_L is found using the methods described above.

ii) A line is fitted to the actual *R-T* relationship between $R = 1$ and $R = 0.75R_L$ as shown in **Figure 2.20** using the least squares method and is forced to pass through the point $T = 0$ and $R = 1$.

iii) A parameter, T_o, defining the slope of the curve, was defined as:

$$T_o = \frac{\mu - 1}{\left(dR_\mu / dT \right)} \tag{2.31}$$

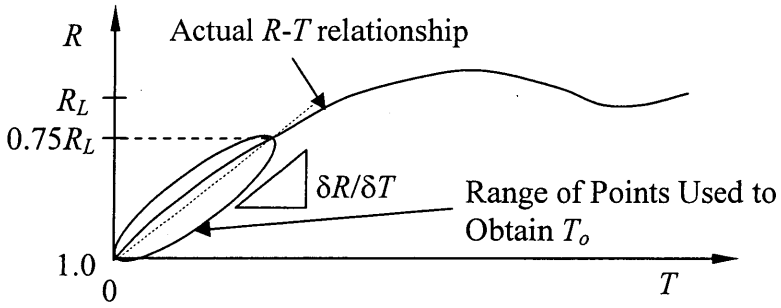

Figure 2.20. Idealized *R-T* relationship for Structures Subject to Severe Loading

(c) Long and Short Period Oscillators

Figure 2.21 shows how both the severity in the short and long period are obtained.

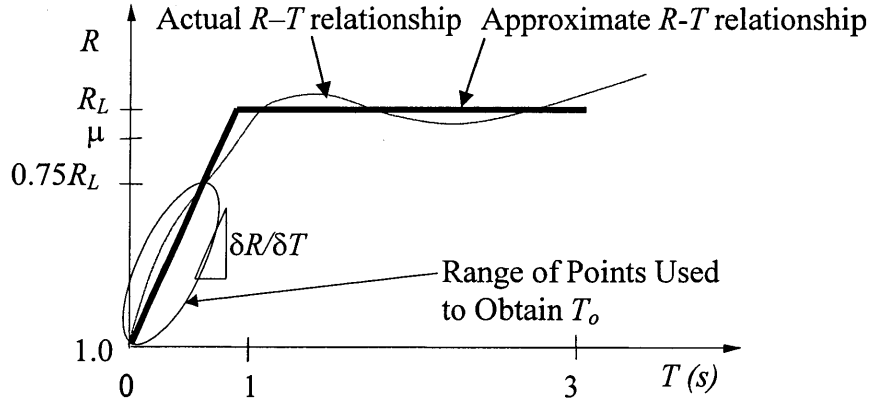

Figure 2.21. Idealized *R-T* relationship

The method shown above describes how the severity of response is obtained for a single ductility factor, μ. For other ductility factors, other parameters, or a more general description of the response may be required to adequately describe the severity. This more general method is described below.

(a) Long Period Oscillators

For long period oscillators the equation for the lateral force reduction factor is:

$$R = R_L \tag{2.32}$$

The parameter R_L is dependent on the ductility, μ. If the ductility is unity, then $R = \mu$. As μ increases, R increases at a lower rate. Equations for R_L may therefore take the following form:

$$R_L = \mu^{\gamma} \tag{2.33}$$

In these equations γ is obtained from the behavior of long period oscillators from **Equations 2.33** and **2.7** according to **Equation 2.34**. When $\gamma = 1$ then $R_L = \mu$ in the long period range.

$$\gamma = \frac{\ln(R_L)}{\ln(\mu)} = \frac{\ln(\mu d_e / d_u)}{\ln(\mu)} = \frac{\ln(\mu C_\mu)}{\ln(\mu)} \tag{2.34}$$

(b) Short Period Oscillators

For short period oscillators the initial slope was approximated by the expression and appropriate values for α and β were provided by:

$$T_o = \alpha\mu^\beta \tag{2.35}$$

The full equation to represent the behavior of both short and long period structures is therefore:

$$R_\mu = min \begin{cases} 1 + (\mu - 1)\left(\dfrac{T}{T_o}\right) & \text{(a)} \\ \mu^\gamma & \text{(b)} \end{cases} \tag{2.36}$$

It was found that there were no consistent strong trends in inelastic response for short period oscillators with location relative to the fault and it was recommended that T_o be given for all types of records by **Equation 2.37**.

$$T_o = 0.094\mu^{0.57} \tag{2.37}$$

For FF records, which were records from stations greater than 100km from the epicenter, the value of γ was 1.18, and for the NF strike normal (SN) records the value of γ could be found from the s vs. r_{rup} plot given in **Figure 2.22**. For ductility of 4, these γ values are equivalent to d_u/d_e of 0.80, 0.83, 1.15 and 1.43 in sectors (1,1), (1,2), (1,3) and (1,5) respectively. Larger d_u/d_e values (and smaller γ values) indicating greater demands may be seen in the region of positive directivity. Trends were not nearly as strong for the NF strike parallel SP records as shown in the plot of d_u/d_e in **Figure 2.23**.

It was expected that demands may be dependent on the site condition where the ground motions were obtained (especially for short period structures). However, site condition effect was not able to be investigated properly. This was because the vast majority of records were from FEMA302 (1997) soil type S_D. No trends were observed for the few records from other site conditions.

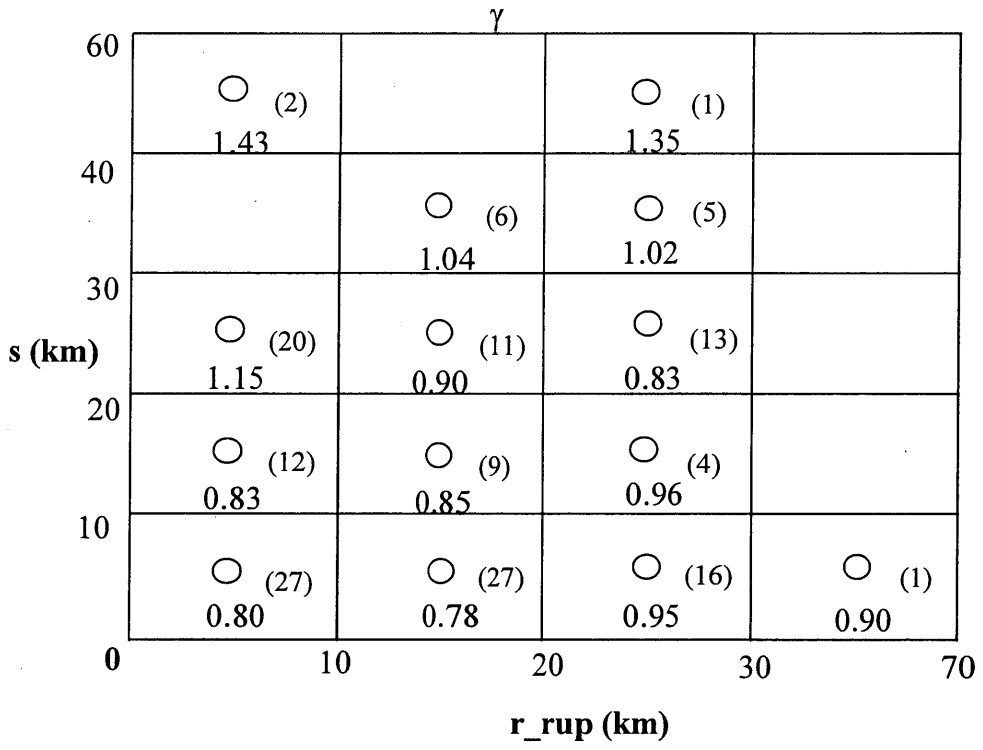

Figure 2.22. Average γ for T=1-3s and μ = 4, plotted on s vs. r_{rup} grid for Strike Normal Records, ζ = 2%

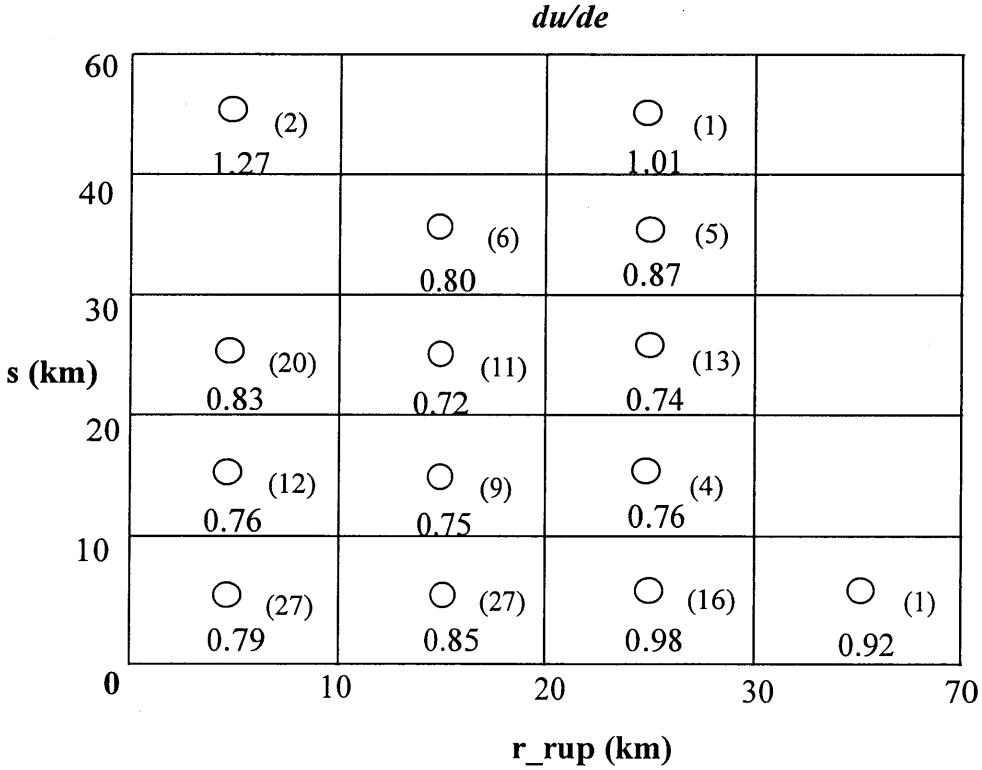

Figure 2.23. Average d_u/d_e for T=1-3s and μ = 4, plotted on s vs. r_{rup} grid for Strike Parallel Records, ζ = 2%

The information obtained from the analysis resulted in quantitative information for design of structures at different locations relative to the fault. A design procedure was proposed.

Limitations of the study carried out by MacRae et al. include:

- The period, T_o, was not computed in the way specified in the report where it was stated that the *R-T* line was forced to go through the point $R = 1$, $T = 0.0$s. This was corrected in the journal paper (MacRae, Morrow and Roeder 2001).
- The average *R-T* relationship for each s-r_{rup} region was obtained from the average *R-T* relationship for each individual record rather than from the average *R-T*-μ relationship in each region. This was corrected in the journal paper (MacRae, Morrow and Roeder 2001). These two changes only changed the parameters for the short period structures and the difference did not change the trends or conclusions.
- A similar method to that used by Reinhorn (1997), Fajfar (1999, 2000) and Chopra & Goel (1999) was used to obtain d_u/d_e. This may be slightly non-conservative as shown by Miranda (2001).
- The lack of earthquake records.

It should be noted that both the studies by Iwan et al. (1998) as well as those by MacRae et al. (2000), indicated that shorter period structures have greater ductility demands for a certain *R* than do longer period structures. Also, both researchers found that for pulse type shaking, shorter period structures have greater ductility demands for a certain *R* than do longer period structures. Iwan et al. (1998) could not compare the demands of actual NF records with those of actual FF records because his study considers only seven NF records and no FF records. MacRae et al. (1999) used 156 NF-SN records and 34 FF records to see if there was a difference in the inelastic response of actual records. While there were some differences, there was no consistent difference or trend from the data they obtained.

2.4. MODELLING OF PG&E MILL TYPE STRUCTURES

A study previously conducted by Roeder and MacRae (1999) described the behavior of a typical PG&E mill-type structure, the Berkeley F substation in Berkeley, CA. A plan of this structure is shown in **Figure 2.24**. The structure is old and was built in 2 different stages in 1909 and 1923. The structure consists of built-up steel framing members with infill concrete walls. In this structure, drawings indicated good connectivity between the walls and the frame. No design was carried out specifically for earthquake.

The structure was assessed according to FEMA273 LDP using a response spectra provided by PG&E shown in **Figure 2.25**. A full 3-D elastic model of the structure was analyzed using SAP-2000. It was found in the study that there were many closely spaced modes. Typical mode shapes consisted of breathing of walls and flexural roof deformation. Peak roof displacements were small, but those at the mid-height of the walls were bigger due to the 2%/50 year spectra as shown in **Figure 2.26**. Typical modal periods and the mass participation in the x and y directions, m_x and m_y, is given in **Table 2.1** .

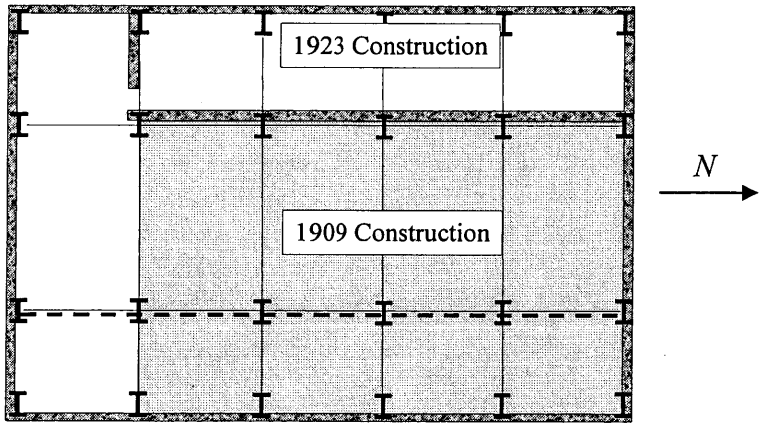

Figure 2.24. Plan of Berkeley F Substation

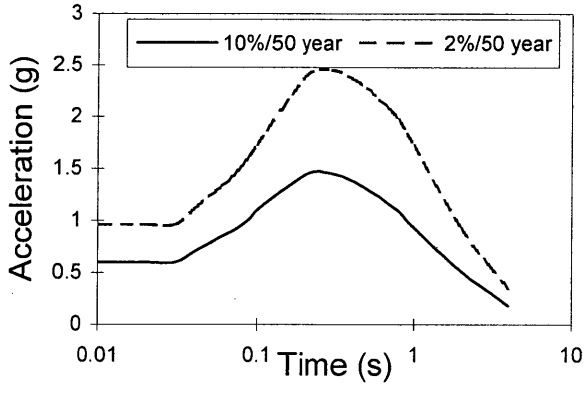

Figure 2.25. Design Response Spectra

Table 2.1. Berkeley Substation Modal Frequencies and Mass Participation In Each Direction

Mode	Period (s)	m_x (%)	m_y (%)
1	0.16	0	13.5
5	0.11	15.7	0
6	0.10	5.4	0.2
7	0.09	0	17.3
19	0.05	0.1	5.8
20	0.05	0.6	30.0
23	0.05	32.3	0.5
26	0.04	5.7	0.3
37	0.03	10.4	0.1
38	0.03	1.2	5.0
58	0.02	0.1	5.0
65	0.02	5.1	0

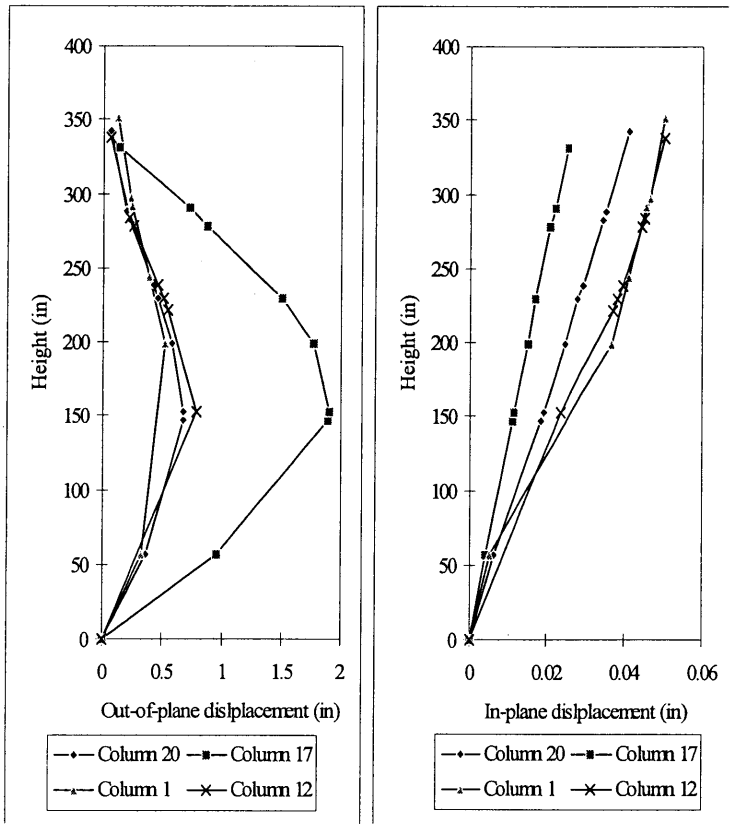

Figure 2.26.Displacements from 2in50 Design Spectra up Height of Building (a) Along the center of a wall, and (b) At a corner of the building

Considering the possible failure modes of shear failure of walls/roof, separation of wall from roof, wall sliding on foundation, wall out-of-plane flexure, separation of wall from mezzanine and problems with the roof truss, and the inherent ductility of each component using *m*-factors, the behavior of the structure was assessed. Analyses considering the possibility of roof-wall as well as wall-foundation connectivity failure were considered. It was found that the structure should remain life safe if the capacity of the roof truss is sufficient.

Simplified methods for modeling the structure to assess it's behavior were also suggested. Each of these models allows non-linear dynamic time-history analysis to be conducted relatively simply, but they lose information on the actual behavior of the structure. These are briefly described in the figures below.

MODEL A

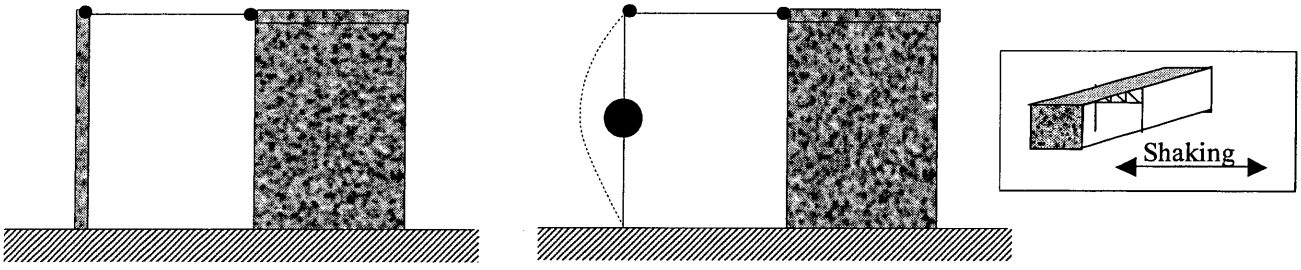

(a) Simple Model (b) 2-DOF Model

Figure 2.27. Model A Representation of Mill Structure

Here, the following effects are lost; torsional effects, wall corner effects, effects of the internal frame and effects of roof flexibility.

MODEL B

Here, the following effects are lost; torsional effects, wall corner effects and effects of roof flexibility.

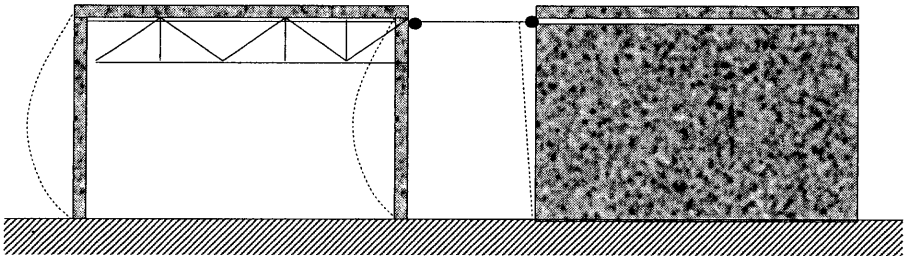

Figure 2.28. Model B Representation of Mill Structure

MODEL C

Here, torsional effects and wall corner effects are lost.

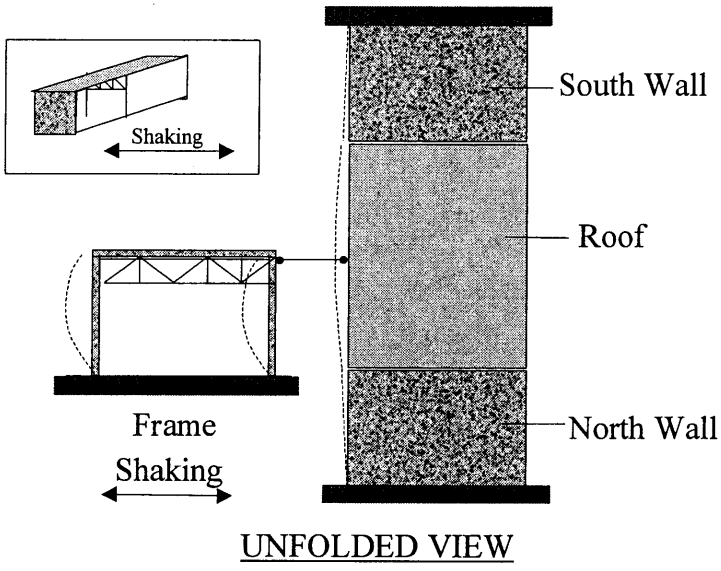

Figure 2.29. Model C Representation of Mill Structure

CHAPTER 3. MODEL, RECORDS AND ANALYSIS TECHNIQUES

3.1. MODEL SELECTED

Single-degree-of-freedom elastic-perfectly plastic (EPP) oscillators were used in this study. The EPP oscillator force-displacement behavior is shown in **Figure 3.1**. These oscillators tend to give slightly greater displacements than oscillators with positive post-elastic stiffness characteristics so results may be slightly conservative for design. A structural elastic damping ratio of 2% was used in all analyses.

For a few selected analyses a bilinear oscillator with a post-elastic stiffness ratio, r, of 0.1 was also used as given in **Figure 3.1b**.

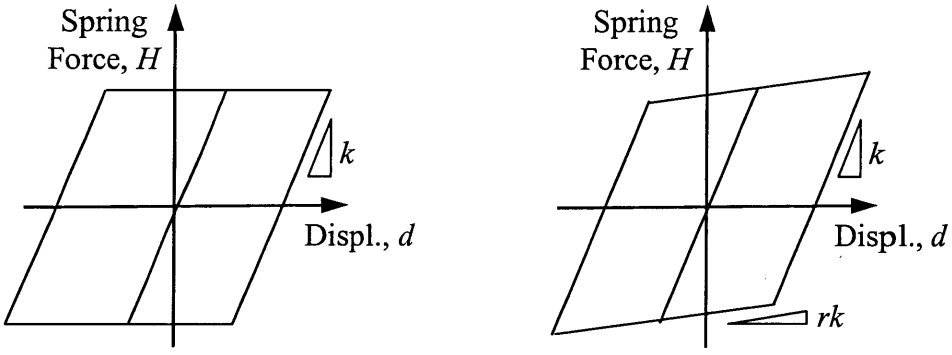

(a) EPP Loop (b) Bilinear Loop

Figure 3.1. EPP Oscillator Force-Displacement Behavior

3.2. GROUND MOTIONS SELECTED

3.2.1. Ground Motion Sources:

a) National Geophysical Data Center Strong Motion Catalog (NGDC SMCAT)

The NGDC Strong Motion Catalog is a collection of over 15,000 digitized and processed accelerograph records dating from 1933 to 1994. The collection is supplied in a three compact disk (CD) set. Three types of records are included on the CDs: Uncorrected, corrected (filtered) and response spectra. Data sources include the United States Geologic Survey (USGS), California Department of Mines and Geology (CDMG), University of Southern California (USC) and other agencies.

b) Woodward-Clyde Directivity Records

Records were provided by Nancy Smith, of Woodward-Clyde Federal Services which included information relating to the position of the fault relative to the site. These 65 sets of records, from 21 different earthquakes, were used as part of a study reported by Woodward Clyde (Somerville, Smith, Graves and Abrahamson, 1997). The 3 components in each set consisted of 2 horizontal components, rotated to fault strike-normal (SN) and fault strike-parallel (SP) components, and 1 vertical component. Earthquakes used for the study included all California crustal earthquakes with magnitudes of 6 or larger for which digital strong motion data and faulting mechanism were available. Sources of the strong motion records included the United States Geological Society (USGS), California Strong Motion Instrumentation Program (CSMIP), California Division of Mines and Geology (CDMG) and other agencies.

The 65 records in the paper were supplemented by 91 other measurements (Smith, 1998) to obtain 156 records. The extra records had a magnitude of earthquake shaking ranging from $M_W = 6.0$ to $M_W = 7.7$ and distances from the fault of 10km-68km. These records came from Asia Minor, Japan Meteorological Agency (JMA), Japan Railway Company (JR) recordings of the 1994 Kobe earthquake and others.

The positions of each site relative to the fault are provided for all records in terms of the parameters given below. The information given for each fault is shown below. The length of rupture, L, was available for all but one of these records. They used the following parameters to describe the position of the site relative to the fault.

- r_{rup}: Rupture distance, which is the closest distance between the fault rupture surface and the site. It is measured as the minimum of (a) the distance measured perpendicular to the fault surface, and (b) the distance from the ground rupture to the site as shown in **Figure 3.2**.
- X: Length ratio, which is equal to s/L
- s The distance from the epicenter to the site in the direction of the fault as given in **Figure 3.3**.
- L The total rupture length. This length was used rather than L', the distance from the epicenter to the site in the direction of the fault.

θ: Horizontal angle between fault plane and site measured from the epicenter
Y: Width ratio (the fraction of fault up dip that fractures toward the site)
ϕ: Vertical angle between fault plane and site measured from the hypocenter

Somerville et al. (1997) argued that the fraction of distance along the fault, *X*, as well as the angle θ, were the most significant parameters affecting near-fault shaking. It should be noted that $s\tan\theta$ does not equal r_{rup} since r_{rup} is measured perpendicular to the fault and $s.\tan\theta$ is a plan dimension. For thrust faults, in which the whole fault moves at once, parameters based on **Figure 3.3** may not be the most adequate ones to describe any NF effects and other parameters may need to be chosen.

Also, corrections to the paper of Somerville et al include the fact that for the Lucerne record, $X = 0.6$, and for the Erzincan record $X = 0.33$ (Abrahamson, 1998).

Soil site characteristics were defined by Smith (1998) as shown in **Table 3.1**. The 1997 UBC (ICBO, 1997) designations and the number of directivity records of each type from the 155 records used are also given. It may be seen that the majority of records were from alluvial sites.

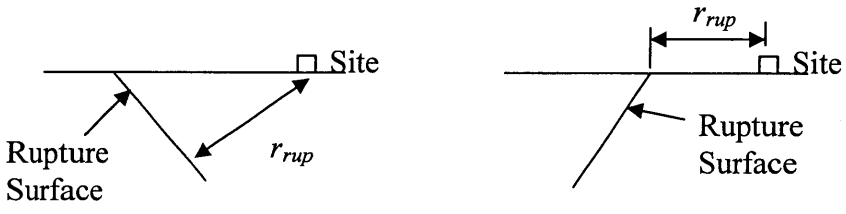

Figure 3.2. Definition of r_{rup} for Different Fault Configurations

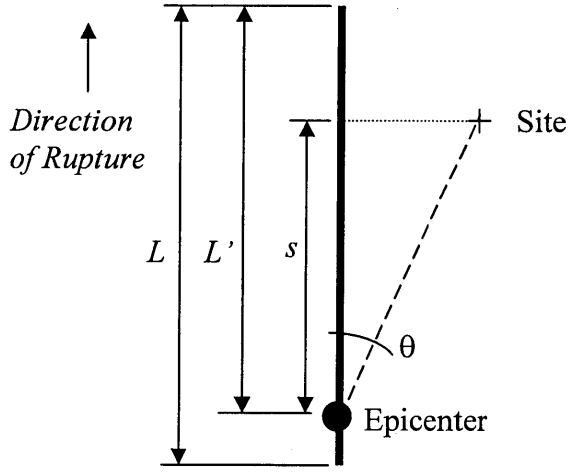

Figure 3.3. Plan of Fault

Table 3.1. Soil Types for WC Directivity Records

Soil Site Designation (Smith, 1998)	Description bases on Shear Wave Velocity, V_s	Approximate Shear Wave Velocity, V_s	Soil Site Designation 1997 UBC (ICBO, 1997)	Number of Directivity Records of Each Type
S1	hard rock	$V_s > 760$m/s	S_B	16
S2	soft rock	760m/s > V_s > 360m/s	S_C	12
S3	alluvium	360m/s > V_s > 180m/s	S_D	122
S4	fill and unconsolidated deposits	180m/s > V_s	S_E	5

c) New Records

Record sets (a) and (b) were used in the previous study by Morrow (1998). New records were provided by Norm Abrahamson of PG&E which are included in this report. Records from 418 stations were obtained from the *1999 ChiChi earthquake* (Taiwan). Of these, 191 sets of records were located within 70km of the rupture surface. The fault ran in the NS direction and the SN component of shaking was therefore considered to be in the EW direction. For the Taiwan stations, these values were provided by Norm Abrahamson of PG&E. Records from 9 stations were obtained from the *1999 Kocaeli earthquake* (Turkey), and records from 4 stations were obtained from the *1999 Duzce earthquake* (Turkey). For the Turkey stations, s and r_{rup}, were provided by Prof. Ellen Raithe of the University of Texas. For the Turkey earthquakes, it was assumed, based on discussion with PG&E, that the fault ran in the EW direction so the SN component of shaking was in the NS direction. All records were obtained on stiff soil sites.

3.2.2. Ground Motion Sets:

(a) Far-Fault Record Set

Source: NGDC SMCAT database

Selection Criteria:

Records representing far field motions were selected based on the following criteria:

1) The epicentral distance must be equal to or greater than 100 km,
2) The earthquake magnitude equal to or greater than 6.
3) Horizontal components only were used

Number of Records: 32 records from 13 earthquakes

Notes: Even though the records have a large epicentral distance, this does not imply a far-fault record as the fault may go directly from the epicenter to the site. However the chance of it being a near-fault record decreases with distance so these records are considered to be far-fault. Subsequent recommendations by Abrahamson (1998) indicate that epicentral distances greater than 60km may be appropriate for far-fault shaking.

(b) Near Fault Directivity Record Set

Source 1: Woodward-Clyde Directivity Records

Selection Criteria:

Sets of records with SN and SP and vertical components were used. These records were from sites at various geographic locations relative to the fault and epicenter.

Number of Record Sets: 155

Source 2: New Records (PG&E, 2000)

Number of Record Sets:
191 - *ChiChi earthquake 1999* (Taiwan)
9 - *Kocaeli earthquake 1999* (Turkey)
4 - *Duzce earthquake 1999* (Turkey)

The name of each earthquake, earthquake magnitude, station name, soil type, s and r_{rup} values and PGA are given for each of the records analyzed in **Appendix**.

Total Number of Record Sets: 359

3.3. SOFTWARE AND ANALYSIS TECHNIQUES

The software used was modified from program written by Dunn (1995) to make inelastic response spectra for bilinear structures. The Newmark linear acceleration method ($\beta = 1/6$) was used for the analyses with a time step of 0.005s. Oscillators with 60 periods ranging from 0.05s to 3.0s with an interval of 0.005s were used. An initial elastic damping ratio of 2% was used for all analyses. Other programs for processing the data and report preparation such as MATLAB (1998) and Microsoft Office (1998) were used.

Two types of analysis were performed. One was carried out to determine quantities required for the CM and another was carried out for the CSM and DCSM.

3.3.1 CM: Computation to Determine C_μ for a Target Ductility

The value of C_μ for the CM was found from inelastic response spectra for oscillators with various periods, T, and target ductilities, μ. For the initial elastic damping ratio, ζ_o, and each T and μ, iteration is required on the yield displacement, d_y, until the required ductility is obtained as shown in **Figure 3.4** for a target ductility of 3. When iteration is complete, then the peak displacement, d_u, yield displacement, d_y, yield force, H_y, and force at peak displacement, H_u, are known. Then C_μ was obtained as d_u/d_e and the lateral force reduction factor could be computed as H_e/H_y.

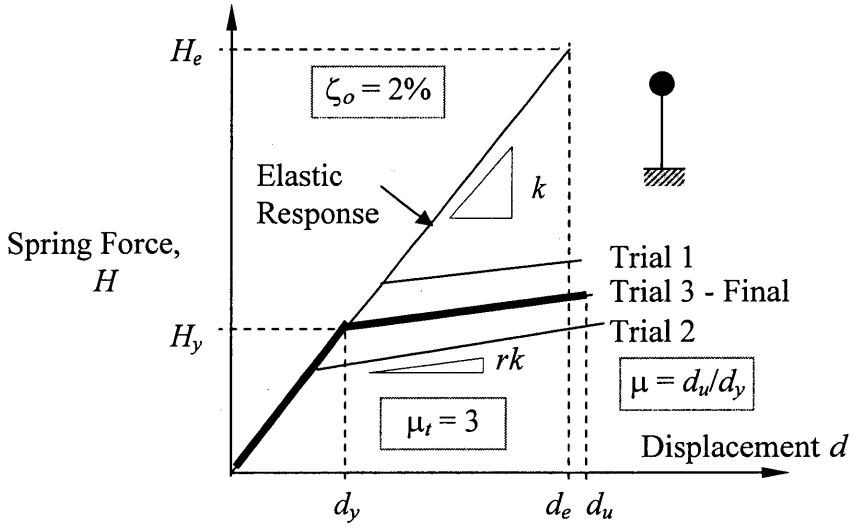

Figure 3.4. Schematic of Iteration Trials Required to Obtain d_y, H_y, and H_u for an Oscillator with T, μ and ζ_o

It should be noted that using this kind of approach, the absolute magnitude of the earthquake acceleration is not required. If the magnitude of design acceleration is doubled, then the inelastic quantities, R, and μ, and C_μ will still be the same although absolute force and displacement quantities will change. Also, it does not matter what combination of stiffness, k, and mass, m, are used for a certain period, so a unit mass was used.

The median (logarithmic mean) values of C_μ and R were taken. The error described by Miranda (2001) when taking the average values is not a problem when the median is used. This is because Median[C_μ] = Median[μ/R] = μ.Median[$1/R$] = $\mu.\sqrt[i]{\Pi[1/R_i]}$ = $\mu.1/(\sqrt[i]{\Pi[R_i]})$. Here $\Pi[R_i] = R_1R_2 \ldots R_n$ for each of the n records used for each analysis at each period. There was a difference as high as 25% between the median and mean for analyses with $\mu = 4$.

3.3.2 CSM: Computation to Find ζ_{eff} and *SR* for a Target Ductility

The method of computing effective damping ζ_{eff} and the elastic displacement reduction factor, *SR*, is also iterative. It is performed using the following steps:

Step 1. For the initial elastic damping ratio, ζ_o, and each T and μ_t, iteration is required on the yield displacement, d_y, until the μ_t is obtained following the procedure outlined in **Section 3.3.1**. The peak displacement, d_u, and force at peak displacement, H_u, are results of this analysis.

Step 2. The total damping, ζ_{eff}, is obtained as for the "equivalent elastic structure" with a period T_{eff}. This period for the "equivalent elastic structure" was found by **Equation 3.1**. It was defined based on the secant stiffness, k_{eff}, to the force at peak displacement, H_u, at the peak displacement, d_u, as illustrated in the schematic of **Figure 3.5**.

The ultimate force, H_u, peak displacement, d_u, effective stiffness, k_{eff}, and effective period, T_{eff}, of the yielding oscillator are:

$$H_u = (1 + r(\mu - 1))H_y$$

$$d_u = \mu d_y$$

$$\begin{aligned} k_{eff} &= H_u/d_u \\ &= (1 + r(\mu - 1))H_y/(\mu d_y) \\ &= (1 + r(\mu - 1))/\mu \,.H_y/d_y \\ &= (1 + r(\mu - 1))/\mu \,.k_o \end{aligned}$$

$$T_{eff} = T_o\sqrt{\frac{k_o}{k_{eff}}} = T_o\sqrt{\frac{\mu}{(1+r(\mu-1))}} = T_o\sqrt{\frac{\mu}{(1+r\mu-r)}} \qquad (3.1)$$

When $r = 0.0$ then $T_{eff} = T_o\sqrt{\mu}$.

Iterative elastic analyses were carried out on this equivalent elastic structure. The effective damping ratio, ζ_{eff}, was changed until the peak displacement was equal to the peak displacement, d_u, from Step 1. The hysteretic damping, ζ_{hyst}, is computed as the total damping, ζ_{tot} (= ζ_{eff}), minus the initial viscous damping, ζ_o, as given in **Equation 3.2**.

$$\zeta_{hyst} = \zeta_{eff} - \zeta_o \tag{3.2}$$

The *SR* value was computed as the elastic displacement of the equivalent structure, $d_{e,eff}$, for the level of damping, ζ_{eff}, divided by the peak displacement, d_u, for the level of damping, ζ_o.

$$SR = d_u / d_{e,eff} \tag{3.3}$$

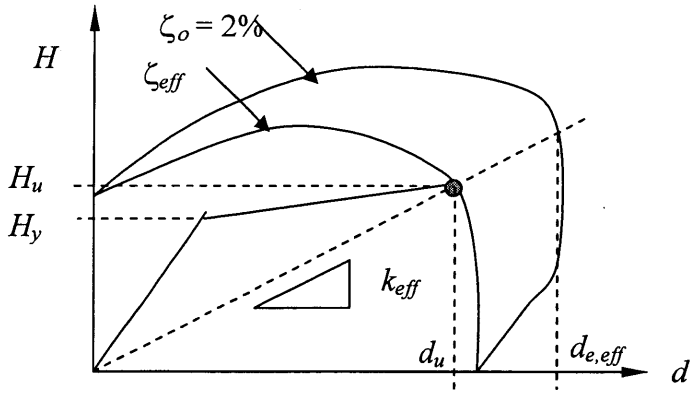

Figure 3.5. Schematic of Iteration Trials Required
to Obtain d_y, H_y, and H_u for an Oscillator with T, μ and ζ_o

3.3.3 DCSM: Computation to Find *SR* for a Target Ductility

The DCSM computations are identical to the CSM computations. However, the damping effect is of no interest and only the *SR*-μ relationship is studied.

CHAPTER 4. EVALUATION OF NEAR FAULT RECORD INELASTIC DEMANDS

4.1. COEFFICIENT METHOD

The *R-T* plot for $\mu = 4$ and a stiffness ratio, *r*, of 0.0 and initial damping ratio, ζ_o, of 2% is given in **Figure 4.1** for the FF records. This is similar to that given by MacRae et al. (1999), except that the median (logarithmic mean), rather than the average of the lines from the different curves was taken. The -1 Sigma and +1 Sigma plots are also given. For $\mu = 4$, $R = 4$ according to the Equal Displacement Method (EDM) and $R = \sqrt{(2\mu-1)} = 2.64$ according to the Equal Energy Method (EEM). Since the median *R* is greater than the EDM value for the longer period far-fault oscillators, the EDM will overestimate the displacement demand and the median value is conservative. The EEM is a better approximation to the –1 Sigma value. Neither method is conservative for structures with very short periods.

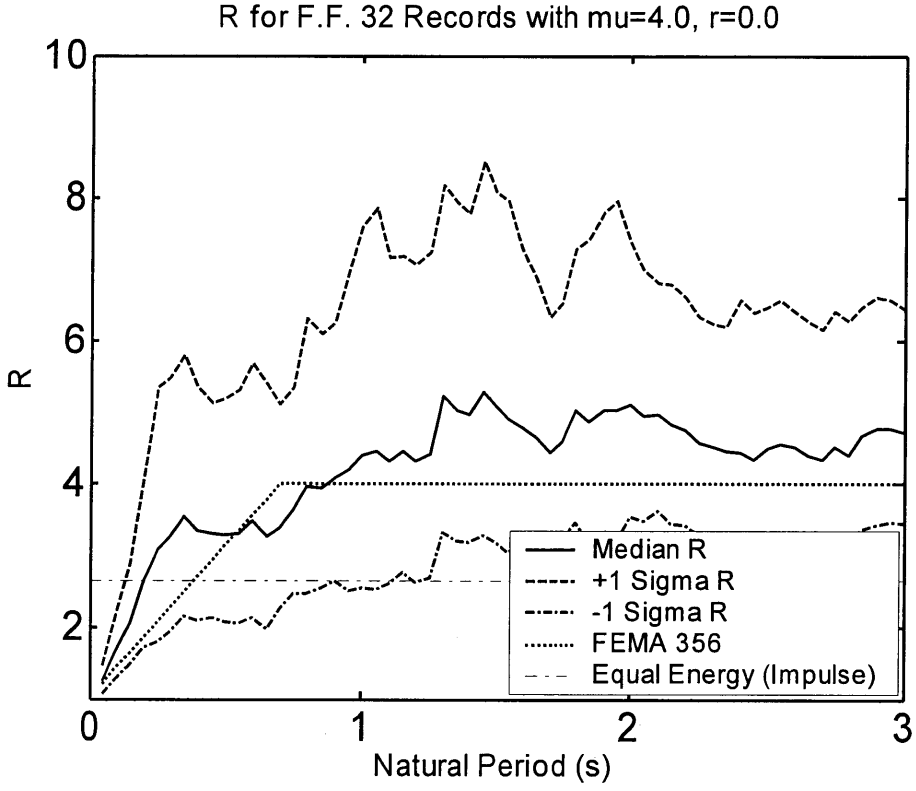

Figure 4.1. *R* vs. *T* Plot for FF Records ($\mu = 4$, $r = 0.0$, $\zeta_o = 2\%$)

A bilinear approximation is made to the FF record median R-T curve following the method used by MacRae and Roeder (1999) in **Figure 4.2** and the C_μ-T curve is given in **Figure 4.3**. **Equation 4.1a** gives the bilinear approximation. The value of γ for the FF records was computed as 1.12 and **Equation 4.1b** gives T_o for estimation of the demand of structures in the short period range.

$$R_\mu = min \begin{cases} 1 + (\mu - 1)\left(\frac{T}{T_o}\right) \\ \mu^\gamma \end{cases} \tag{4.1a}$$

$$T_o = 0.123\mu^{0.77} \tag{4.1b}$$

Since the bilinear approximation is non-conservative near the intersection of the lines in the bilinear approximation, a parabolic curve is used to give a less conservative approximation. The parabola is defined as having a slope which is the same as the ascending line of $(\mu\text{-}1)/T_o$ at the T = 0s and R = 1. The line passes through this point T = 0s and R = 1, and the slope of the parabola is zero when it reaches the flat line.

Since the intersection of the lines in the bilinear approximation occurs when

$$1 + (\mu - 1)\left(\frac{T}{T_o}\right) = \mu^\gamma \tag{4.2}$$

then the period where intersection occurs, T_{int}, is

$$T_{\text{int}} = \frac{(\mu^\gamma - 1)}{(\mu - 1)} T_o \tag{4.3}$$

The parabola merges with the flat line, $R = \mu^\gamma$, at the period:

$$T_{merge} = 2T_{\text{int}} = \frac{(\mu^\gamma - 1)}{(\mu - 1)} 2T_o \tag{4.4}$$

And the equation of the curve containing the parabola is:

$$R = \begin{cases} \dfrac{-\left(\dfrac{(\mu - 1)}{T_o}\right)^2}{4(\mu^\gamma - 1)} T^2 + \dfrac{(\mu - 1)}{T_o} T + 1, & T < \dfrac{(\mu^\gamma - 1)}{(\mu - 1)} 2T_o \\ \mu^\gamma, & T \geq \dfrac{(\mu^\gamma - 1)}{(\mu - 1)} 2T \end{cases} \tag{4.5}$$

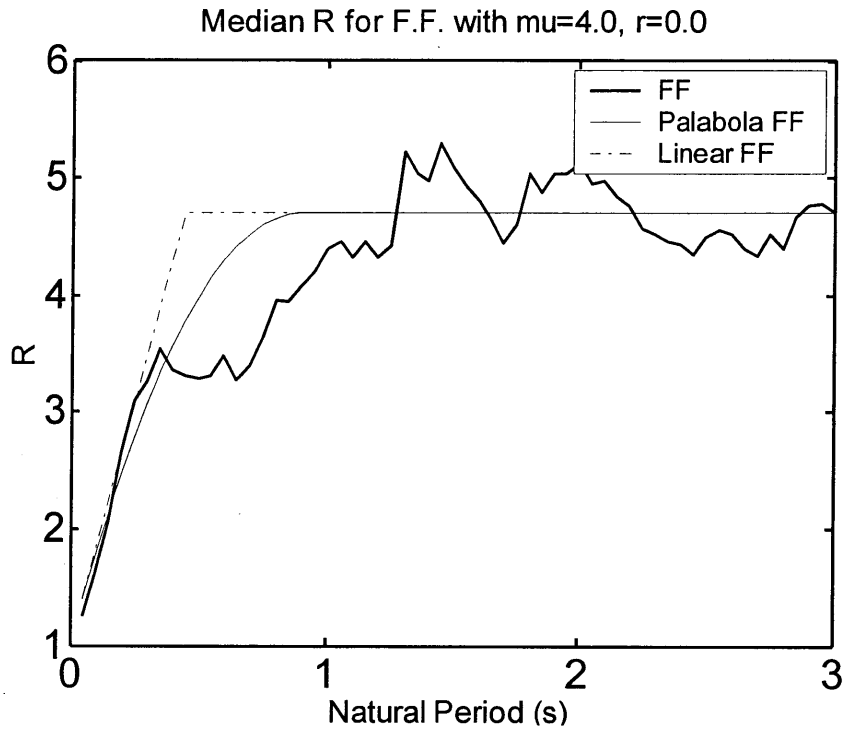

Figure 4.2. Median R vs. T Plot for FF Records ($\mu = 4$, $r = 0.0$, $\zeta_o = 2\%$) with Bilinear and Parabolic Approximations

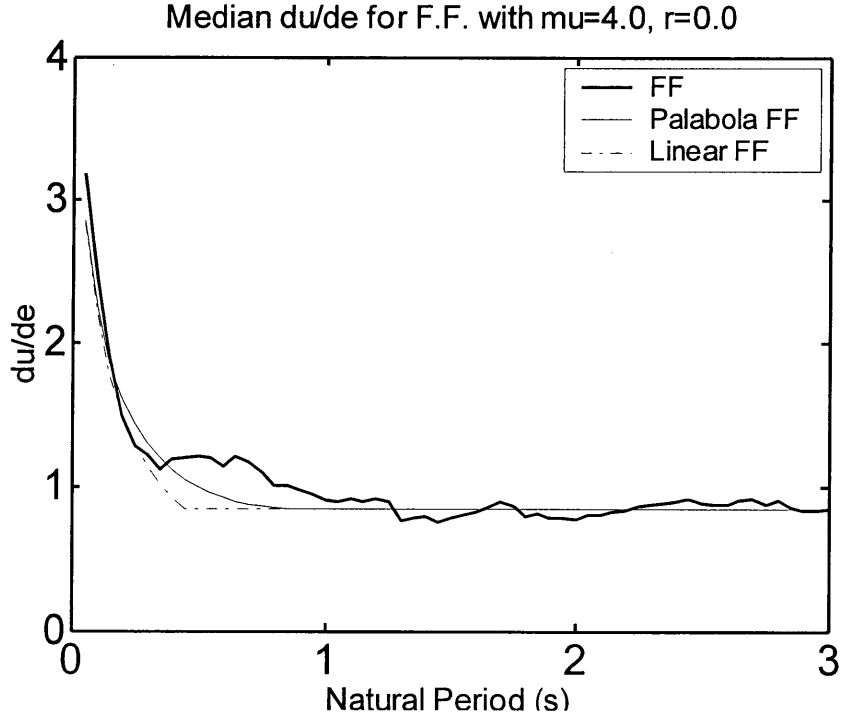

Figure 4.3. Median C_μ ($= d_u/d_e$) vs. T Plot for FF Records ($\mu = 4$, $r = 0.0$, $\zeta_o = 2\%$) based on Bilinear and Parabolic Approximations to the R-T Curve

Since $C_\mu = d_u/d_e = \mu/R$, for the bilinear approximation:

$$C_\mu = \begin{cases} 1 + (\mu - 1)\left(\dfrac{T}{T_o}\right), & T < \dfrac{(\mu^\gamma - 1)}{(\mu - 1)} T_o \\ \mu^{1-\gamma}, & T \geq \dfrac{(\mu^\gamma - 1)}{(\mu - 1)} T_o \end{cases} \tag{4.6}$$

or

$$C_\mu = \max \begin{cases} 1 + (\mu - 1)\left(\dfrac{T}{T_o}\right) \\ \mu^{1-\gamma} \end{cases} \tag{4.7}$$

and for the parabolic approximation

$$C_\mu = \begin{cases} \dfrac{\mu}{\left(-\dfrac{\left(\dfrac{(\mu - 1)}{T_o}\right)^2}{4(\mu^\gamma - 1)} T^2 + \dfrac{(\mu - 1)}{T_o} T + 1 \right)}, & T < \dfrac{(\mu^\gamma - 1)}{(\mu - 1)} 2T_o \\ \mu^{1-\gamma}, & T \geq \dfrac{(\mu^\gamma - 1)}{(\mu - 1)} 2T_o \end{cases} \tag{4.8}$$

In order to show how good the approximation for long period oscillators is in **Equations 4.6** or **4.8**, a C_μ-μ plot for (s,r_{rup}) Sector (1,3) is given in **Figure 4.4**. The actual line was obtained from the average C_μ for oscillators with periods between 1.0 and 3.0s which are subject to records in Sector (1,3) and which have a target ductility of 4. The approximation to C_μ was obtained from **Equation 4.8b** where the value of γ used was 0.90 which was found from **Equation 4.9** using the average C_μ for oscillators in this sector with $\mu = 4$ which was $C_\mu = 1.15$ as shown in **Figure 4.5.** It may be seen that the equation does not match totally at a ductility other than 4, but it follows the trends in actual response.

$$\gamma = 1 - \frac{\log(C_\mu)}{\log(\mu)} \tag{4.9}$$

For the longer period oscillators, a plot of C_μ for a ductility, μ, of 4, is given in **Figure 4.5** and γ for each sector is given in **Figure 4.6**. It may be seen that the demand tends to increase as the distance along the fault increases from the epicenter in the first few sectors. However, this is not true for sector (1,5) where there are 3 records.

For the short period oscillators, T_o is found from **Equation 2.35** for the median R-T relationship in each of the sectors and it is shown in **Figures 4.7** for $\mu = 4$. Larger T_o implies more severe inelastic demand. A trend of increasing T_o in the direction of positive directivity is not observed. Best fit values for κ and β for each sector are given in **Figures 4.8 and 4.9**. It may also be seen

that there are no trends in κ or β with directivity. Using the median value of κ for all NF records of 0.123, the median value of β was obtained as shown in **Figure 4.10**. Smaller β implies smaller T_o, and hence smaller response. Again no trends are given for β indicating that the short period oscillators are not affected significantly by near-fault effects. The average β was 0.64 for all segments. If variation based on sector is ignored then the average ratio of T_o for all NF records is:

$$T_o = 0.123\mu^{0.64} \tag{4.10}$$

A *R-T* plot showing the best fit showing the parabolic approximation to the NF records is given in **Figure 4.11**. The median $C_\mu = d_u/d_e$, computed based on $\mu = 4$ is given in **Figure 4.12** and the approximations for the NF records are shown in **Figure 4.13** for the records in the sectors 11, 12 and 13 as shown in **Figure 2.16**. It may be seen that the curve fits seem reasonably well but it may be slightly conservative for the shorter period structures as a result of the curve fit method.

Since many of the PG&E structures are short period, *R-T* and C_μ-*T* plots for $\mu = 4$ and $r = 0.0$ for periods up to 0.5s are shown in **Figures 4.14** and **4.15**. It may be seen that there are no strong trends with earthquake record along the length of the fault.

A full study was not carried using all strike parallel records. However, the Taiwan strike parallel (SP) records, the difference between the elastic and inelastic response is not very different in sector (1,3) as shown in **Figure 4.16**. This finding is different from that by MacRae, Morrow and Roeder as shown in **Chapter 2**.

Figure 4.17 shows the ratio of $C_{\mu,NF}$ to $C_{\mu,FF}$ for a ductility of 4. This is equivalent to the ratio of peak displacements of NF and FF oscillators for the same target ductility. It may be seen for structures with a fundamental period, *T*, less than about 0.8s that NF shaking does not tend increase the demands. A significant increase in demand, up to 1.6 times, occurs for longer period structures in the sectors in the region of positive directivity. These trends are consistent with what was seen before. The same ratio is plotted for sector (1,3) in **Figure 4.18**. It may be seen that the demand generally increases with ductility when T > 1s and generally decreases for shorter period oscillators.

The scatter in response to SN records for a typical sector is given in **Figure 4.19**. This scatter is measured as the standard deviation of the natural logarithm of the responses, *SIGMA*(ln*x*), with respect to the approximation to C_μ, $\hat{x}$, according to **Equation 4.11**. Here x_i is the value of C_μ for each of the records analyzed.

$$SIGMA(\ln x) = \sqrt{\frac{1}{n-1}\sum_{i=1}^{n}\left(\ln x_i - \ln \hat{x}\right)^2} \tag{4.11}$$

The value equivalent to the average plus one standard deviation, which is the 68% confidence limit or the 84th percentile is referred to as "+1 Sigma", and it is computed as:

$$+1 \text{ Sigma} \quad = e^{\left(\ln \hat{x} + SIGMA(\ln x)\right)} = \hat{x}e^{\left(SIGMA(\ln x)\right)} \tag{4.12}$$

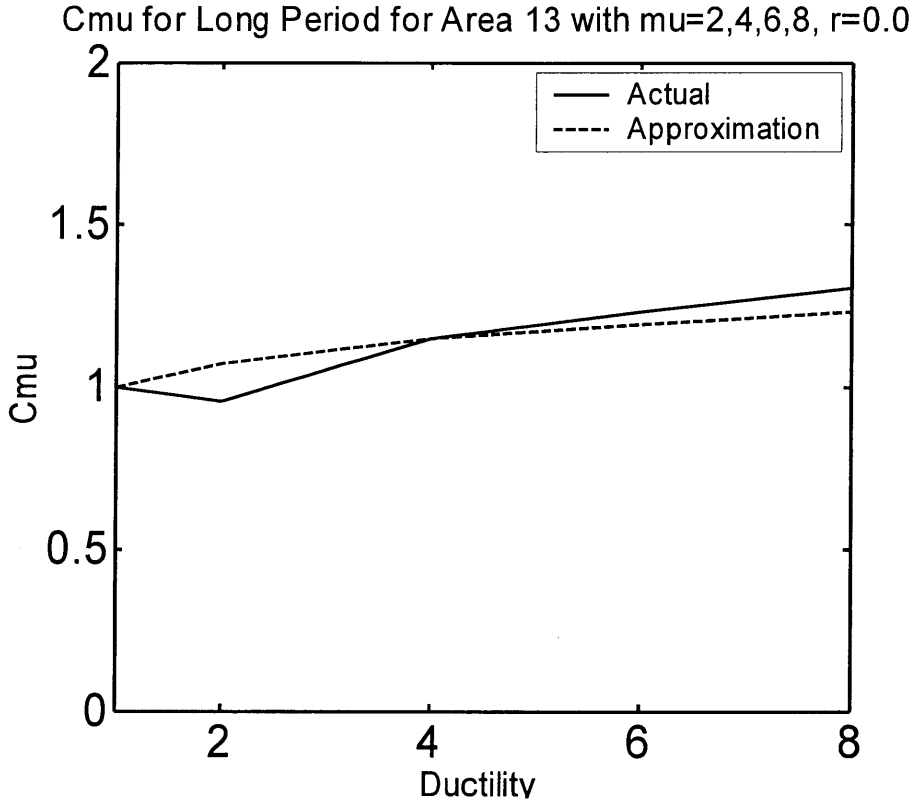

Figure 4.4. C_μ-μ plot for Long Period Oscillators for Records in Sector (1,3) ($\mu = 4$, $r = 0.0$, $\zeta_o = 2\%$) and Approximation (SN records)

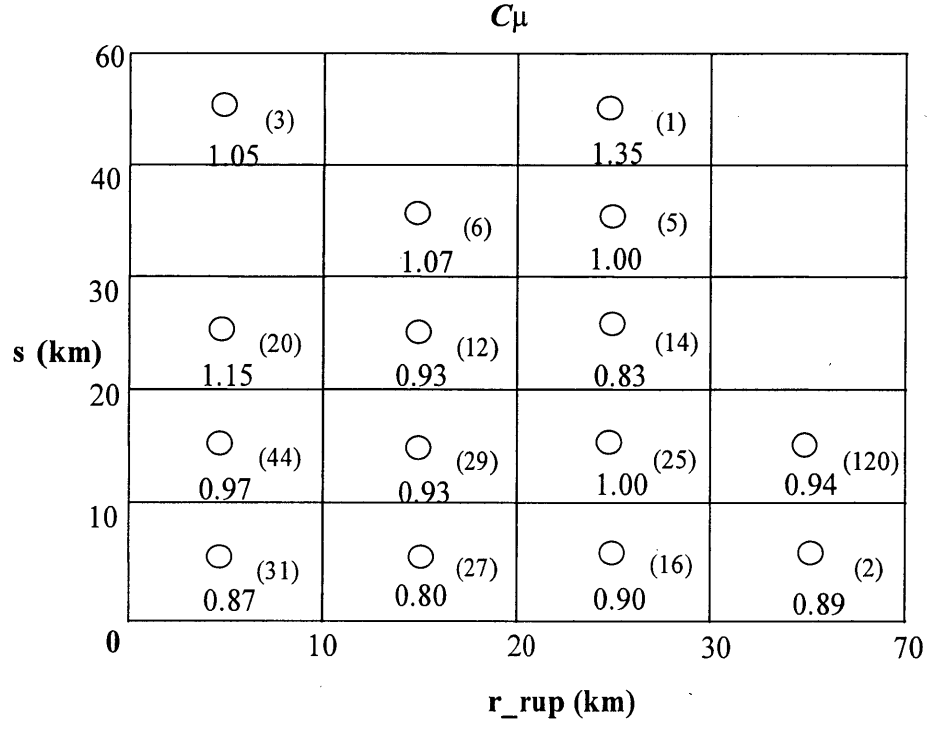

Figure 4.5. C_μ plot for Long Period Oscillators in Each Sector (SN records) ($r = 0.0$, $\zeta_o = 2\%$, $\mu = 4$)

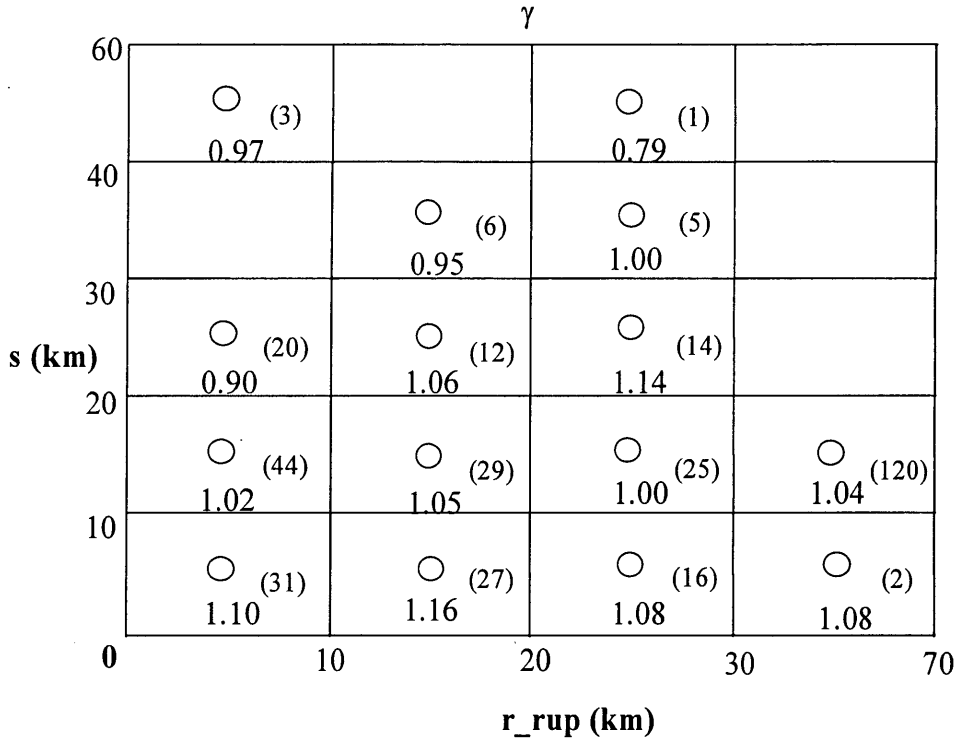

Figure 4.6. γ plot for Long Period Oscillators in Each Sector (SN records)
($r = 0.0$, $\zeta_o = 2\%$)

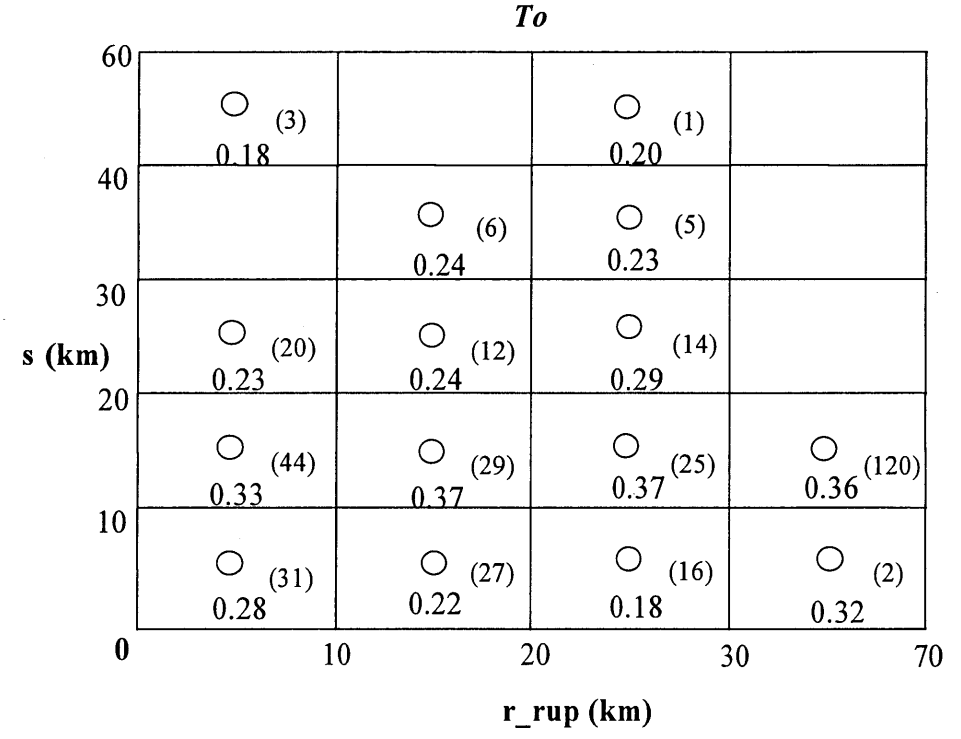

Figure 4.7. Best fit T_o plot for Short Period Oscillators in Each Sector (SN records)
($r = 0.0$, $\zeta_o = 2\%$, $\mu = 4$)

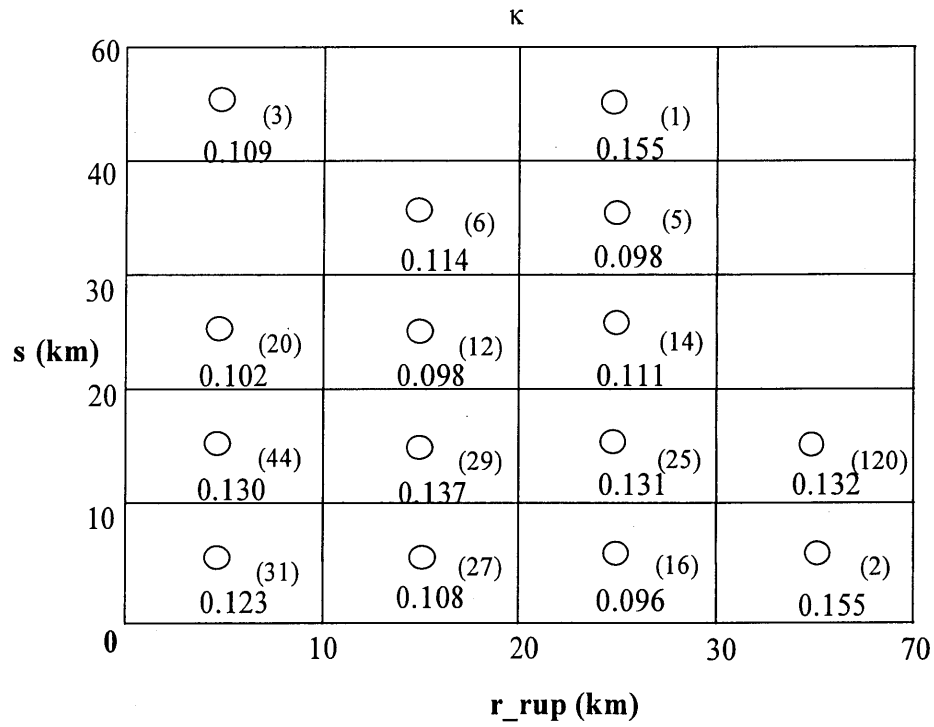

Figure 4.8. Best fit κ plot for Short Period Oscillators in Each Sector (SN records) ($r = 0.0$, $\zeta_o = 2\%$)

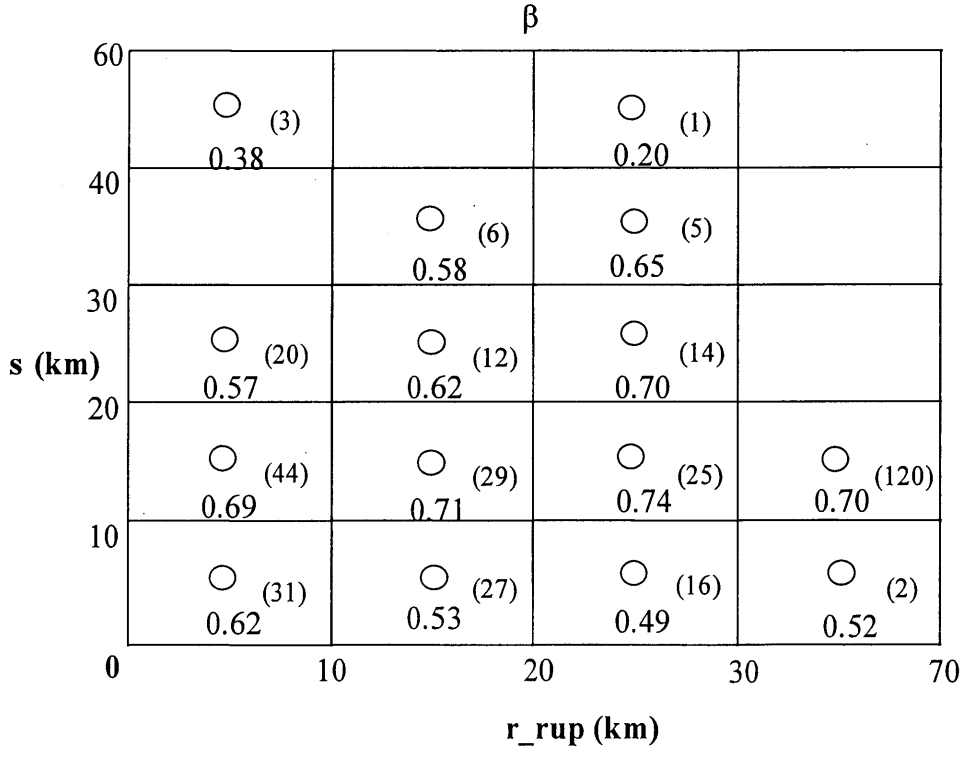

Figure 4.9. Best fit β plot for Short Period Oscillators in Each Sector (SN records) ($r = 0.0$, $\zeta_o = 2\%$)

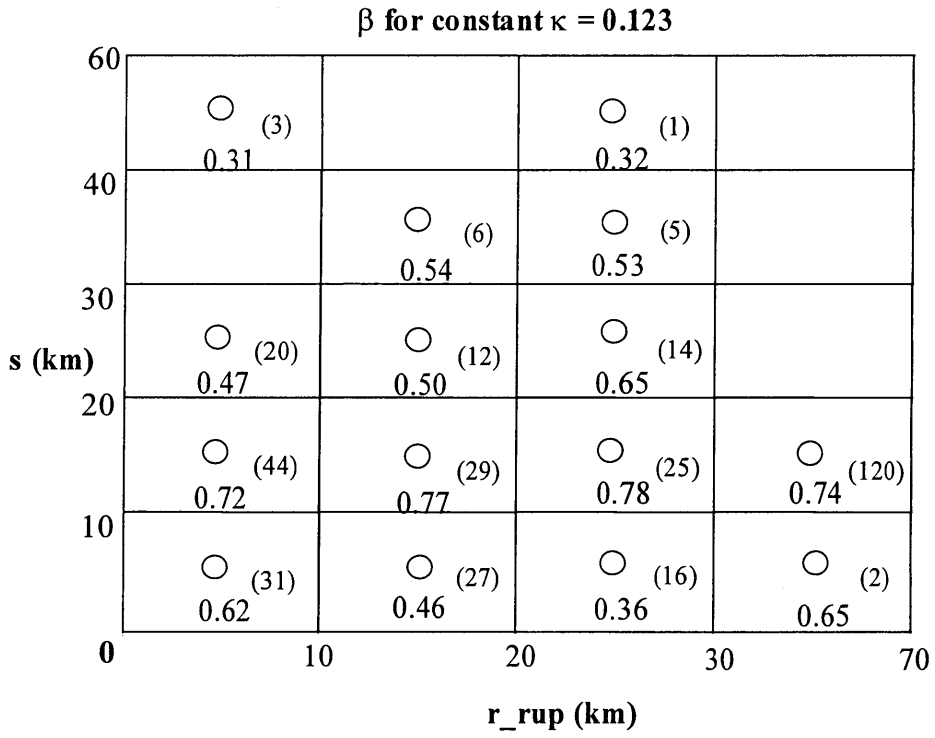

Figure 4.10. Best fit β plot for Short Period Oscillators in Each Sector using Constant κ
$r = 0.0$, $\zeta_o = 2\%$, SN records

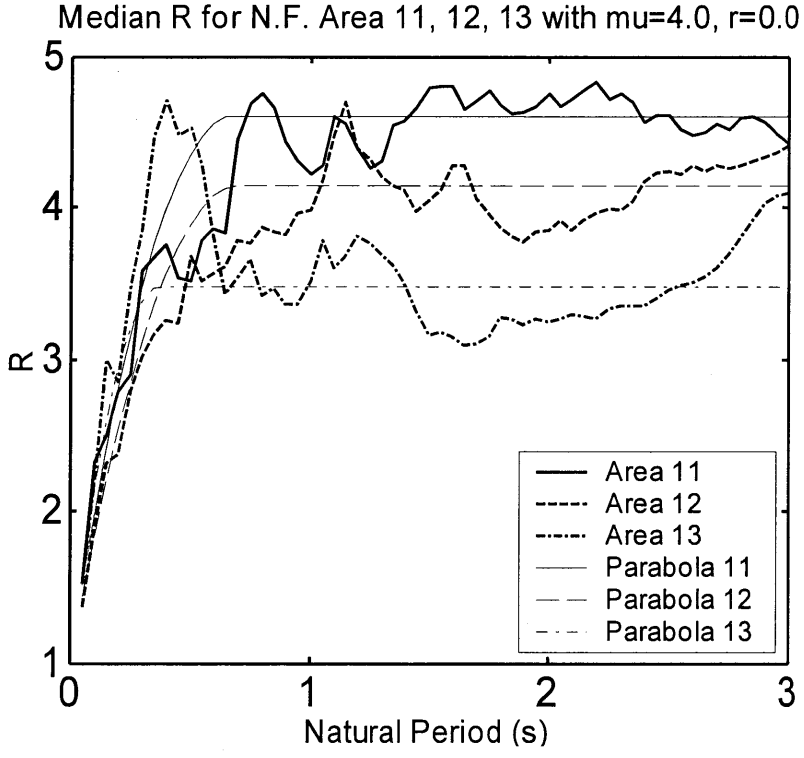

Figure 4.11. *R-T* plot for Sector (1,1) to (1,3) and Approximations
($r = 0.0$, $\mu = 4$, $\zeta_o = 2\%$), SN records, $T = 0$-3s

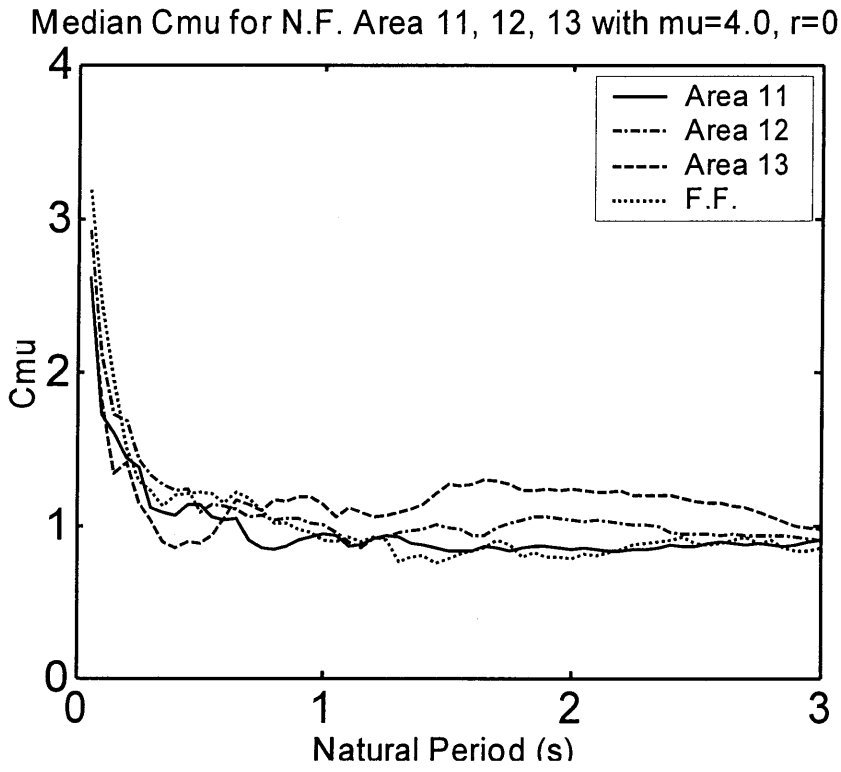

Figure 4.12. C_μ-T plot for Sector (1,1) to (1,3) SN records and FF records ($r = 0.0$, $\mu = 4$, $\zeta_o = 2\%$), T = 0-3s

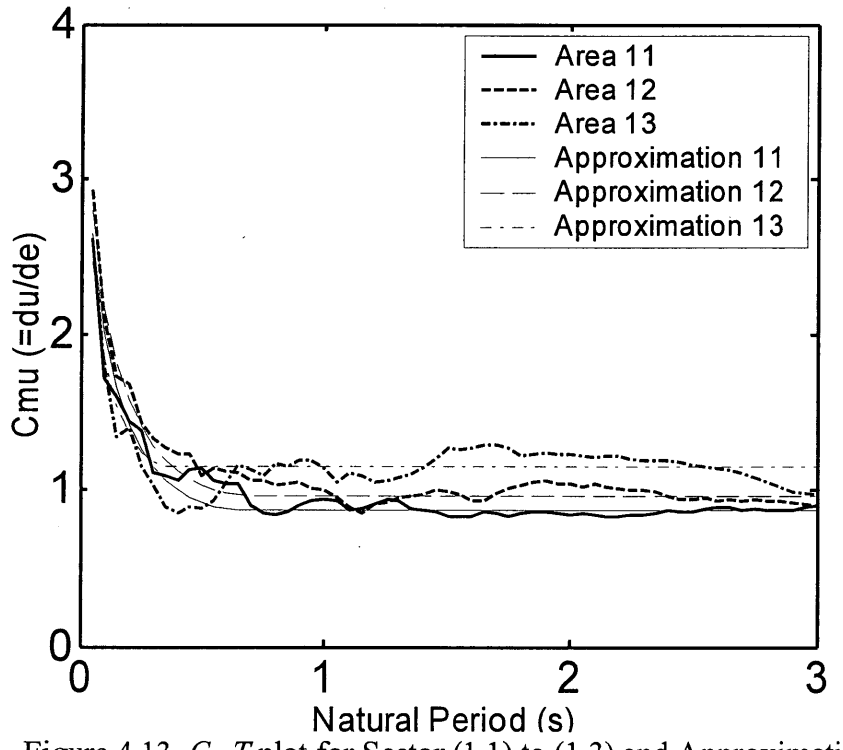

Figure 4.13. C_μ-T plot for Sector (1,1) to (1,3) and Approximations ($r = 0.0$, $\mu = 4$, $\zeta_o = 2\%$), SN records, T = 0-3s

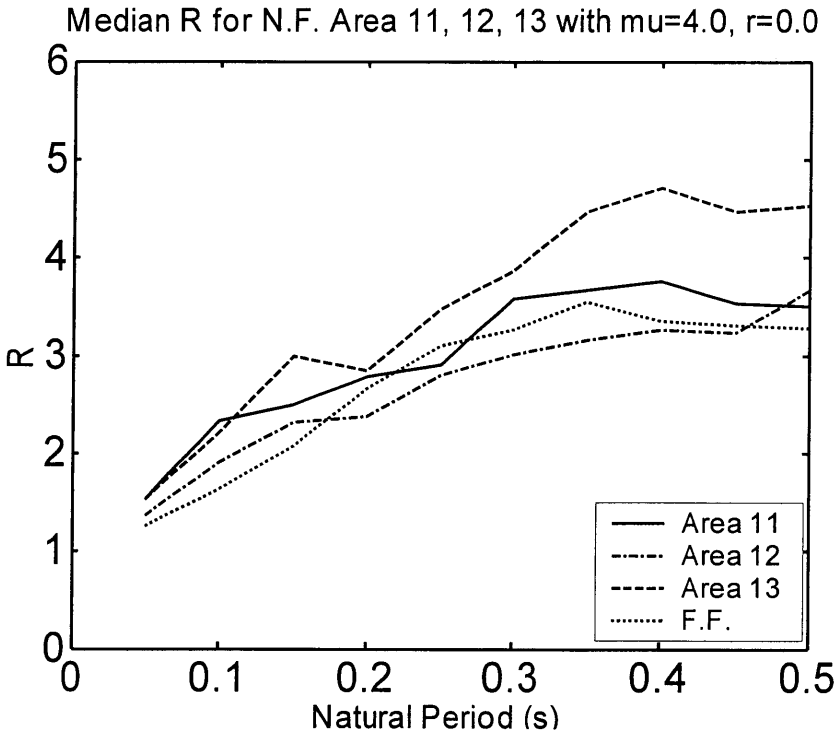

Figure 4.14. *R-T* plot for Sector (1,1) to (1,3) for Short Period Oscillators ($r = 0.0$, $\mu = 4$, $\zeta_o = 2\%$), SN records

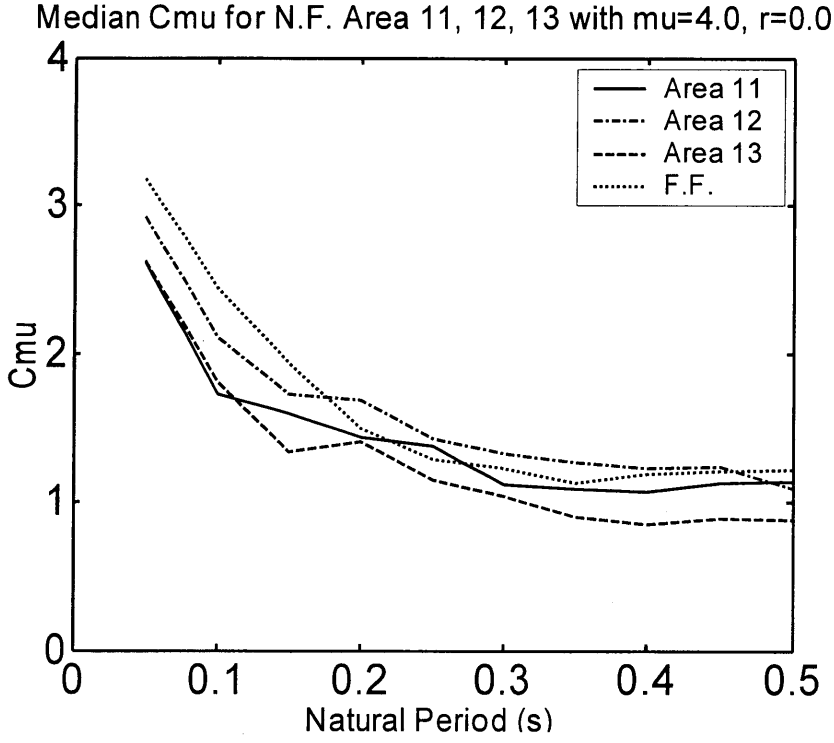

Figure 4.15. C_μ-*T* plot for Sector (1,1) to (1,3) for Short Period Oscillators ($r = 0.0$, $\mu = 4$, $\zeta_o = 2\%$), SN records

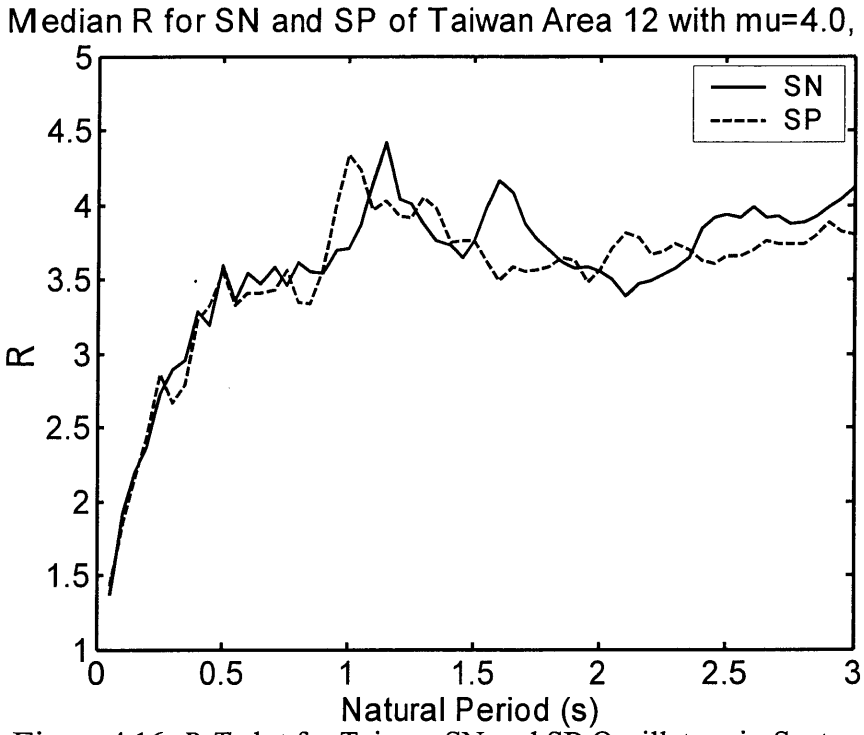

Figure 4.16. *R-T* plot for Taiwan SN and SP Oscillators in Sector 1,3 ($r = 0.0$, $\zeta_o = 2\%$, $\mu = 4$)

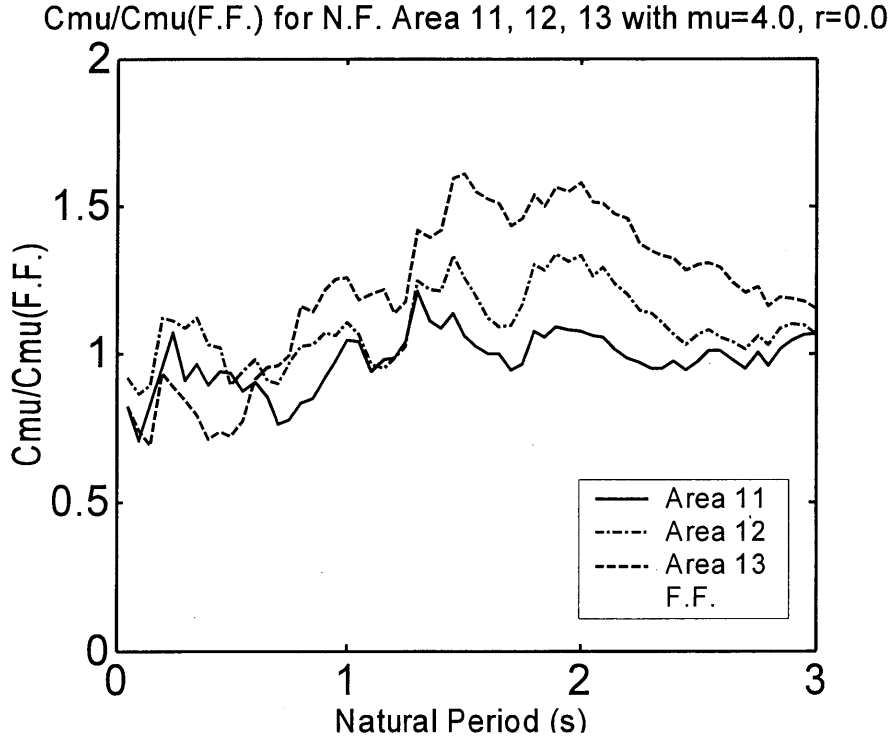

Figure 4.17. C_μ(NF)/ C_μ(FF) plot for SN records for Various Sectors ($r = 0.0$, $\zeta_o = 2\%$, $\mu = 4$)

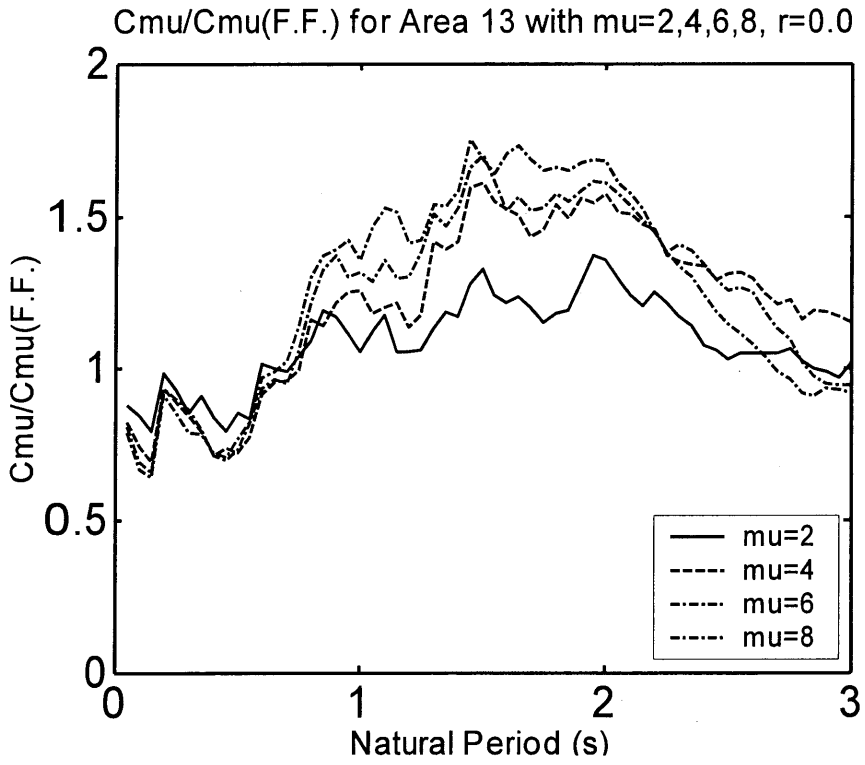

Figure 4.18. C_μ(NF)/ C_μ(FF) plot for SN records for Sector 1,3 ($r = 0.0$, $\zeta_o = 2\%$)

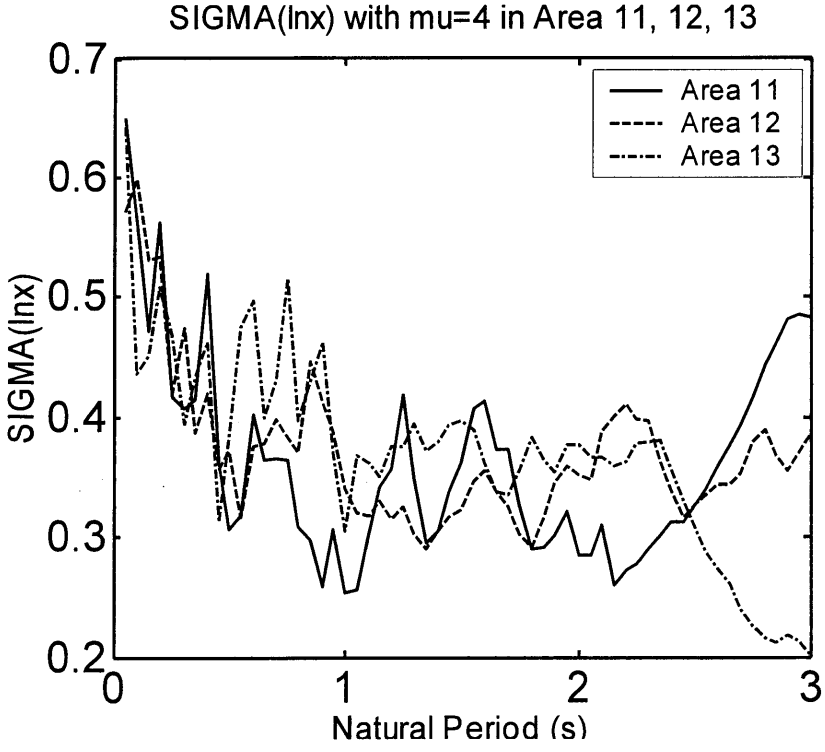

Figure 4.19. SIGMA(ln C_μ) Plot for FF Records and SN Records in Sectors (1,1), (1,2) & (1,3) ($r = 0.0$, $\mu = 4$, $\zeta_o = 2\%$)

4.2 CAPACITY SPECTRA METHOD

Relationships between μ-T_{eff}, μ -ζ_{eff} and ζ_{eff}-SR are required for the CSM. These are described below.

4.2.1. Effective Damping, ζ_{eff}, Ductility, μ, Relationship

The actual damping ratio for 2 records is given in **Figure 4.20**. It may be seen that the damping to these two records, USA01058 and JAPAN03145 obtained from NGDC SMCAT (1995) give an effective damping which is significantly different from the ATC-40 and Gulkan procedures. Both records show a high effective damping at short periods, sometimes greater than 100%, which decreases at long periods. It may be seen that:

a) The second record, Japan03145, shown exhibits some "negative hysteretic damping", ζ_{hyst}, since the total effective damping, ζ_{eff}, is less than the initial viscous damping, ζ_o, of 2%. It also shows "negative effective damping" since ζ_{eff} is less than zero. Negative damping indicates that a structure in free vibration will not have a displacement response which damps out. Instead the response grows. In the application shown here, the meaning of *negative damping* is that the peak displacement of the yielding oscillator is greater than the response of an elastic oscillator at the effective period with zero damping. The magnitude of the negative damping is relatively meaningless. It is dependent on the length of time that the analysis is run. If the analysis were carried out over a longer time and the extra ground acceleration were zero, then a lower value of effective damping would be obtained. If the time history analysis were carried out for a very long time, then the damping would tend to zero. However, the values obtained are used in the analysis since the result would be conservative for design.

b) The damping ratios over most of the period range are less than either the damping ratios estimated by the method of Gulkan and Sozen (1975) and by ATC-40 (1997). Displacements would therefore be expected to be larger than the displacement obtained by either of these methods. The standard methods to estimate damping are therefore unsafe.

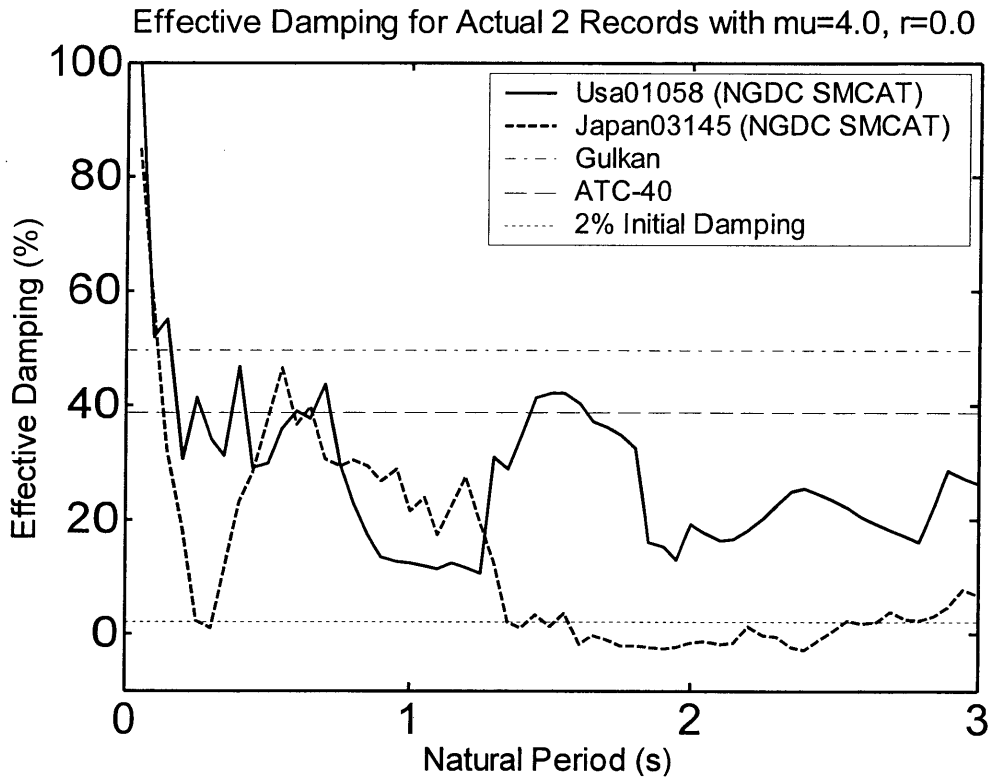

Figure 4.20. Effective Damping For Actual Records ($\mu = 4$, $r = 0.0$, $\zeta_o = 2\%$)

The effective damping trends for 32 FF records are shown in **Figure 4.21** for a ductility of 4. This is the average, rather than the median, because of the presence of negative numbers. It may be seen that effective damping decreases significantly with period. Again the ATC-40 and Gulkan and Sozen methods are unsafe for these structures. The line indicating the mean minus 1 standard deviation (-1SD) is close to zero damping.

The effective damping for ductilities of 2, 4, 6 and 8 are plotted together in **Figure 4.22**. It may be seen that effective damping generally increases as the ductility increases from 2 to 4 as would be expected for $r = 0$ according to the **Equation 2.13**. However, for ductilities, μ, from 4 to 8, the effective damping seems to be almost independent of ductility. In some cases the effective damping for $\mu = 8$ is between that from $\mu = 2$ and $\mu = 4$. A comparison of the damping with the impulse equations is given in **Figure 4.23**. These equations give a much better estimate of damping especially for long period structures.

The effect of changing the oscillator post-elastic stiffness is given in **Figure 4.24**. A positive post-elastic stiffness ratio, r, of 0.1 causes a decrease in ζ_{eff} at short periods and an increase at longer periods. The value of ζ_{eff} therefore changes less with period than when $r = 0.0$. The effective damping ratio is significantly less than the prediction by ATC-40.

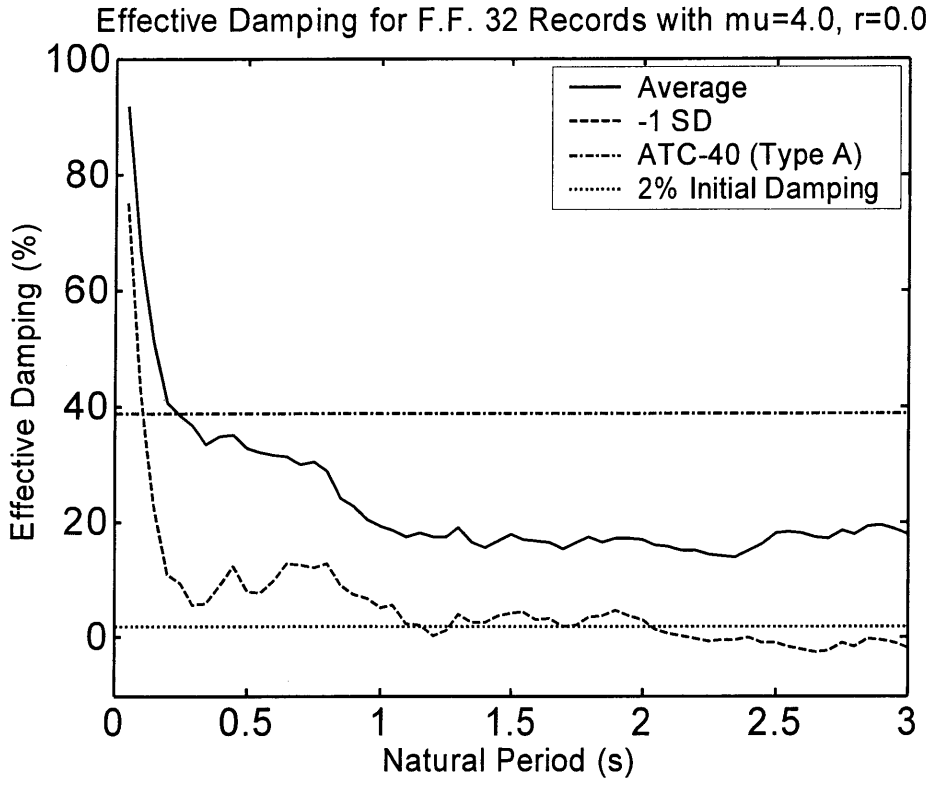

Figure 4.21. Effective Damping, ζ_{eff}, For FF Records ($\mu = 4$, $r = 0.0$, $\zeta_o = 2\%$)

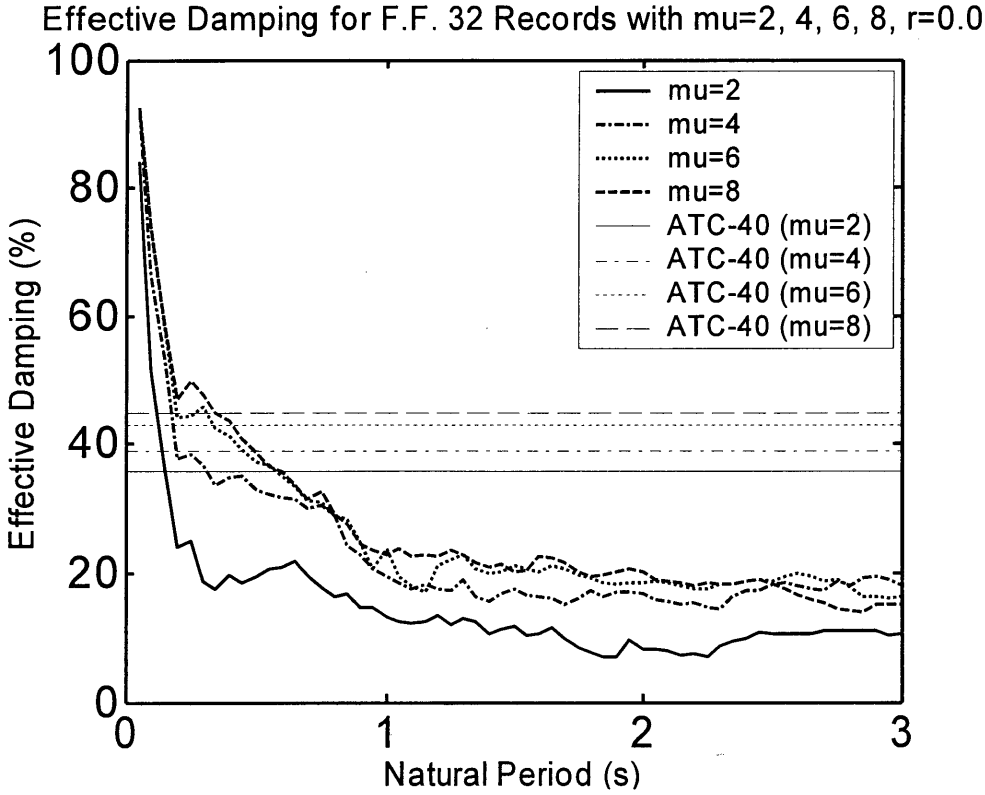

Figure 4.22. Effective Damping, ζ_{eff}, for Ductilities, μ, of 2, 4, 6 and 8 ($r = 0.0$, $\zeta_o = 2\%$) FF Records, Comparison with ATC-40

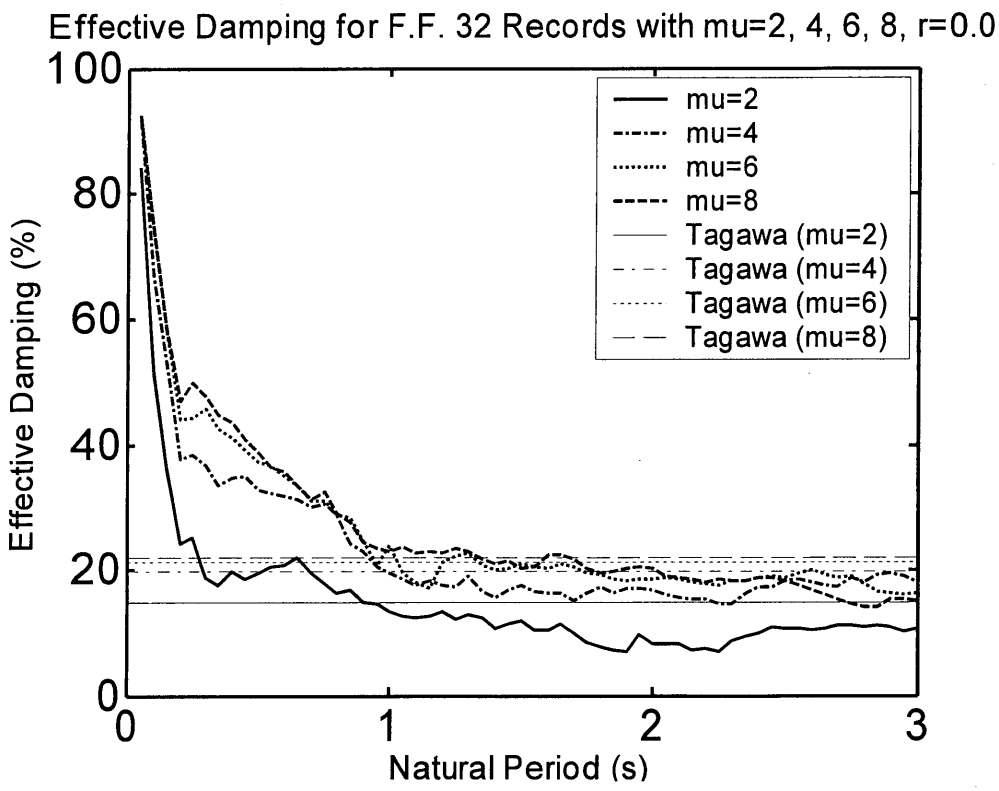

Figure 4.23. Effective Damping, ζ_{eff}, for Ductilities, μ, of 2, 4, 6 and 8 ($r = 0.0$, $\zeta_o = 2\%$) FF Records, Comparison with Equation Approximating Impulse Loading

Since it has been shown in the papers referenced by Fenwick and Bull (2002) that oscillators with the same strength and stiffness with fat or pinched hysteresis loops show similar displacements irrespective of the fatness of the loop (except for those oscillators with non-linear elastic characteristics or progressive yielding in one direction), the amount of hysteretic energy dissipation does not control the response of an oscillator. Only the backbone curve of the hysteresis loop is important to control the response. While a number of researchers have indicated that hysteretic energy dissipation is not important to estimate displacements, the logical consequence of this finding does not seem to have been stated anywhere explicitly yet.

The logical consequence of this finding is that the *effective damping* used to estimate the response for the types of loop described above is independent of the energy dissipation. That is, one equation for effective damping can be used for oscillators with fat loops (steel structures), with moderately pinched loops (RC structures) and with very pinched loops (timber structures). This independence of effective damping on the hysteretic energy dissipation is not represented in the method by Gulkan and Sozen (1994) where hysteretic damping is found directly as a function of estimated hysteretic energy dissipation. The finding also helps to explain why researchers using a Takeda hysteresis loop (e.g. Kowalsky, Priestley and MacRae, 1995) find that the CSM calibration by Gulkan and Sozen or ATC-40 estimates demands well, while those using bilinear loops (e.g. Chopra and Goel, 1999 and this report) find that the CSM calibration by Gulkan and Sozen or ATC-40 may be very non-conservative in estimating the demands.

Using the arguments described above, effective damping values for the bilinear oscillators described above are therefore applicable to structures with pinched hysteretic loops.

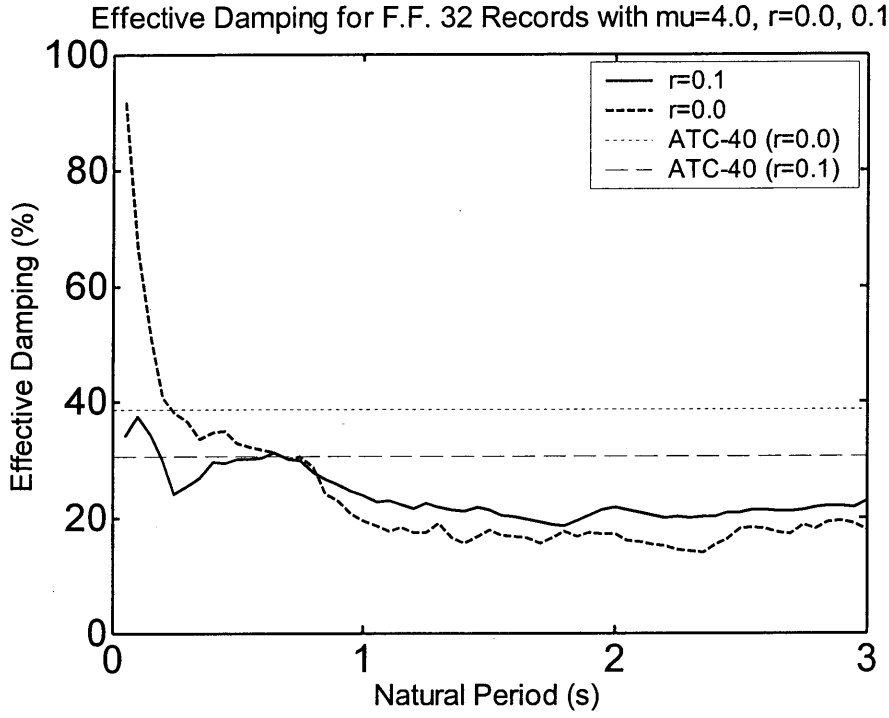

Figure 4.24. Effective Damping, ζ_{eff}, for FF Records, $r = 0.0$ and $r = 0.1$ ($\mu = 4$, $\zeta_o = 2\%$)

The effective damping for different regions close to the fault is given in **Figure 4.25**. Here it may be seen that the *effective damping tends to increase as the distance along the fault increases.* This implies that design using this method should be carried out with a less severe damping relationship (or greater damping) in the region of positive directivity than that closer to the epicenter. These trends are different from that of the Coefficient Method (CM) where more severe relationships were needed in the region of positive directivity. **Figure 4.26** shows the effective damping below a period of 0.5s. There do not seem to be strong trends with position along the fault since the records in Sector 1,2 tend to have higher effective damping than the records in Sector 1,1 or Sector 1,3 for periods less than 0.2s, and at periods greater than 0.3s there is very little difference in the effective damping for the records close to the fault. A similar plot to **Figure 4.25**, showing the scatter in the response is given in **Figure 4.27**.

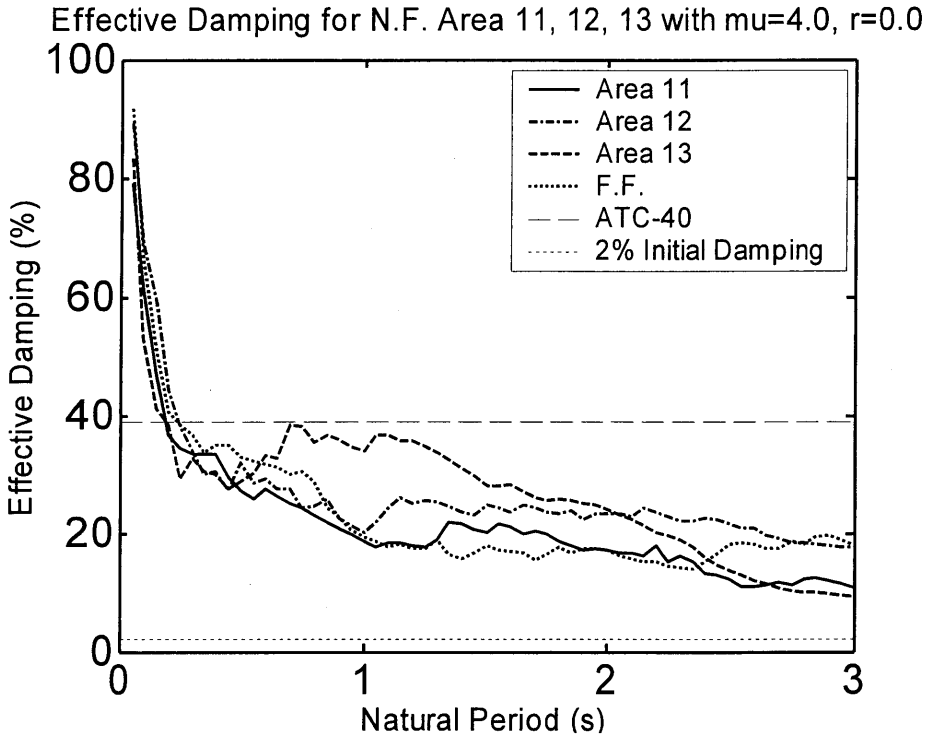

Figure 4.25. Average Effect of Position Along the Fault on ζ_{eff} ($r = 0.0$, $\mu = 4$, $\zeta_o = 2\%$)

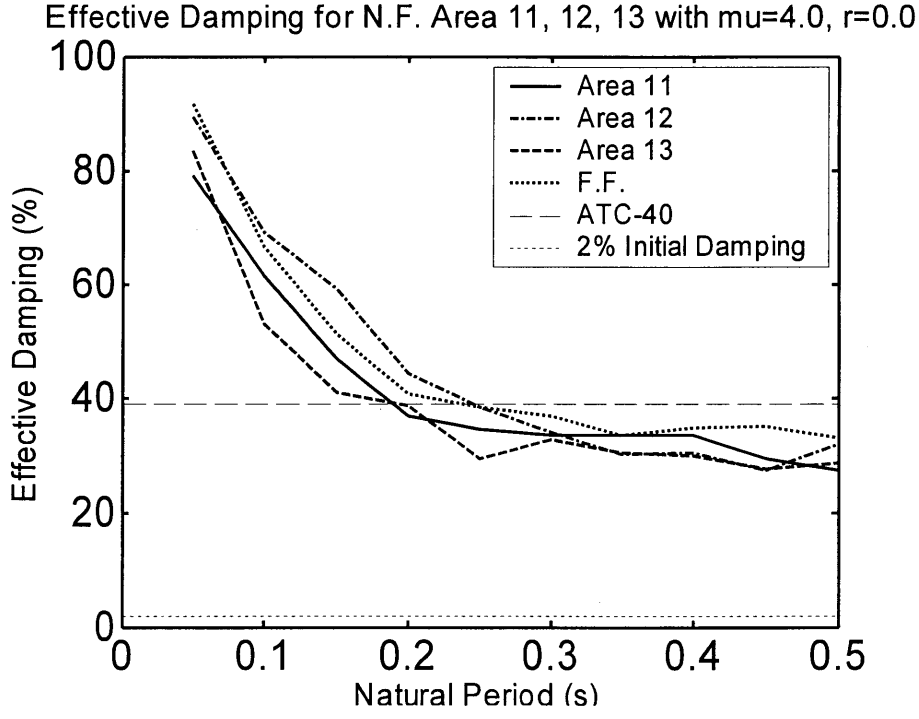

Figure 4.26 Average Effect of Position Along the Fault on ζ_{eff} ($r = 0.0$, $\mu = 4$, $\zeta_o = 2\%$) – Short Period Structures

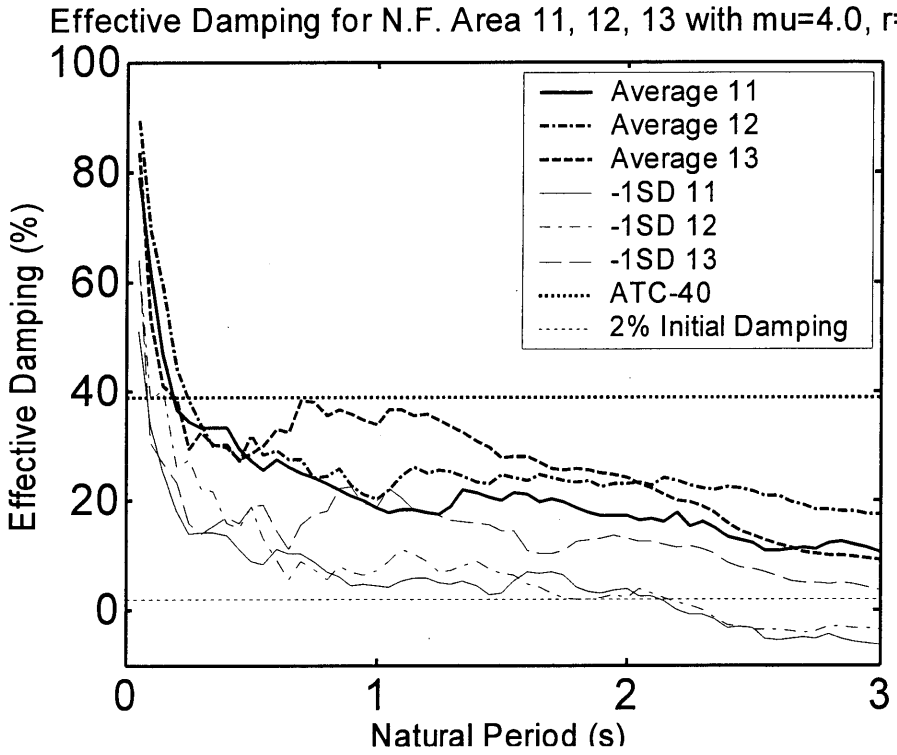

Figure 4.27. Average Effect of Position Along the Fault with Scatter of ζ_{eff} ($r = 0.0$, $\mu = 4$, $\zeta_o = 2\%$)

4.2.2. *SR* - ζ_{eff} Relationship

For the far-field records, a plot of *SR* versus *T* for various ζ_{eff} values was obtained by conducting elastic analyses of the different records with the different damping ratios and it is given in **Figures 4.28 and 4.29**. It is plotted over a period range of *T* = 0-6s since the effective period of a structure with a fundamental period of 3s and a ductility of 4 is 6s according to **Equation 2.11**. The *SR* values were computed as the elastic displacement for the total damping ratio of interest, $d_{max,\zeta}$, divided by that with 2% damping, $d_{max,\zeta=2\%}$. The ATC-40 damping value, which is based on 5% damping, was corrected to consider 2% damping as described in **Section 2.1.3.4** using **Equation 4.11**. This gives SR_A of 0.60, 0.43 and 0.33 for total damping ratios of 10%, 20% and 30% respectively and SR_V of 0.67, 0.53 and 0.45 respectively. AIJ (1993) *SR* values tend to be slightly smaller than the SR_A values. The jump in the predicted *SR* due to the different SR_A and SR_V curves at the transition period may be seen in **Figure 4.29**. A smooth transition, rather than the abrupt one given is likely to represent the behavior of real oscillators better.

$$SR_A = \frac{(3.21-0.68\ ln(\zeta_{eff}\%))/2.12 > 0.33}{(3.21-0.68\ ln(2\%))/2.12} \quad \text{(a)}$$

$$SR_V = \frac{(2.31-0.41\ ln(\zeta_{eff}))/1.65 > 0.50}{(2.31-0.41\ ln(2\%))/1.65} \quad \text{(b)} \qquad (4.11)$$

It may be seen that for very short period structures *SR* tends to unity. As the period tends to infinity, *SR* will also tend to unity as discussed in the **Chapter 2**. However, a constant approximation is probably not unreasonable over a period range from *T* = 0.2-6s say. It may be seen that *SR* values are generally greater than the average ATC-40 SR_A values (given in the short period range) for 30% damping shown. After the transition, the actual *SR* is less than the ATC-40 SR_V values but the actual *SR* becomes similar to SR_V by a period of 3s. This means that ATC-40 *SR* estimates are non-conservative only for short-period structures.

Figure 4.30 shows the *SR* for (r_{rup},*s*) Sectors (1,1), (1,2) and (1,3) with the damping ratios of 10%, 20% and 30%. *SR* is higher, indicating more severe demands in region (1,1) over much of the period range. **Figure 4.31** shows the scatter in *SR* for one case.

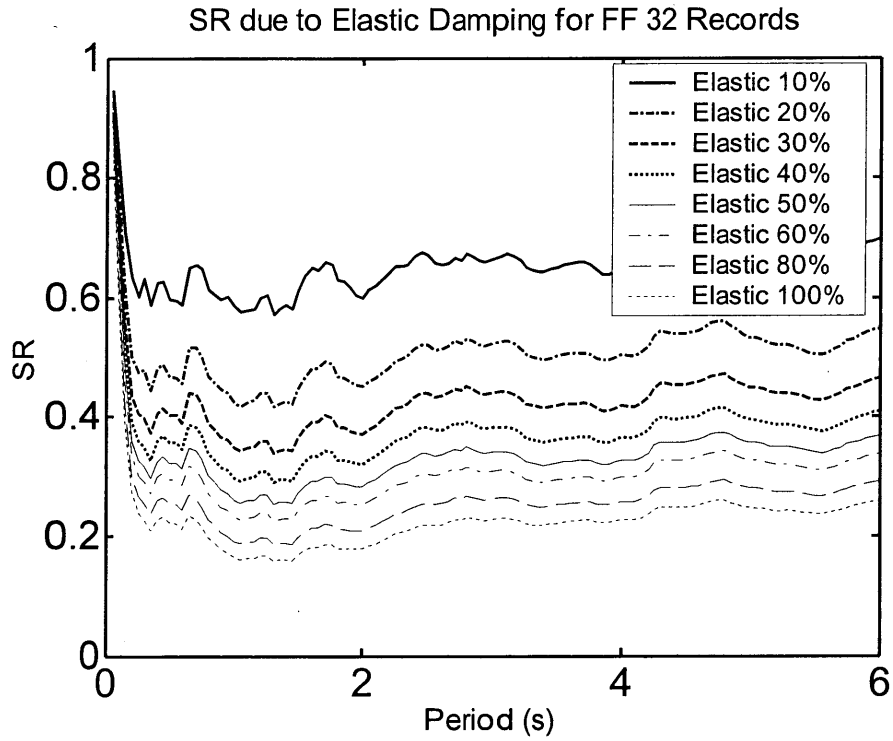

Figure 4.28. *SR*-ζ_{eff} Relationship for FF Records (ζ_o = 2%)

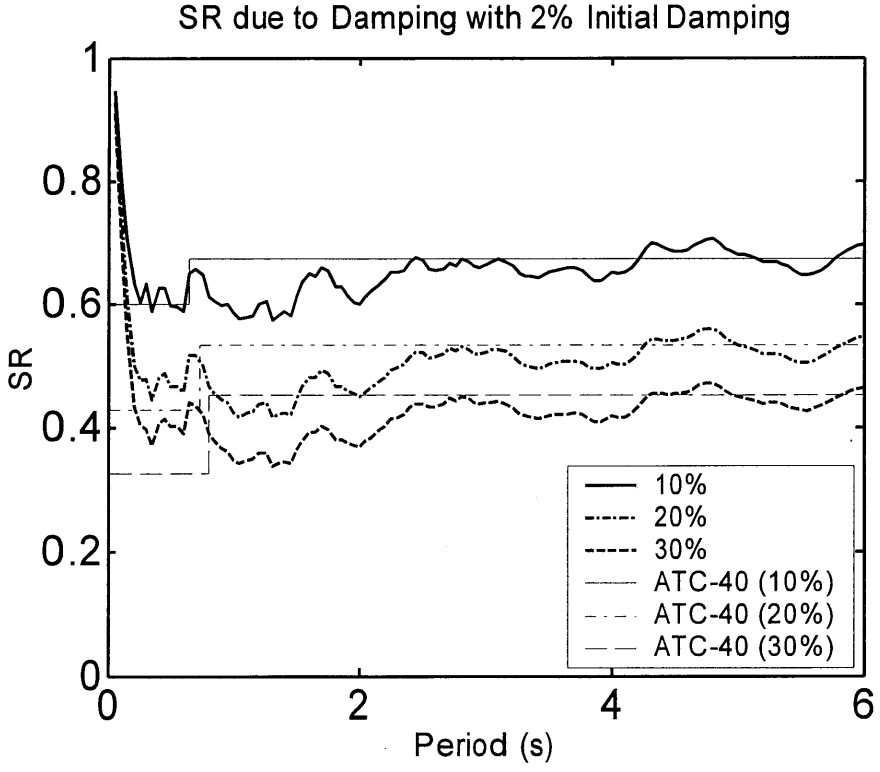

Figure 4.29. *SR*-ζ_{eff} Relationship for FF Records (ζ_o = 2%)
Comparison with ATC-40

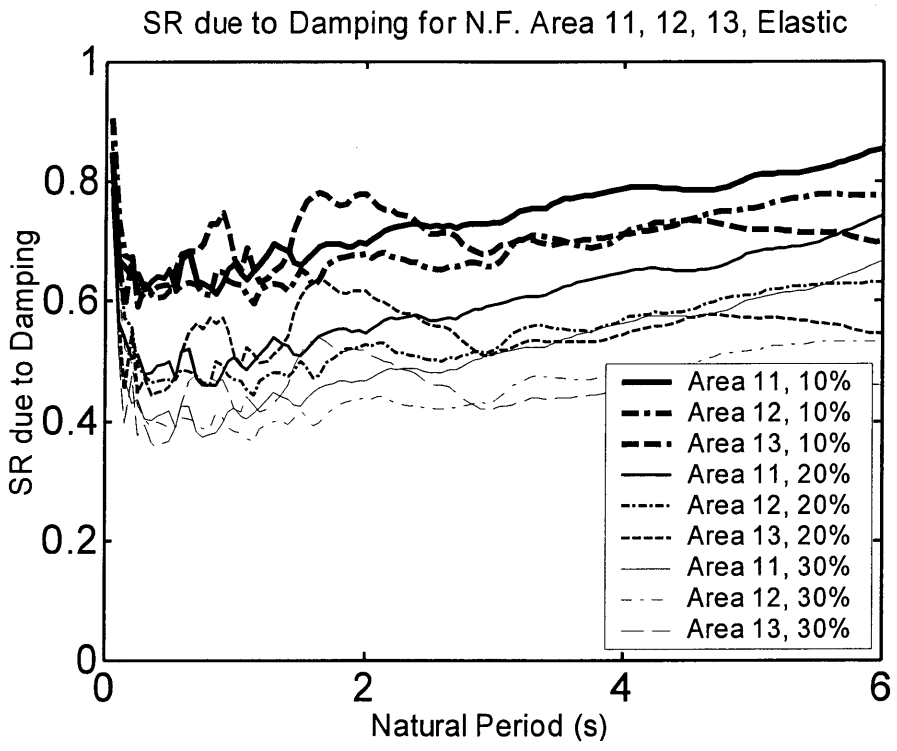

Figure 4.30. *SR-T* Plot for Records
at Different Locations to the Fault (ζ_{eff} = 10%, 20% 30%, ζ_o = 2%)

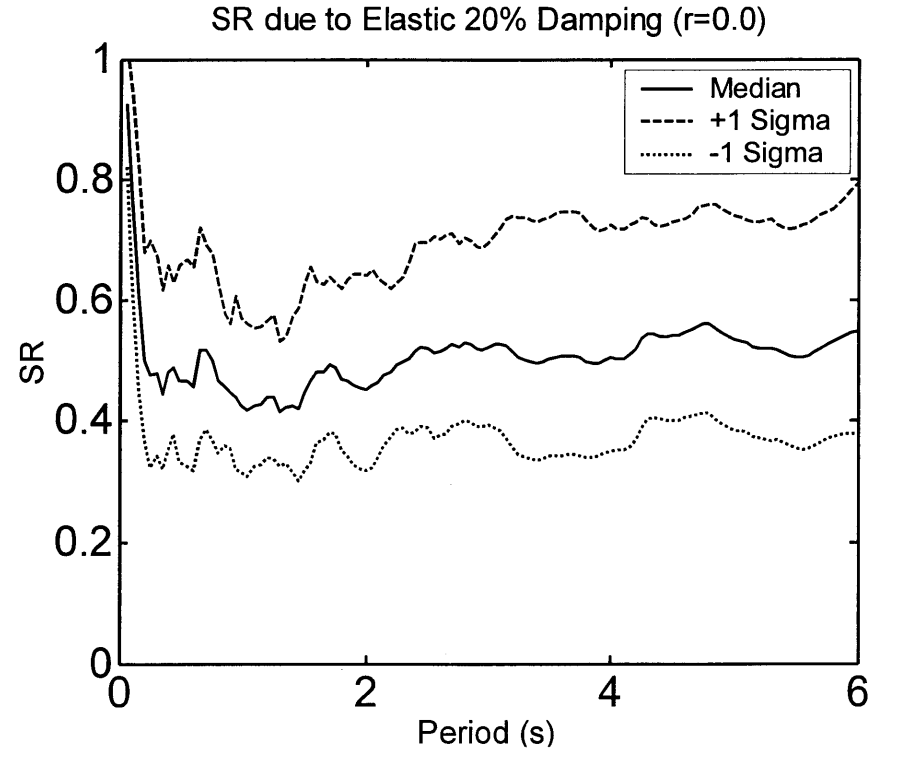

Figure 4.31. *SR-T* Plot FF records showing Scatter (ζ_{eff} = 20%, ζ_o = 2%)

4.2.3. *SR*- ζ_{eff} and ζ_{eff}-μ Relationship

The inelastic displacement response is determined by both the *SR*-ζ_{eff} and ζ_{eff}-μ relationships. By putting them together we get an *SR*-μ relationship. An *SR*-*T* line for FF oscillators is given in **Figure 4.32** for $\mu = 4$ and $r = 0.0$ where T is the fundamental (initial elastic natural) period of the oscillator. Elastic analysis at the effective period of the structure, T_{eff}, were scaled using **Equation 2.11** to obtain the fundamental period, T_o.

It may be seen that the *SR*-μ relationship does not follow a line of constant period, *T*. Instead it tends to cross lines of increased damping as the period shortens from about 1.5s. This is shown in the blow up of the short period range in **Figure 4.33**. This is consistent with the higher effective damping with shorter periods for a fixed ductility seen in previous plots. This trend is less for $r =$ 0.1 as shown in **Figures 4.34** and **4.35** where the inelastic response line tends to follow a curve of constant damping.

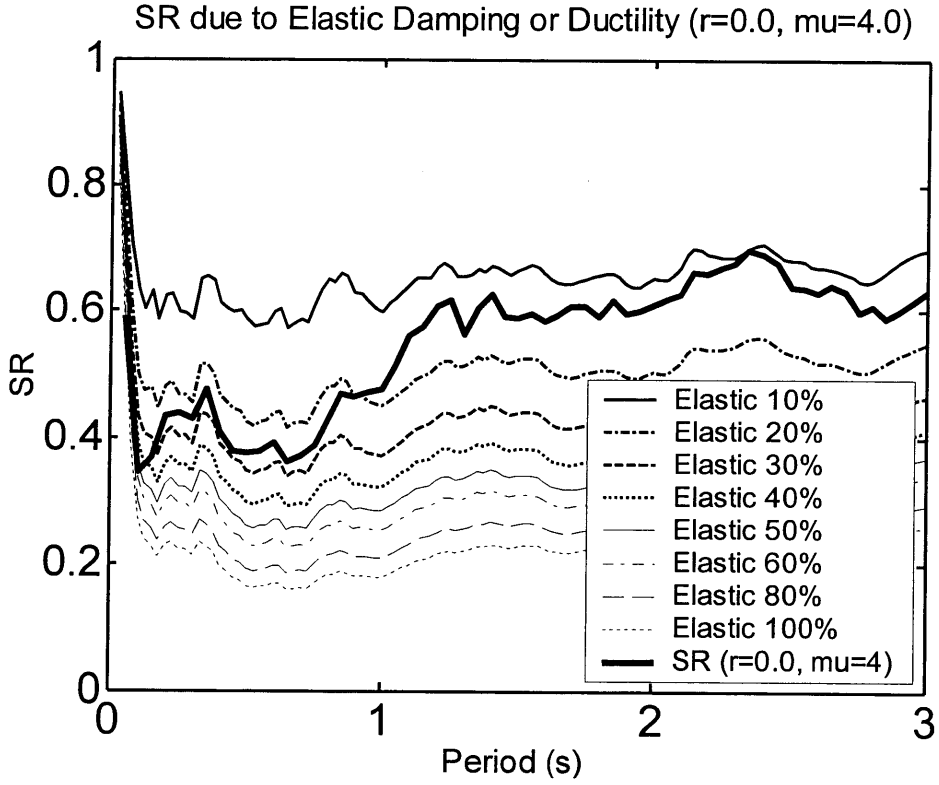

Figure 4.32. SR for Different Values of Damping for FF Records
($\mu = 4$, $r = 0.0$, $\zeta_o = 2\%$)

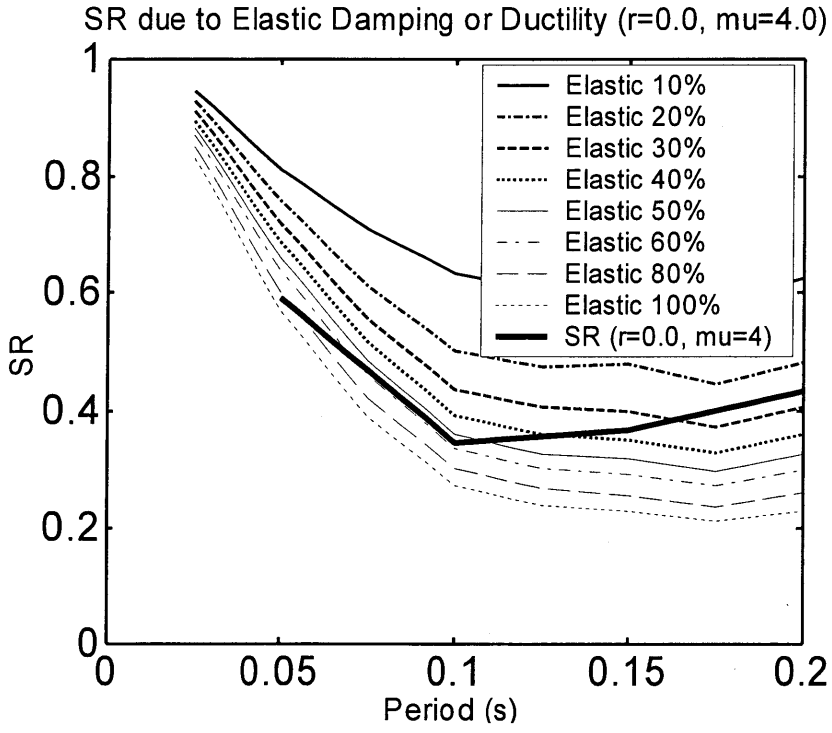

Figure 4.32. SR for Different Values of Damping for FF Records
Short Period Oscillators ($\mu = 4$, $r = 0.0$, $\zeta_o = 2\%$)

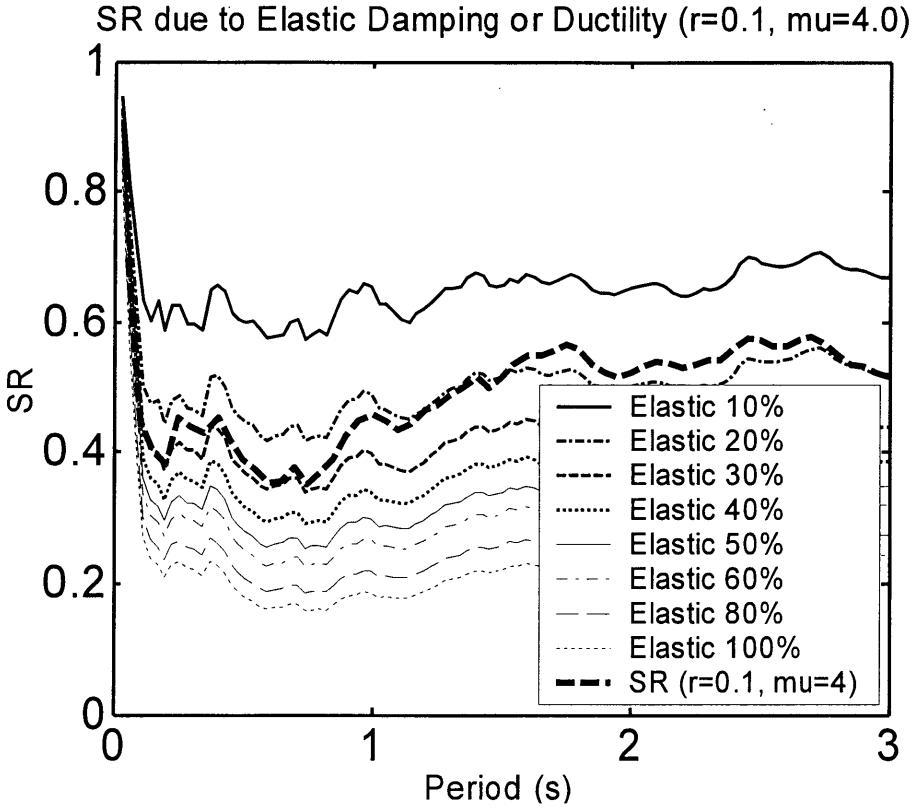

Figure 4.34. SR for FF Records with $\mu = 4$ ($r = 0.1$, $\zeta_o = 2\%$)

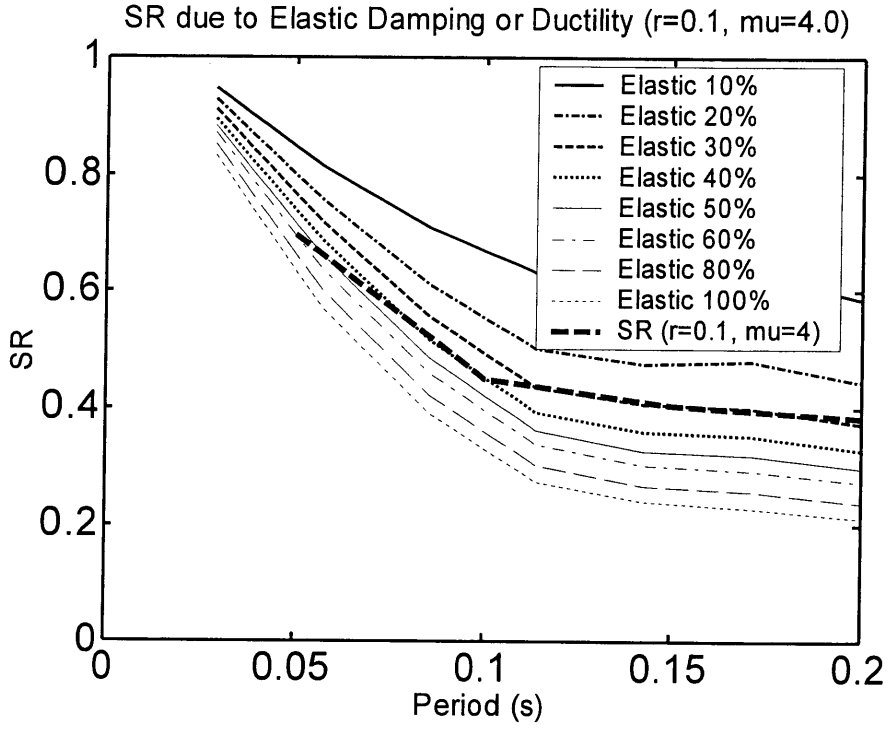

Figure 4.35. SR for FF Records with $\mu = 4$ ($r = 0.1$, $\zeta_o = 2\%$), Short Period Oscillators

4.3. DIRECT CAPACITY SPECTRA METHOD (DCSM)

4.3.1. Actual *SR*-μ relationship

The actual relationship for the two far-field records analyzed previously with $\mu = 4$, $r = 0$ and $\zeta_0 = 2\%$ is given in **Figure 4.36**. For the Japan03145 record, *SR* is sometimes greater than unity indicating negative damping. A range in SR values are also obtained with the different artificial records as shown in **Figure 4.37**. SR plots for the FF records for $r = 0$ and $\zeta_o = 2\%$ with $\mu = 2$, 4, 6 and 8, are given in **Figure 4.38 to 4.41**. The mean and +1 sigma values are shown. The logarithmic values were considered to be better indicators of the actual response and variation in response than the average and standard deviation used previously. However, in previous graphs the average and standard deviation were often used since the mean could not be found for negative values. **Figure 4.40 to 4.41** indicate that *SR* tends toward unity as the period decreases from about 0.1s. It tends to increase with increasing period from about 0.1s.

Figure 4.42 shows that the differences in median *SR* with period for different ductilities. It may be seen that this relationship is not particularly sensitive to ductility, especially for ductilities greater than 2. Also, the ATC-40 prediction is seldom conservative for the different oscillators. A ductility, μ, of 2 requires a larger *SR* value than the other ductilities.

Figure 4.43 shows that the differences in median SR with period for different bilinear factors, *r*, of 0.0 and 0.1. *SR* is greater with $r = 0.1$ for shorter period structures and lower for longer period structures. A high *SR* indicates a more severe response for a given ductility, $r = 0.0$ is more severe for periods greater than about 0.6s. ATC-40 estimates for *SR* give a lower value for the $r = 0.0$ loop since the effective damping is greater than for the $r = 0.1$ loop. This is opposite to what is actually seen for the longer period structures.

The effect of location relative to the fault is given in **Figure 4.44** and **Figure 4.45**. In this case the initial natural period, *T*, (rather than the effective period, T_{eff}) of the oscillators analyzed is plotted along the *x*-axis. The elastic analyses to compute *SR* were carried out using the elastic period, T_{eff}. For this ductility, the natural period, *T*, is one half of the effective period, T_{eff}, according to **Equation 2.11**. For oscillators with a period, $T < 1$s, there do not seem to be significant trends in the different sectors. For longer periods, the lowest *SR*, and hence the greatest reduction in elastic displacement, occurred in sector (1,3) for oscillators with a fundamental period between 1.0s and 2.3s. This implies a greater reduction in displacement than that in sector (1,1) which is closer to the epicenter. All of the lines are greater than the ATC-40 prediction. The trends are different from those obtained from the *R*-*T*-μ plots where greater demands were found in the region of positive directivity.

The lack of greater demand from NF directivity records indicates that no special account needs to be made for NF effects on structures designed by the CSM.

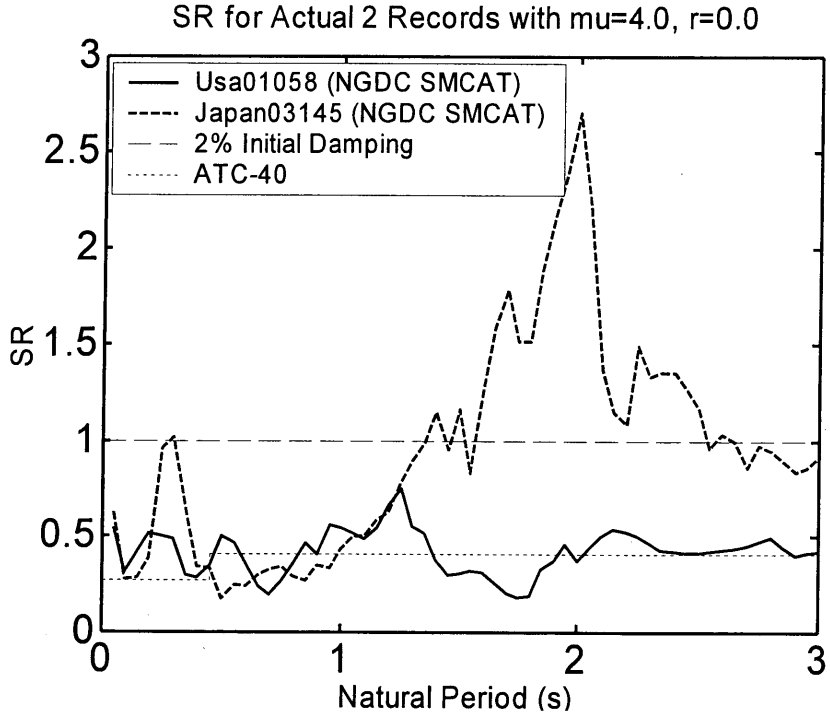

Figure 4.36. *SR-T* Relationship for Two Records
($\mu = 4$, $r = 0$ and $\zeta_o = 2\%$)

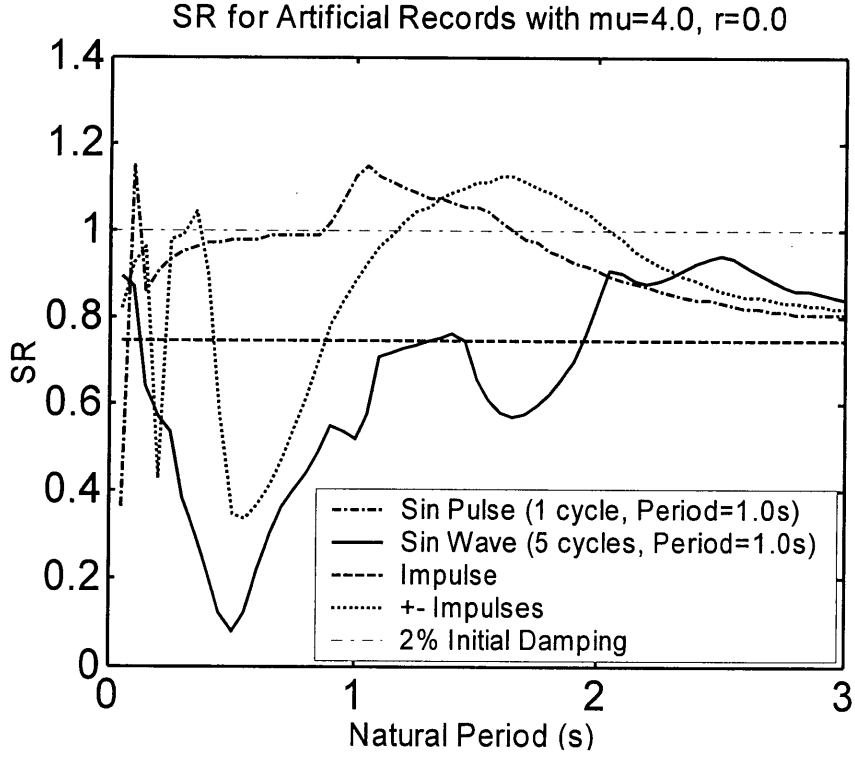

Figure 4.37. *SR-T* Relationship for Artificial Records
($\mu = 4$, $r = 0$ and $\zeta_o = 2\%$)

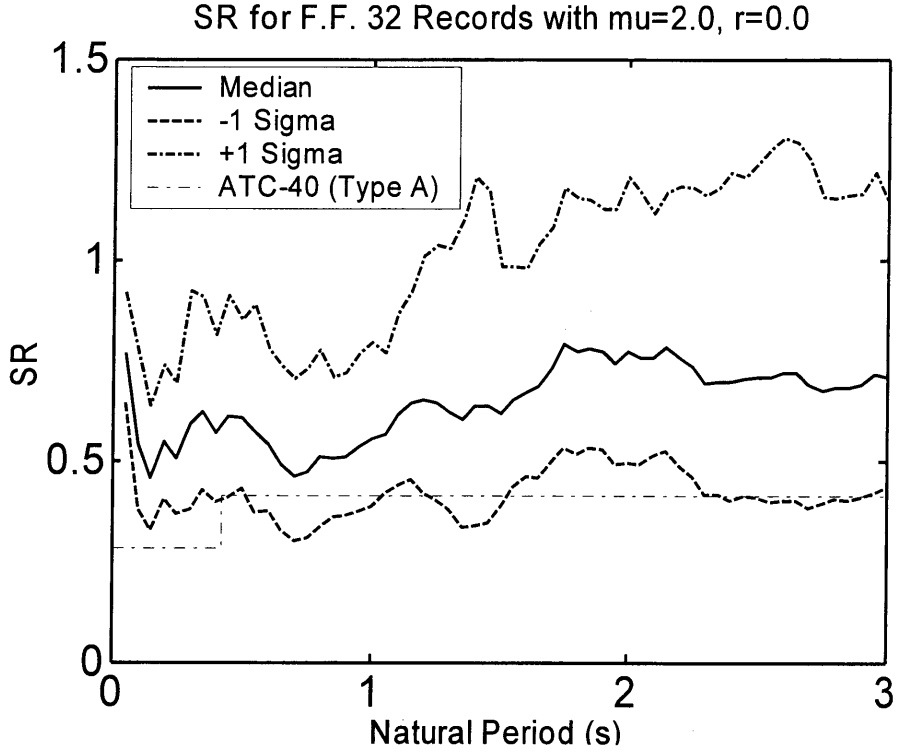

Figure 4.38. *SR-T* Relationship for FF Records
($\mu = 2$, $r = 0$ and $\zeta_o = 2\%$)

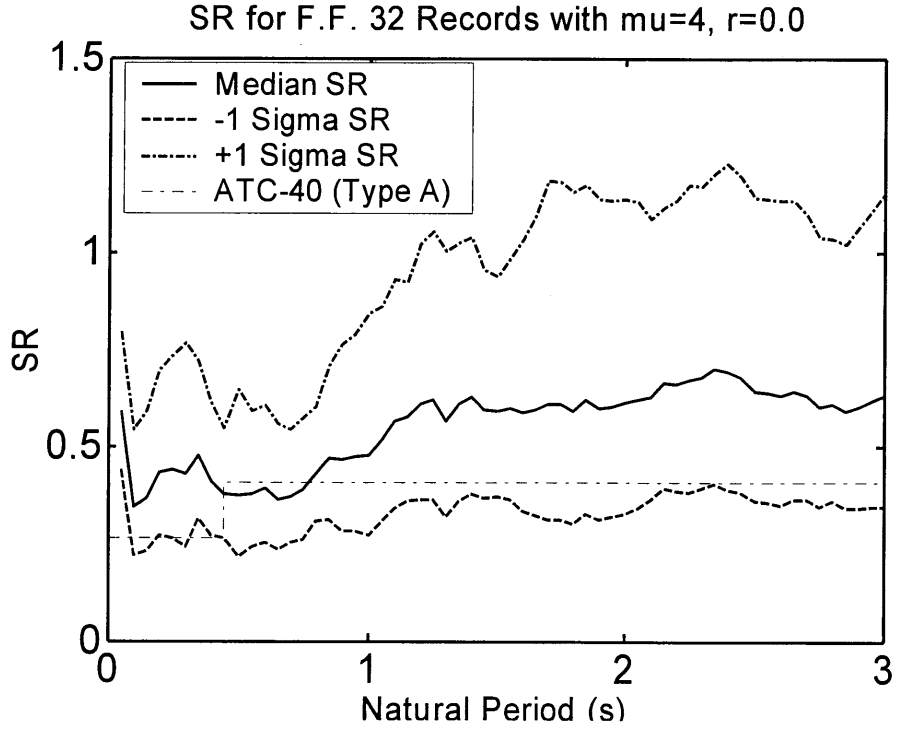

Figure 4.39. *SR-T* Relationship for FF Records
($\mu = 4$, $r = 0$ and $\zeta_o = 2\%$)

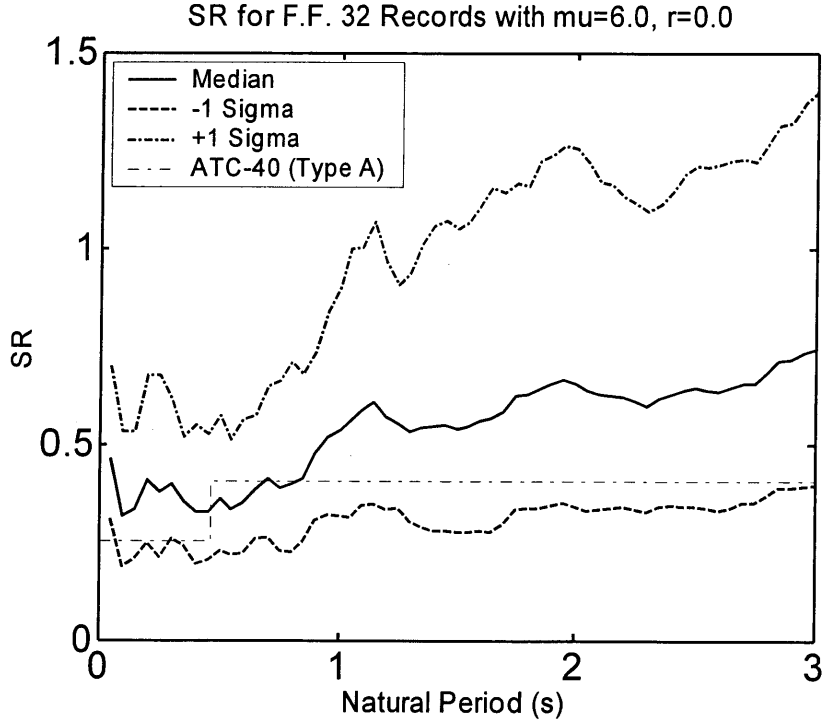

Figure 4.40. *SR-T* Relationship for FF Records
($\mu = 6$, $r = 0$ and $\zeta_o = 2\%$)

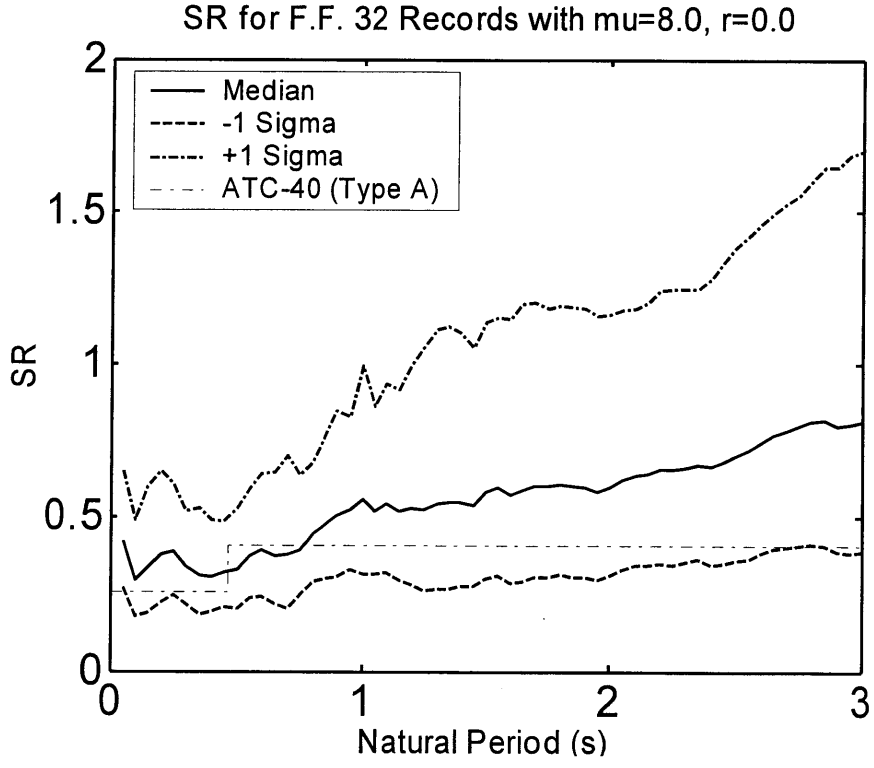

Figure 4.41. *SR-T* Relationship for FF Records
($\mu = 8$, $r = 0$ and $\zeta_o = 2\%$)

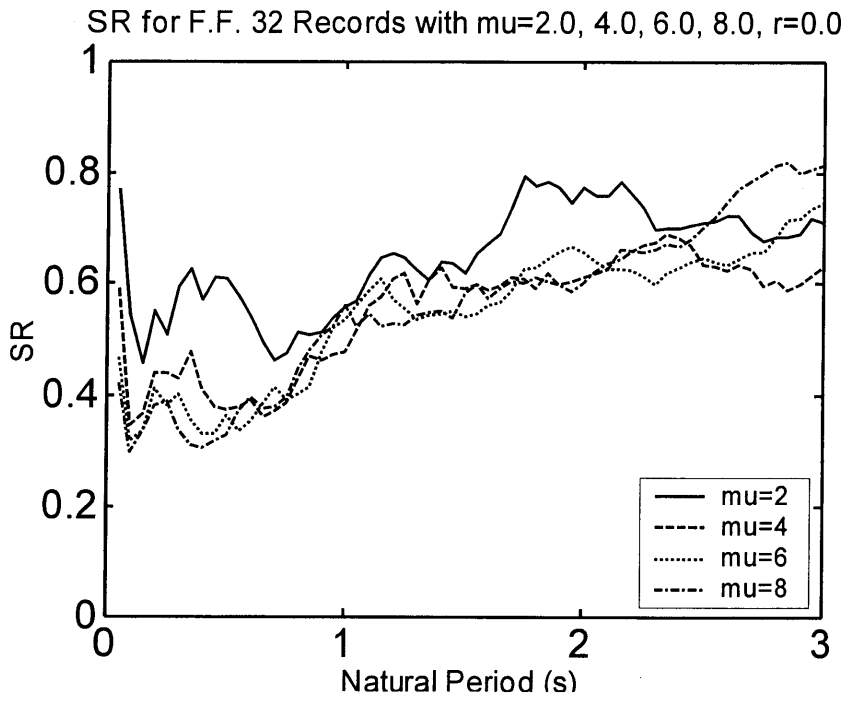

Figure 4.42. *SR-T* Relationship for FF Records
($\mu = 2, 4, 6$ & 8, $r = 0$ and $\zeta_o = 2\%$)

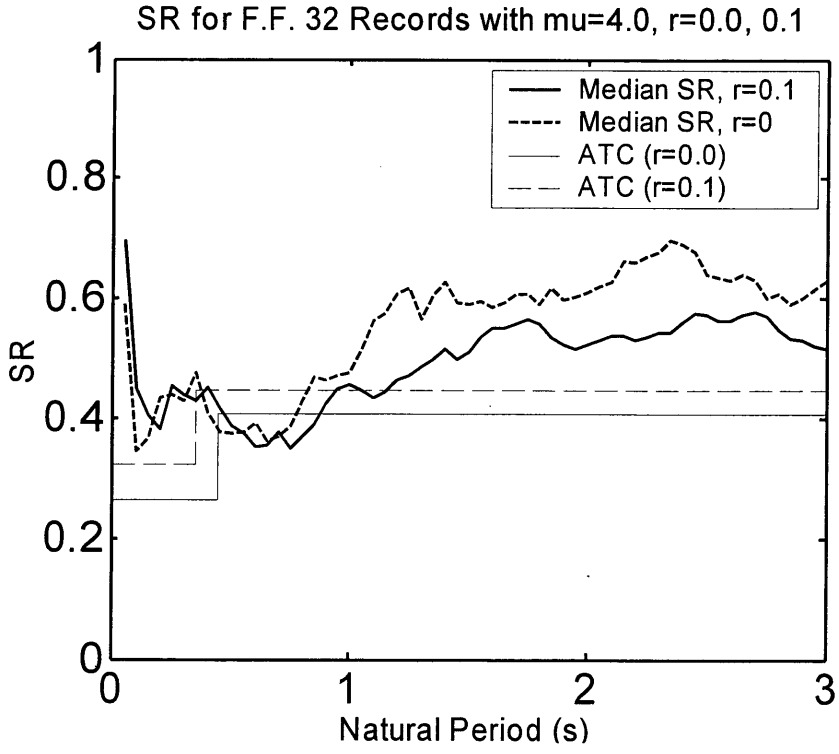

Figure 4.43. *SR-T* Relationship for FF Records
($\mu = 4$, $r = 0$ & 0.1, and $\zeta_o = 2\%$)

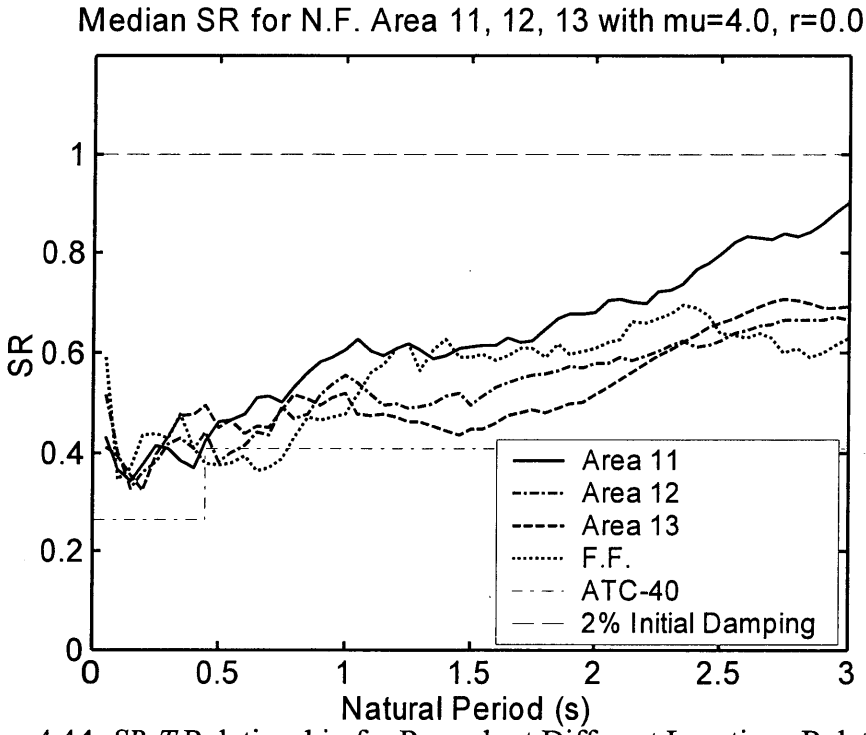

Figure 4.44. *SR-T* Relationship for Records at Different Locations Relative to the Fault ($\mu = 4$, $r = 0$ and $\zeta_o = 2\%$)

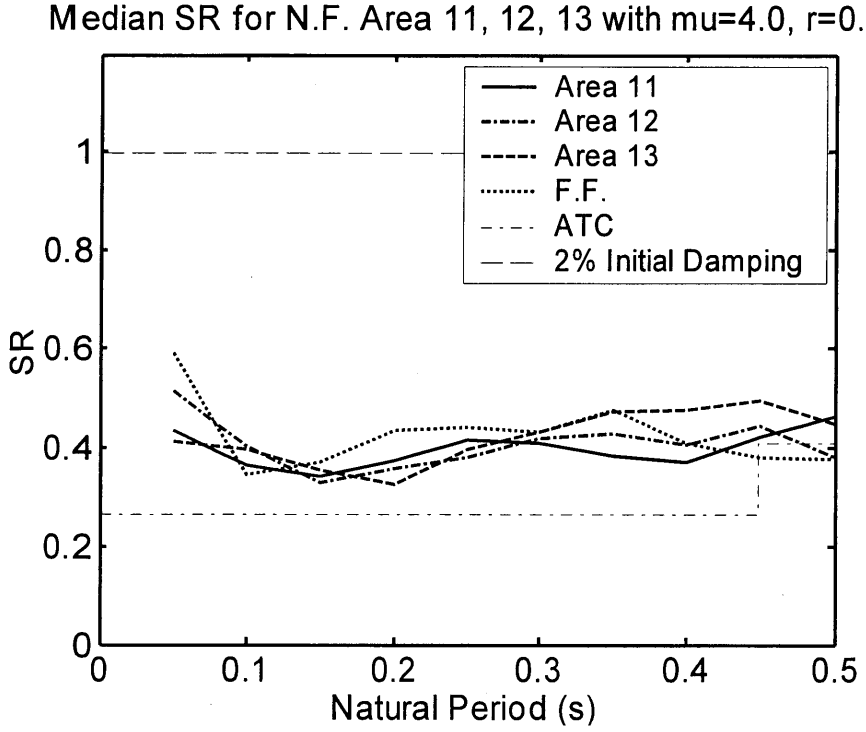

Figure 4.45. *SR-T* Plot for Records at Different Locations to the Fault Short Period Oscillators ($\mu = 4$, $\zeta_o = 2\%$)

4.4 COMPARISON OF DISPLACEMENTS PREDICTED BY DIFFERENT METHODS

Three methods to predict the inelastic demands on structures were described above. They were the Coefficient Method (CM), the Capacity Spectra Method (CSM) and the Direct Capacity Spectra Method (DCSM). Each of the methods was calibrated to predict the actual spectral displacement for a particular target ductility. The accuracy of the CM and DCSM are described below. The accuracy of the CSM is not provided because the scatter of the damping-ductility relationship, as well as the scatter of the ductility-*SR* relationship, when obtained separately and combined, are large. The DCSM was considered to give a better indication of scatter in the CSM.

The scatter of displacement of the FF records for $\mu = 4$ and $\zeta_o = 2\%$ is given in **Figure 4.46** when $r = 0.0$ and in **Figure 4.47** when $r = 0.1$. These graphs were obtained as follows:

1. Median elastic spectra was found from the records analyzed and plotted on the figures.
2. The predicted actual displacements were obtained by applying the actual calibration factor for the CM (as a C_1-T relationship for a ductility of 4), and from the DCSM (as a *SR*-T relationship for a ductility of 4) to the median elastic response. In addition, the inelastic response of every record for a ductility of 4 was found. The median response of these curves was also found. The 3 lines obtained; CM peak displacement estimation; CSM peak displacement estimation; and actual median peak displacement were drawn on the figures. These 3 lines lay on top of each other since the methods were well calibrated.
3. The +1 Sigma values were obtained using the median inelastic displacement and the logarithmic standard deviation from **Figure 4.19** and **Figure 4.39** according to **Equation 4.12**. These lines were then plotted on the graph.

When the DCSM (or CSM) and CM relationships are calibrated properly, they estimate the same median demand as the actual median demand. However, the scatter in the relationships are different depending on the scatter in inelastic demand. It may be seen that the "+ 1 Sigma" displacement response for both the CM and DCSM is similar for both methods up to a period of about 1.5s (corresponding to an effective period of 3s) when $r = 0$. When $r = 0.1$, the DCSM has slightly less scatter than the CM. For greater periods, the DCSM indicates considerably more scatter than the CM. Different amounts of scatter in the DCSM may be obtained if alternative definitions are used for T_{eff}. It should be noted that the scatter shown does not represent the scatter in the actual estimation of the displacement from the different records, it only measures the scatter in inelastic response defined by these two methods. For $r = 0$, median elastic displacements are less than actual displacements up to a period of about 0.9s and for $r = 0.1$ it is similar to the actual displacement. For greater periods, elastic displacements are greater than median displacements.

Figure 4.48 and **Figure 4.49** show the CM and CSM method estimation predictions for the FF records when these methods are calibrated according to FEMA356 and ATC-40 respectively. It may be seen that while FEMA356 tends to be slightly conservative over the entire range of periods shown, ATC-40 is generally non-conservative in estimating the median displacement demand. When $T < 0.8$s and $r = 0.1$ the CSM estimate is reasonable. **Figures 4.50** and **Figure 4.51** show the FEMA356 CM and ATC-40 CSM predictions divided by the actual median demands. This gives an indication of the error in estimation of inelastic demand from these two methods for $\mu = 4$, $\zeta_o = 2\%$ and $r = 0.0$ and 0.1 respectively. While the CSM may estimate displacements less than 60% of the actual median displacement, the CM estimates displacements more than 30% greater at some periods.

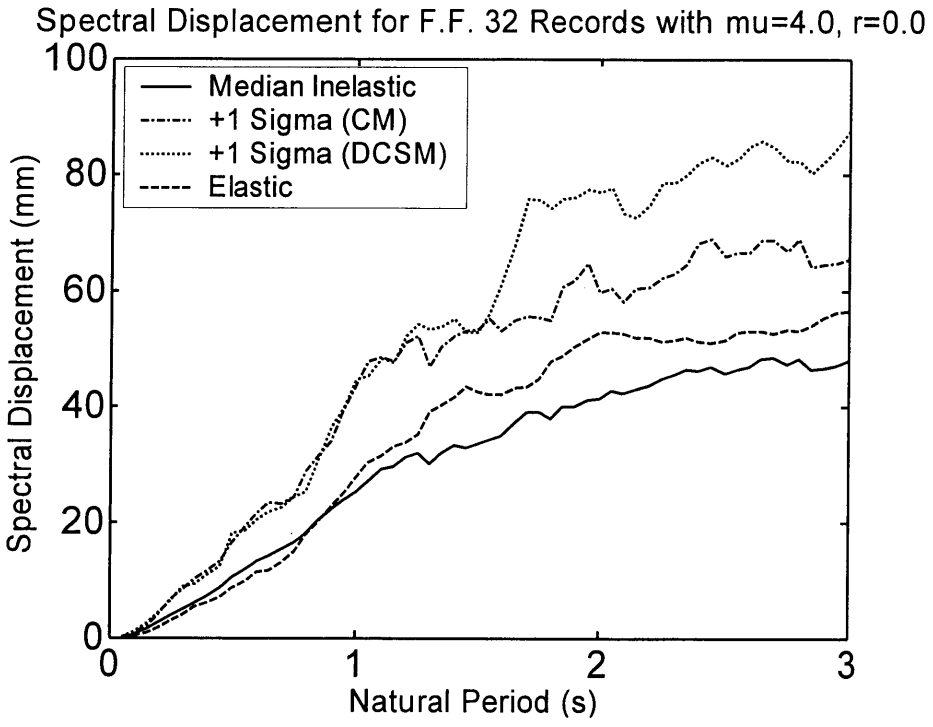

Figure 4.46. Median FF Record Displacement and the Scatter due to Perfectly Calibrated Inelastic Displacement Prediction Methods (CM and DCSM Methods) ($\mu = 4$, $r = 0$ and $\zeta_o = 2\%$)

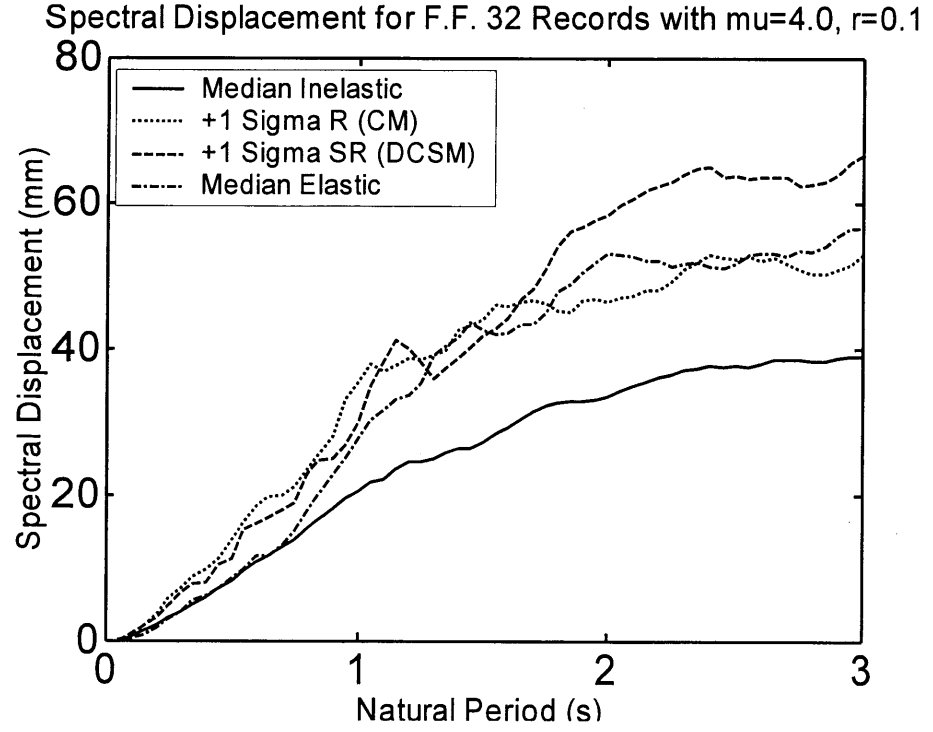

Figure 4.47. Median FF Record Displacement and the Scatter due to Perfectly Calibrated Inelastic Displacement Prediction Methods (CM and DCSM Methods) ($\mu = 4$, $r = 0.1$ & $\zeta_o = 2\%$)

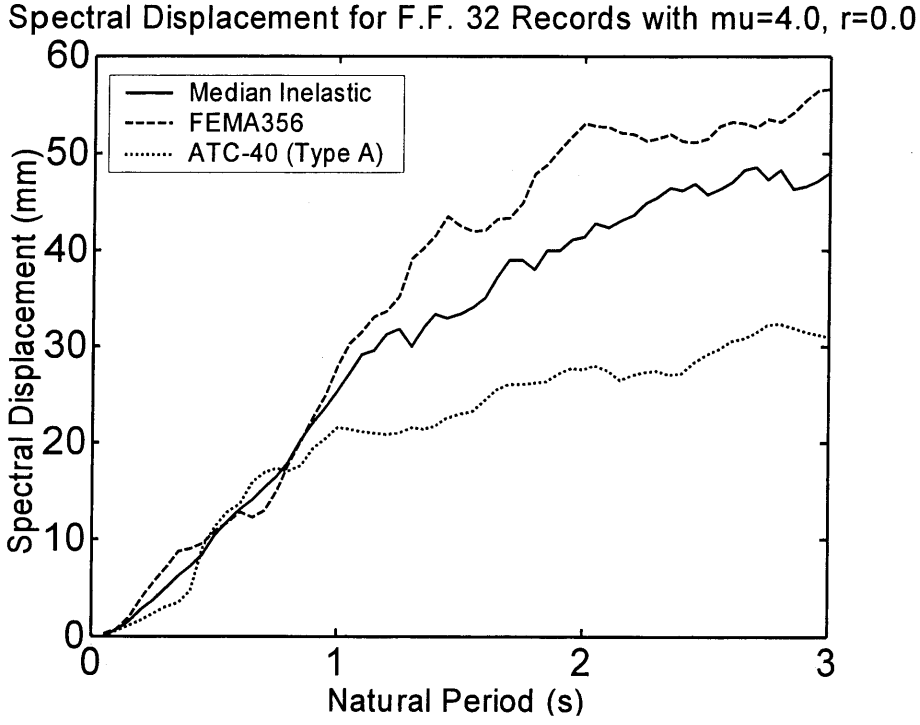

Figure 4.48. Median FF Record Displacement, FEMA302 CM and ATC-40 CSM Average Displacement Estimates Given Elastic Spectra ($\mu = 4$, $r = 0.0$ and $\zeta_o = 2\%$)

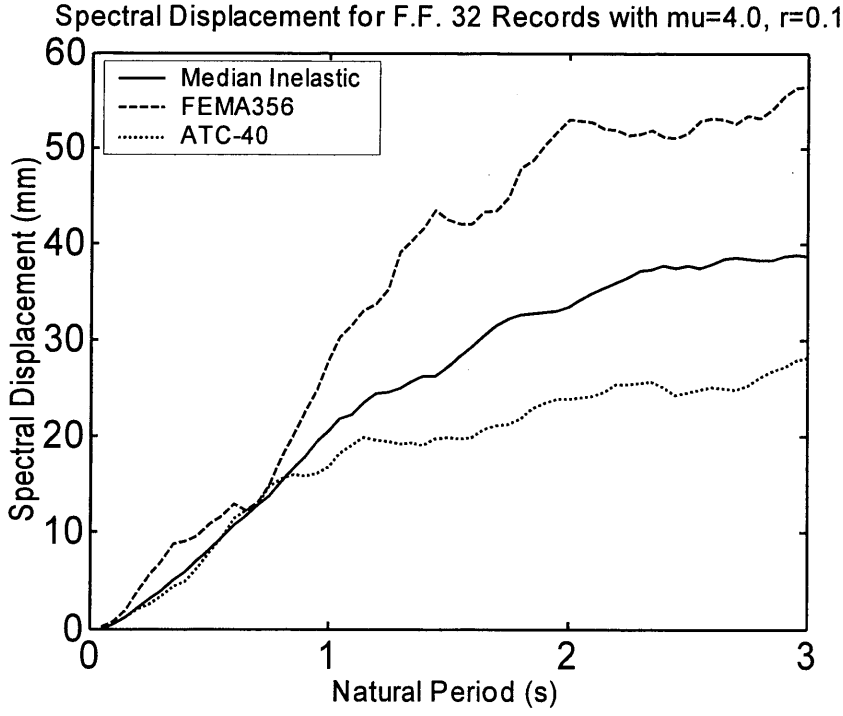

Figure 4.49. Median FF Record Displacement, FEMA302 CM and ATC-40 CSM Average Displacement Estimates Given Elastic Spectra ($\mu = 4$, $r = 0.1$ and $\zeta_o = 2\%$)

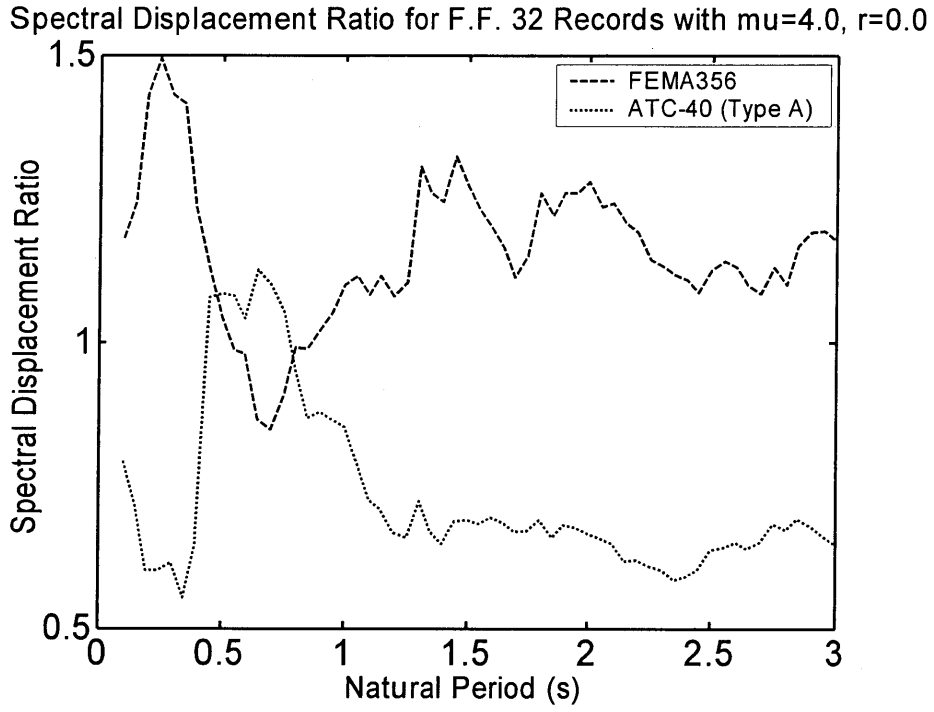

Figure 4.50. Ratio of FEMA302 CM and ATC-40 CSM Average Displacement Estimates Given Elastic Spectra to Median FF Record Displacement ($\mu = 4$, $r = 0.0$ and $\zeta_o = 2\%$)

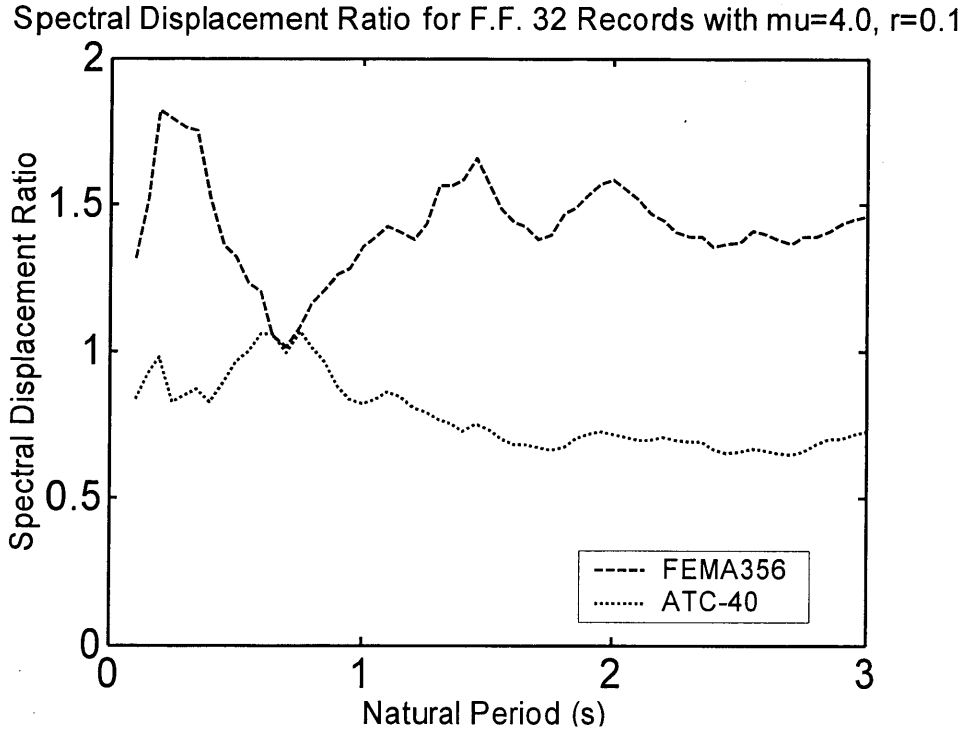

Figure 4.51. Ratio of FEMA302 CM and ATC-40 CSM Average Displacement Estimates Given Elastic Spectra to Median FF Record Displacement ($\mu = 4$, $r = 0.1$ and $\zeta_o = 2\%$)

CHAPTER 5. DISCUSSION OF BEHAVIOR AND DESIGN IMPLICATIONS

Several interesting aspects of behavior were seen in the previous analysis. This begs answers to the following questions:

1. Why does the damping curve decrease with period?
2. Why does the damping curve vary with r the way it does?
3. Why is there is little difference in the damping curve for different ductilities?
4. How does NF shaking change the estimation of effective damping?
5. How should design be carried out for PG&E structures?

5.1. UNDERSTANDING EFFECTIVE DAMPING DECREASE WITH PERIOD

Two attempted methods to providing partial understanding are described below.

5.1.1. Argument based on traditional (CM-type) displacement prediction methods

i) Long Period Structures:

If it is assumed that the Equal Displacement Method (EDM) is appropriate for long period structures then the elastic and inelastic displacement response will be the same. For high strength structures, the effective damping is greater than the initial damping as shown in **Figure 5.1a**. For weaker structures, it may be seen that the total effective damping, ζ_{eff}, which would predict the peak displacement d_u is less than the initial elastic damping, ζ_o. This implies a negative hysteretic damping, ζ_{hyst}, in this case.

ii) Medium Period Structures:

If it is assumed that the EDM is appropriate for medium as well as long period structures then the elastic and inelastic response will have the same displacement as shown in **Figure 5.1b**. In this case the total effective damping, ζ_{eff}, which would predict the peak displacement d_u is greater than the initial elastic damping, ζ_o. This implies a hysteretic damping, $\zeta_{hyst} = \zeta_{eff} - \zeta_o$.

iii) Short Period Structures:

It is well known that the EDM method underestimates the displacements of short period yielding structures. The equal energy method (EEM), or even the equal acceleration method (EAM) may be appropriate for short period structures. Peak displacements will therefore be greater than d_e as shown in **Figure 5.1c**. It may be seen that a large amount of damping is required to estimate the displacements.

iv) Very Long Period Structures:

Following the EDM, the total effective damping, ζ_{eff}, which would predict the peak displacement, d_u, may be less than the initial elastic damping, ζ_o, for all ductilities implying a negative hysteretic damping, ζ_{hyst}, as shown in **Figure 5.1d**.

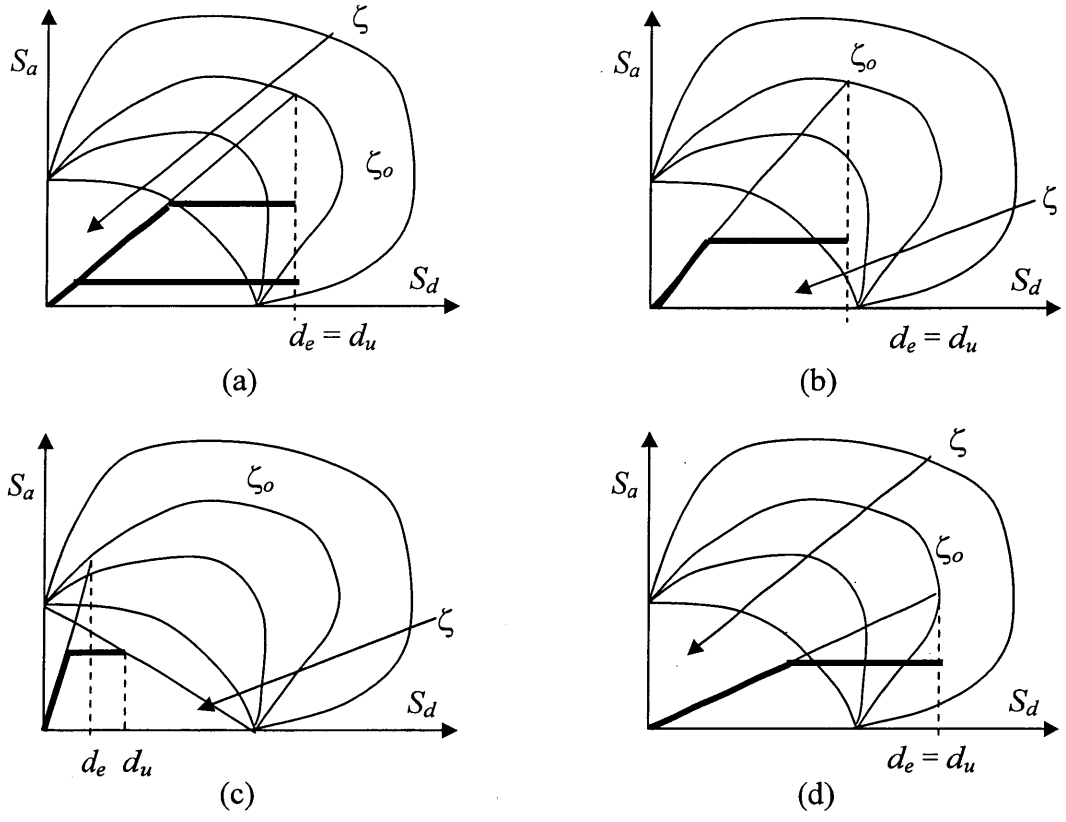

Figure 5.1. Explanation of Change in Effective Damping
with Period using Acceleration-Displacement Plots

By looking at the expected response to short, medium and long period oscillators in **Figure 5.1**, it may be seen that the effective damping should decrease with period.

5.1.2. Argument based on Trends using Artificial Records

Artificial Records may be used to understand this effective damping-period relationship. A series of artificial records are shown in **Figure 5.2**.

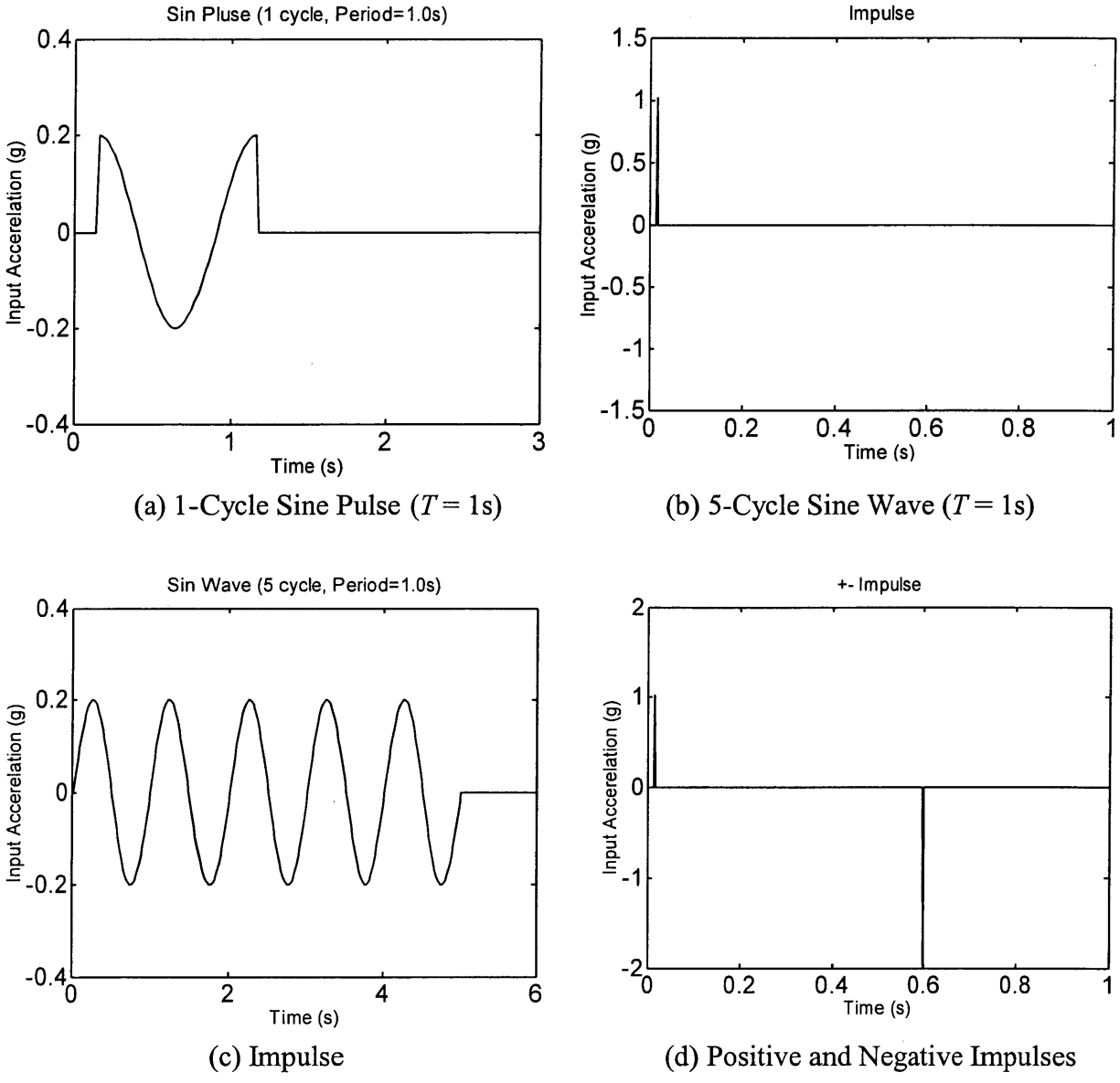

(a) 1-Cycle Sine Pulse ($T = 1$s)

(b) 5-Cycle Sine Wave ($T = 1$s)

(c) Impulse

(d) Positive and Negative Impulses

Figure 5.2. Artificial Records

The response to the artificial records is given in **Figure 5.3**. It may be seen that a wide variety of response may be obtained. All of these records have an effective damping which is less than that predicted by Gulkan and Sozen (1974) after a period of 0.7s. The pure impulse record has an effective damping of about 23% for all periods. This is similar to the estimation of 19.8% for impulses from **Equation 2.14**. The sinusoidal pulse seems to have the lowest effective damping in general. However, no simple and reasonable relationship between ductility and effective damping seems possible. This approach does not really help to explain the observed behavior.

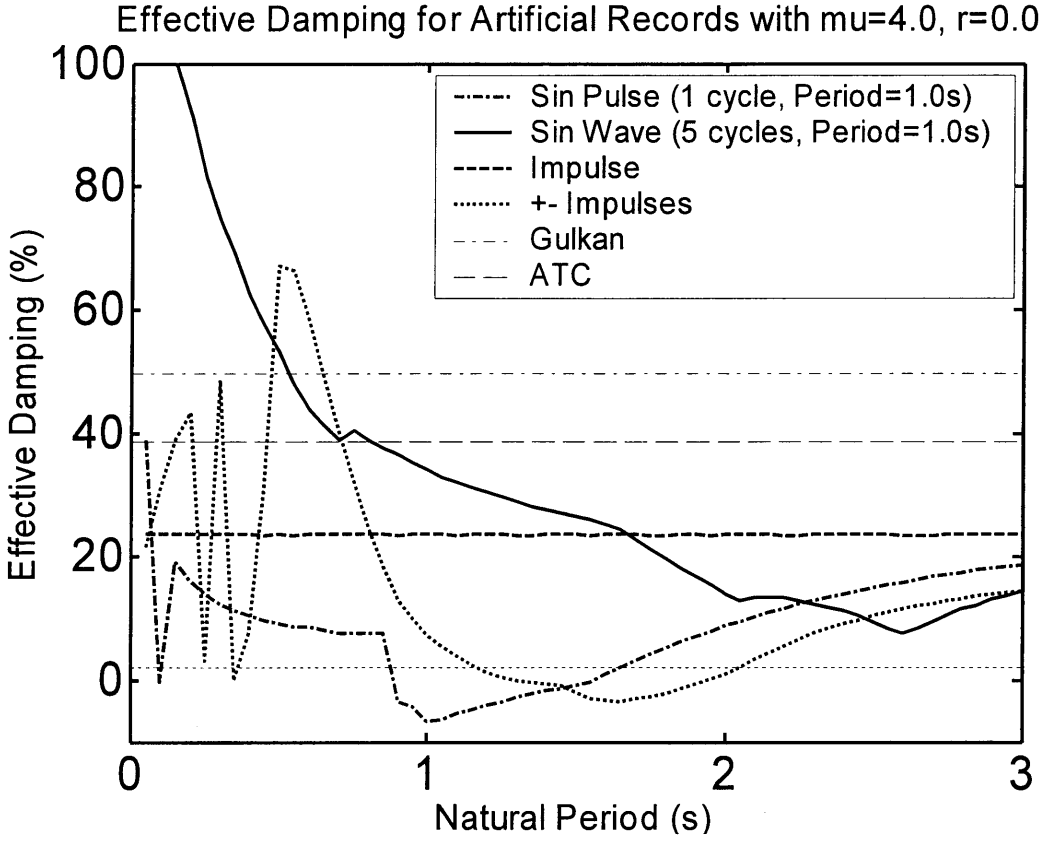

Figure 5.3. Effective Damping for Artificial Records ($r = 0.0$, $\zeta = 2\%$, $\mu = 4$)

5.2. UNDERSTANDING BILINEAR FACTOR EFFECT ON EFFECTIVE DAMPING

For a short period structure with a positive bilinear factor the change in effective damping may be understood using the similar arguments to those used above with reference to **Figure 5.4**. The damping will be less than for an EPP structure as shown in **Figure 5.4a**, and for a long period structure it will be greater as shown in **Figure 5.4b**. This is consistent with observations.

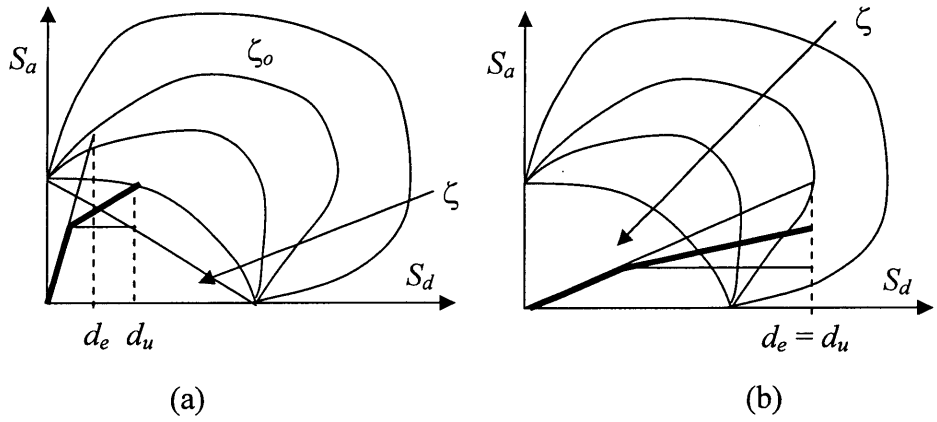

Figure 5.4. Explanation of Change in Effective Damping
with Bilinear Factor using Acceleration-Displacement Plots

5.3. UNDERSTANDING DUCTILITY EFFECT ON EFFECTIVE DAMPING

For a structure with period indicated by the diagram below, if the EDM works, then all of the structures have peak displacements which lie on the same damping curve as shown in **Figure 5.5**. In this case, damping is independent of ductility for large ductilities. This is consistent with **Figure 4.22**. For very low ductilities, such as $\mu = 1.25$ say, then the damping effect will be lower than for the higher ductilities. For shorter period structures, then damping will increase with greater ductility. The opposite is true for very long period structures.

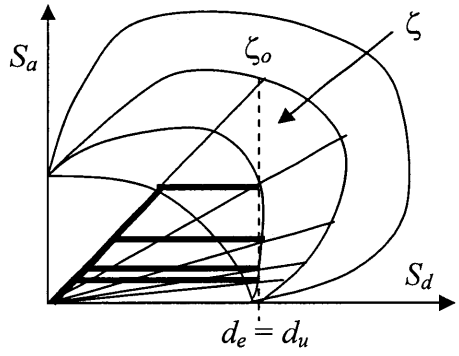

Figure 5.5. Explanation of Change in Effective Damping
with Ductility using Acceleration-Displacement Plots

5.4. UNDERSTANDING NF SHAKING EFFECT ON EFFECTIVE DAMPING

Two approaches are used to explain this:

1) **Figure 5.6** shows the elastic response spectra of the records in areas (1,1), (1,2) and (1,3). Since only the shape of these response spectra is important when looking at the response, these have been normalized to the same value at a period of 1.0s. It may be seen that the shape is similar for oscillators in all areas up to a period of about 1.5s. At greater periods, the displacement increases in the region of positive directivity. A structure subject to records in area (1,1), and in area (1,3), with the same elastic displacement, the same strength, and the same peak displacement is shown in **Figure 5.7**. Since the shape of the records is different, the oscillator subject to the (1,3) shaking is likely to require a greater effective damping to represent the oscillator behaviour well. This explanation is obviously simplistic but it may provide some insight.

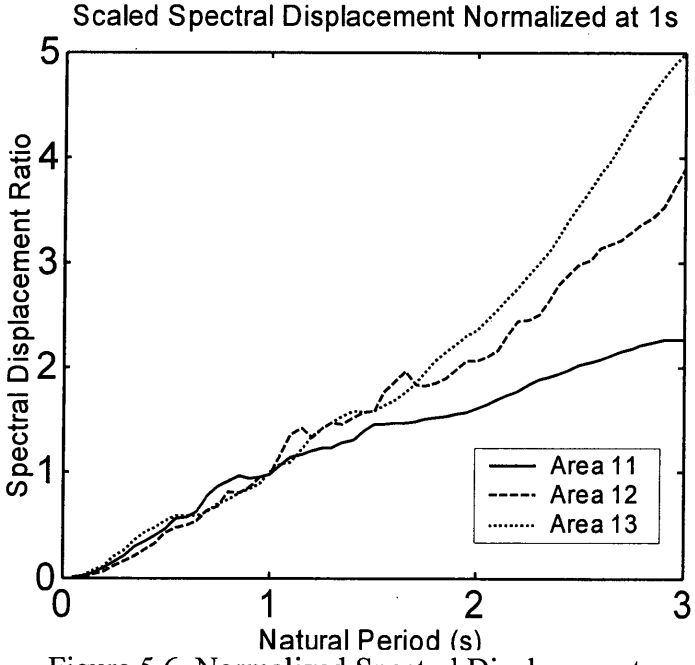

Figure 5.6. Normalized Spectral Displacements

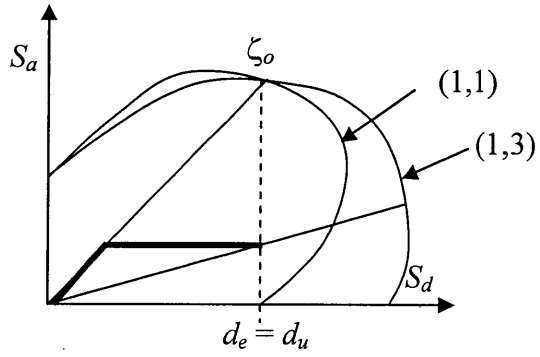

Figure 5.7. Explanation of Change in Effective Damping with Ductility using Acceleration-Displacement Plots

2) Chapter 4 showed that the behaviour of short period structures is not affected much by directivity effects. It is well known that a structures with a period shorter than the period of displacement pulse is likely to have a greater ductility for a certain response modification (or lateral force reduction factor), R, than a similar structure with a period longer than the period of the pulse. However, for an actual earthquake record, there may be significant short period shaking which will swamp the effect of the pulse for very short period oscillators. This is investigated below using an individual oscillator. An earthquake ground motion for the FF record Jap03145 (NGDC SMCAT, 1996) is given in **Figure 5.8** below. The displacement history and the acceleration-displacement plot of a short period oscillator (T = 0.05s), damping of 2% and target ductility of 4 are given in **Figures 5.9 and 5.10** for r = 0.0 and in **Figures 5.11 and 5.12** for r = 0.1 respectively. It can be seen in both cases that the oscillator has one jump in displacement which occurs at a time of about 4.5s. The oscillator inelastic response seems to be affected by a very small amount of the record which has significant is high frequency components, rather than by any long period pulse which may be present in the record. Oscillators with other periods sometimes indicated several jumps in displacement over a very short time intervals. The demands of a long period record pulse are likely to be swamped by the high frequency components for very short period oscillators and NF effects on these oscillators tend to be insignificant. It may be seen that an effective damping of 48%, computed according to Gulkan and Sozen (1974) above, overestimates the actual response and that an effective damping of 100% would give a better estimate of the actual response for the oscillator with r = 0. In this case that r = 0.1, 63% damping, rather than the ATC-40 (1997) value of 33% is needed to correctly estimate the response. The single jump in displacement is different than the more cyclic response seen for longer period 2.4s oscillator in **Figures 5.13 and 5.14** respectively. This more cyclic behavior is more representative of that assumed by Gulkan and Sozen (1974). However, it may be seen that a hysteretic damping ratio or –4.78% for the substitute structure would be necessary to capture the response. This is consistent with the decrease in damping with period shown in **Chapter 4**.

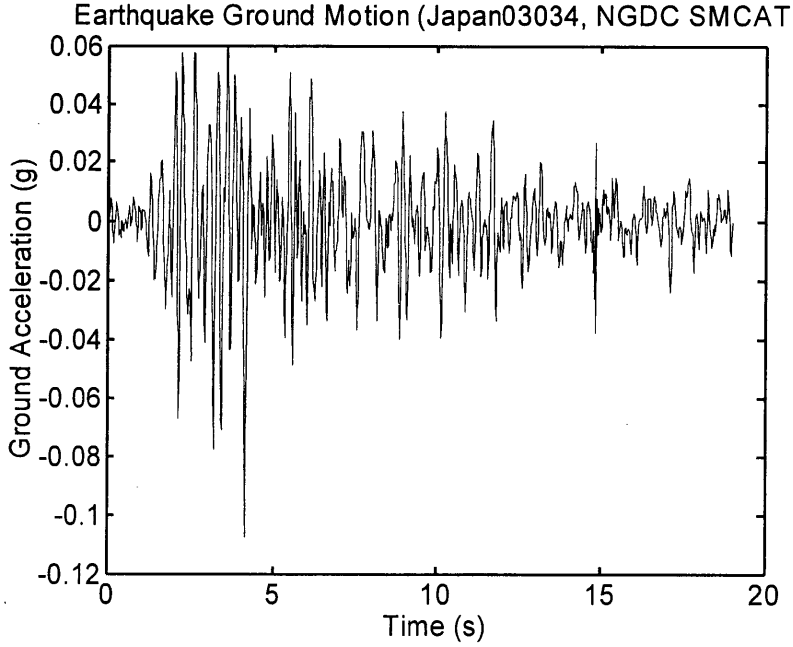

Figure 5.8. Earthquake Ground Motion (Jap03145)

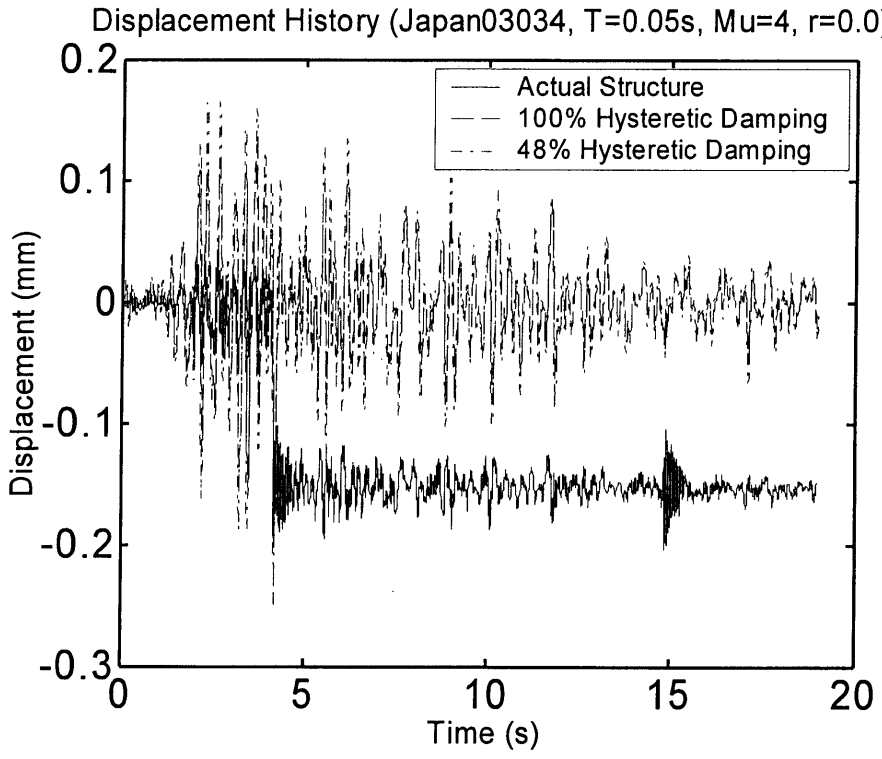

Figure 5.9. Displacement History of Oscillator ($r = 0.0$, $\zeta = 2\%$, $\mu = 4$, $T = 0.05$s)

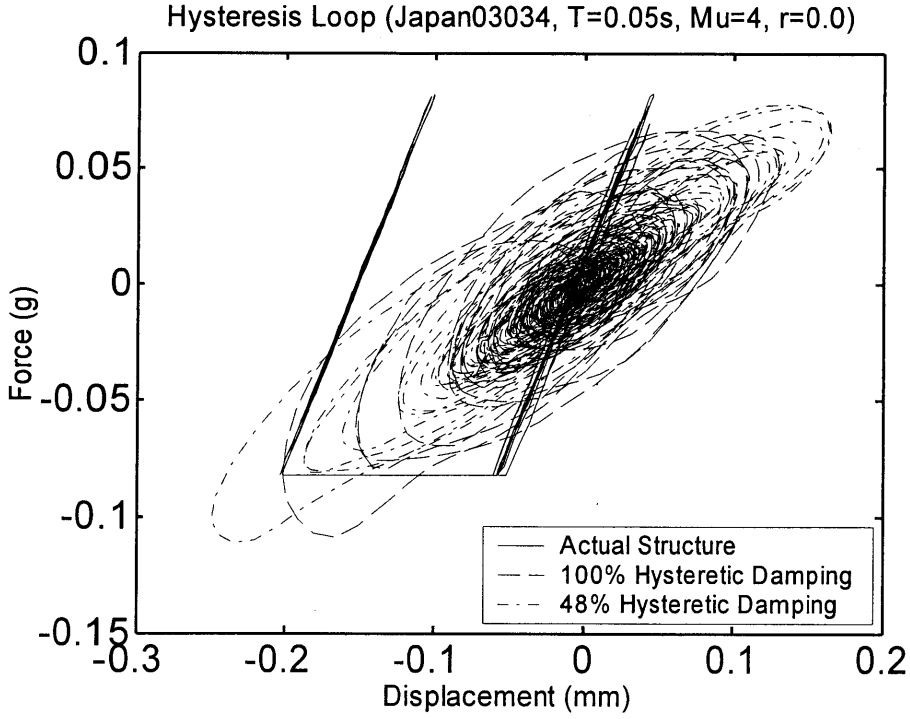

Figure 5.10. Acceleration-Displacement Hysteretic Behavior of Oscillator ($r = 0.0$, $\mu = 4$, $\zeta_o = 2\%$, $T = 0.05$s)

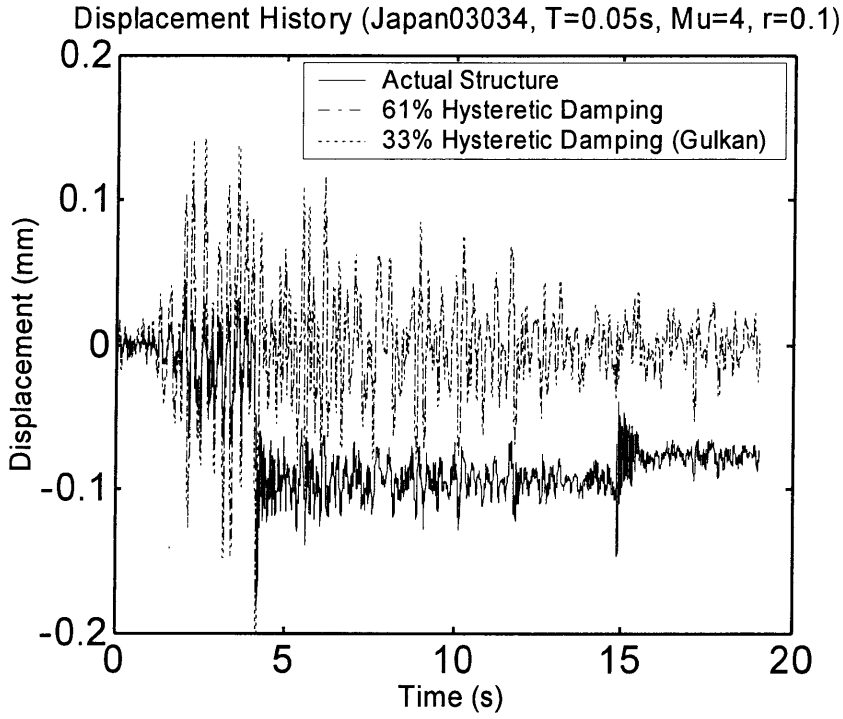

Figure 5.11. Displacement History of Oscillator ($r = 0.1$, $\zeta = 2\%$, $\mu = 4$, $T = 0.05$s)

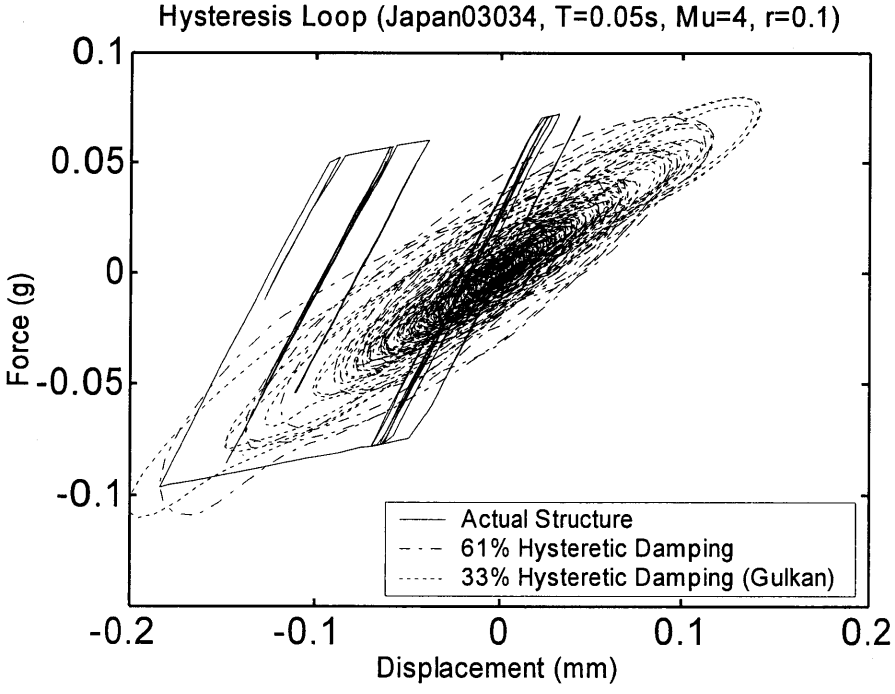

Figure 5.12. Acceleration-Displacement Hysteretic Behavior of Oscillator ($r = 0.1$, $\mu = 4$, $\zeta = 2\%$, $T = 0.05$s)

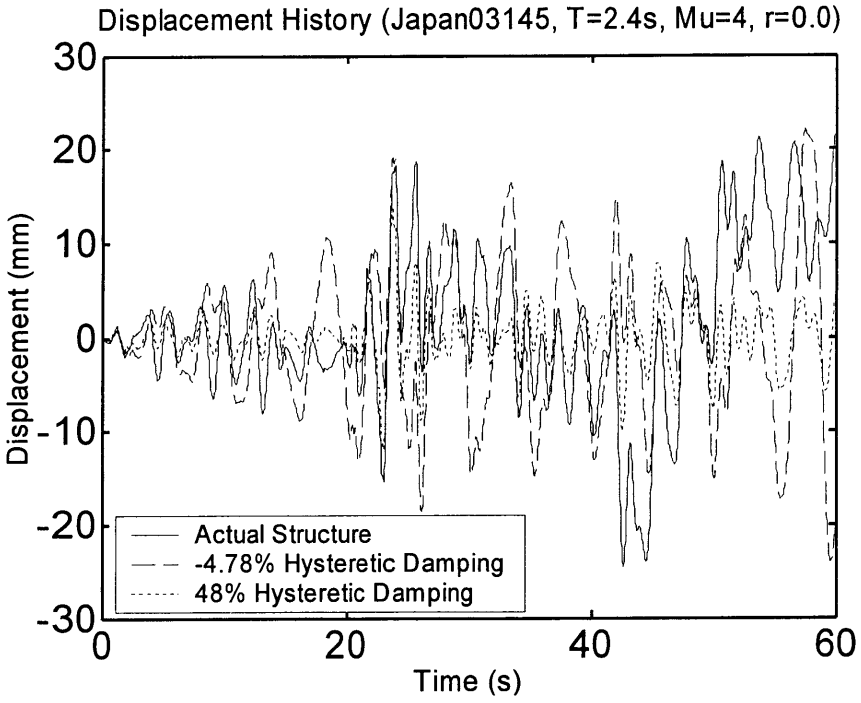

Figure 5.13. Displacement History of Oscillator ($r = 0.0$, $\zeta = 2\%$, $\mu = 4$, $T = 2.4$s)

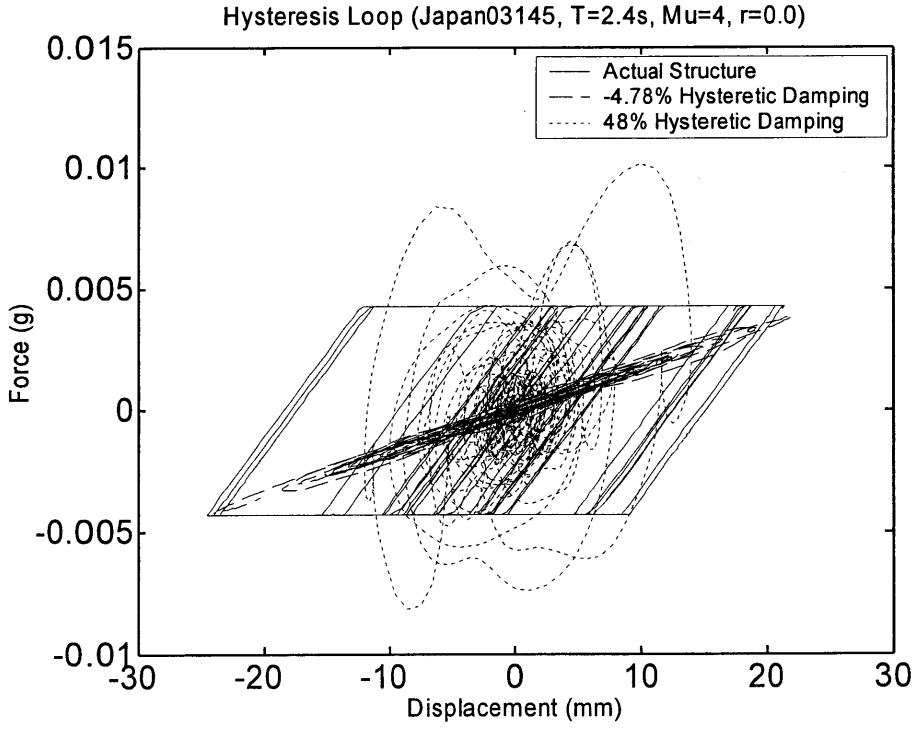

Figure 5.14. Acceleration-Displacement Hysteretic Behavior of Oscillator ($r = 0.0$, $\mu = 4$, $\zeta_o = 2\%$, $T = 2.4$s)

It was hypothesized that one possible reason for the greater demand in the short period structures was that they are affected by only a very small part of the earthquake record, as seen previously in **Figure 5.10**. However, the elastic response at the effective period of the structure is related to other parts of the record, which do not necessarily cause the response of short period structures. The effective damping required for the full record would therefore be greater than that required for the part of the record causing the inelastic demand. To evaluate how the length of the record affects the effective damping, the earthquake ground motion Jap03145 (NGDC SMCAT, 1996) is again used. The full record is referred to as ABC. The partial earthquake record is Part B, which consists of the acceleration-time record from 3.95-4.35s, as shown in **Figure 5.15**. This region, B, was responsible for the large demand seen earlier. The force-displacement curve and the acceleration-displacement plot of an oscillator with a period of 0.05s, damping of 2% and target ductility of 4, are given in **Figures 5.16 and 5.17** respectively to record B only. The oscillator has one jump in displacement and the same displacement as that seen previously. Again a damping ratio for the partial record of 100% is required, which is the same as that for the full record. **Figure 5.17** shows that there is a difference in response from the full record (ABC) and for the short portion (B) only. However, for short period structures, the curves show very similar response. It seems that the length of the record used in the analysis is not important for this short-period oscillator. This hypothesis to explain why shorter period structures have higher damping therefore falls apart. In **Figures 5.10 and 5.16**, for the yielding oscillator the force vs. displacement term is shown and for the equivalent elastic oscillator, the hysteretic damping, ζ_{hyst}, and elastic, $\omega^2 u$, terms only of the equation of motion, given below, are shown.

$$\ddot{u}_t + \zeta_o \dot{u} + \zeta_{hyst} \dot{u} + \omega^2 u = 0 \tag{5.1}$$

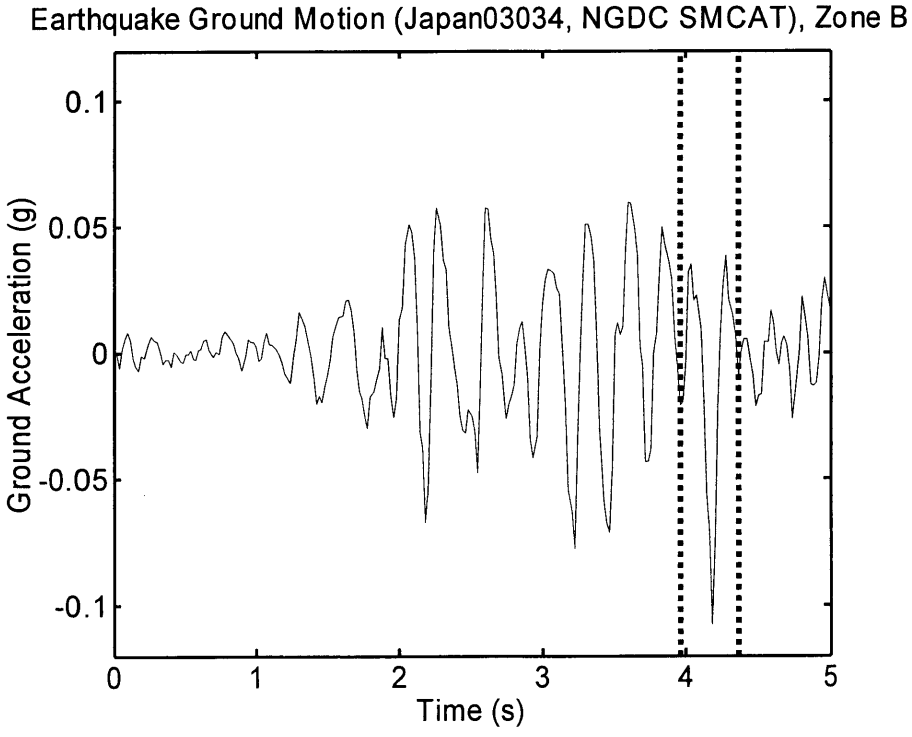

Figure 5.15. Splitting Up Ground Motion into Zones A, B, C

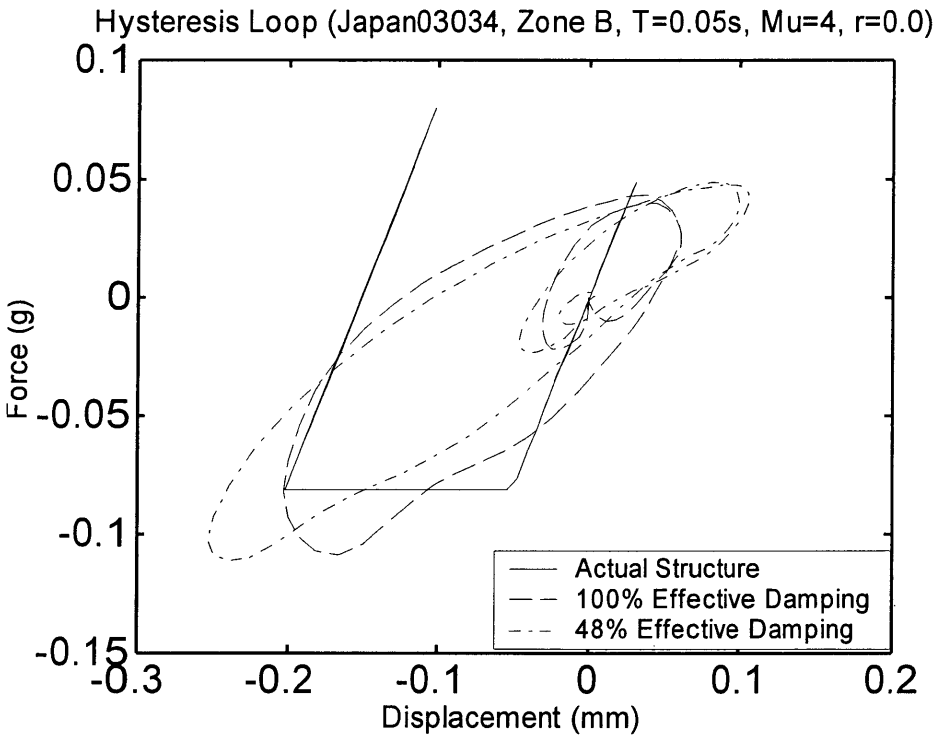

Figure 5.16. Acceleration-Displacement Hysteretic Behavior of Oscillator Elastic and Hysteretic Damping Terms Shown ($r = 0.0$, $\zeta_o = 2\%$, $T = 0.05$s) for Record B

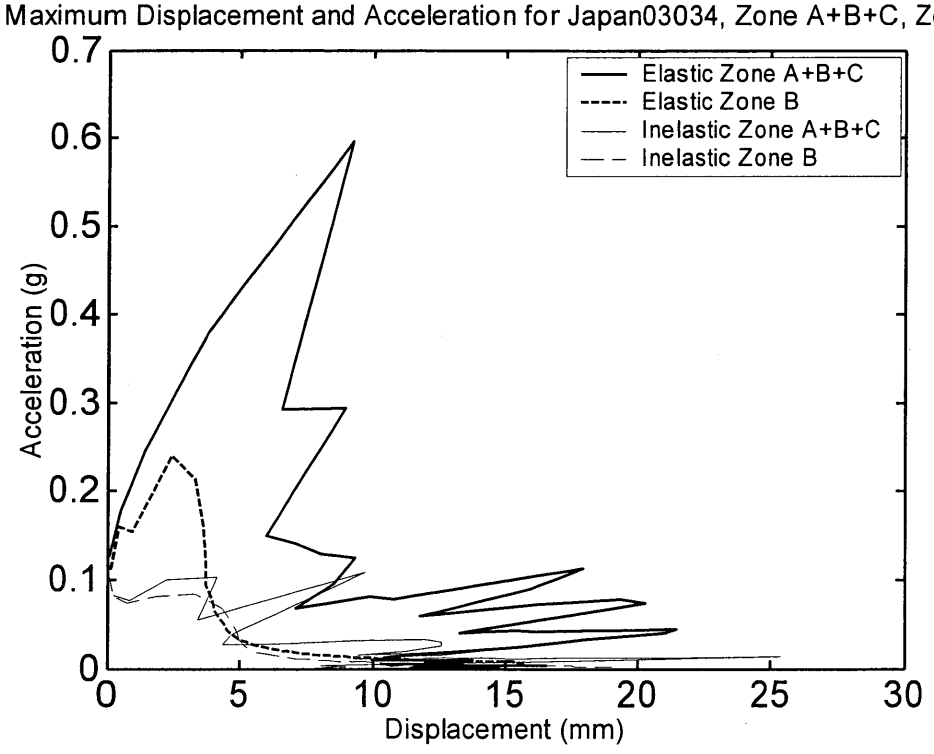

Figure 5.17. Elastic and Inelastic Response with Zones ABC and B ($r = 0.0$, $\zeta_o = 2\%$)

5.5. DEVELOPMENT OF DESIGN METHODOLOGY

5.5.1. Decisions Regarding Design Methodology

Based on discussion with PG&E and with Ronald Hamburger in May 2001, it was decided that the following approach should be recommended for PG&E.

a) Method for Estimating Inelastic Displacements

Estimation of inelastic displacements for design and evaluation of structures should be made with the Coefficient Method (CM), (FEMA356, FEMA273), rather than with the CSM. This was because:

1. Design by the CM (FEMA356) rather than the CSM (ATC40) is the way design is likely to go in the future.
2. The CSM (ATC40), is not necessarily conservative for short period structures ($T < 0.7s$) and it is quite non-conservative for longer period ($T > 0.7s$) structures using the current ATC40 equations.
3. It may be difficult to come up with simple and reasonable SR-ζ and ζ-μ relationships.
4. The CSM produces greater variation in response for structures with a fundamental natural period, T, greater than about 1.5s.

b) Method for Modeling Mill-Type Buildings

While there are many ways that we can model the structure including full LDP, simplified LDP or NSP. Only the full 3-D LDP should be used for assessment. This is because other methods are too simplistic to capture all of the likely 3-D behavior which includes torsion, roof diaphragm action, breathing and roof displacement modes. A 3-D NDP can not be carried out easily by consultants or researchers. Also, the full LDP takes only 2-3 days for the input and analyses by experienced users so it is not overly expensive or time consuming.

5.5.2. Methodology to Assess Inelastic Demand at a Site

A method to determine the likely average demand on a SDOF structure due to near-fault ground shaking, as well as a demand level which provides a consistent factor of safety to that of existing methods, is described below.

(a) Average Demand

The average demand may be computed using the parabolic or bilinear approximation to the actual demand. The bilinear relationship only is shown below due to its simplicity. Using the empirical relationship between T_o and μ from **Equation 4.1b**, the C_μ-R or C_I-R equation is given in **Equations 5.2 and 5.3**. In this equation the unknown γ, may be found from **Figure 4.6**.

$$C_I = d_u/d_e = \mu/R = \frac{1+(R-1)\left(\frac{T_o}{T}\right)}{R} \geq R^{\frac{1}{\gamma}-1} \qquad (5.2)$$

$$C_I = d_u/d_e = \mu/R = \frac{1+(R-1)\left(\frac{0.123\mu^{0.77}}{T}\right)}{R} \geq R^{\frac{1}{\gamma}-1} \qquad (5.3)$$

It may be seen that use of this equation is already complicated for short period structures since μ appears in **Equation 5.3** and iteration is needed. Fortunately, it is seldom necessary to calculate the demand for short-period structures due to NF shaking since it was shown in **Figure 4.17** that for periods less than 0.8s NF effects can be ignored.

(b) Design Level Demand

For design, it is desirable to modify the demand from far-fault shaking to include near-fault effects. To provide a similar level of conservatism to that used in present design, we can take find the design displacement for any records, $d_{u,design}$, be they near fault or far fault as:

$$d_{u,design} = \frac{d_{u,design,\ standard\ records}}{d_{u,\ average,\ standard\ records}} \times d_{u,average\ for\ record\ type\ considered} \qquad (5.4)$$

where $d_{u,design,\ standard\ records}$ is the standard design level shaking displacement according to the specification being used. This is probably from the equal displacement method (EDM) for far-fault longer period structures in countries following that approach. The average likely design level displacement for normal records, $d_{u,\ average,\ standard\ records}$, may be found from analysis of records as may the average ultimate displacement $d_{u,average\ for\ record\ type\ considered}$ for the record type considered.

In the context of FEMA356 it may be written as:

$$d_{u,design} = d_{u,design,\ standard\ records} \times \frac{C_{1\ average\ for\ record\ type\ considered}}{C_{1\ average,\ standard\ records}} \tag{5.5}$$

For long period earthquake records, if the average value of γ for standard records can be taken as that for FF records, then

$$d_{u,design} = d_{u,design,\ standard\ records} \times \frac{R^{1/\gamma-1}_{\ average\ for\ record\ type\ considered}}{R^{1/\gamma-1}_{\ average,\ standard\ records}}$$

$$= d_{u,design,\ standard\ records} \times R^{1/\gamma_{NF}-1/\gamma_{FF}} \tag{5.6}$$

Since, γ for far fault records is 1.12, then

$$d_{u,design} = d_{u,design,\ standard\ records} \times R^{1/\gamma_{NF}-1/\ 1.12} \tag{5.7}$$

$$= d_{u,design,\ standard\ records} \times R^{1/\gamma-0.893} \tag{5.8}$$

Alternatively, C_1, for NF shaking could be obtained as

$$C_{1,NF} = C_{1,FF}\, R^{1/\gamma-0.893} \tag{5.9}$$

To determine whether or not a structure is a short period one it is necessary to compute μ as

$$\mu = d_u/d_y \tag{5.10}$$

And T_o for FF records as:

$$T_o = 0.123\mu^{0.77} \tag{4.1b}$$

From **Equation 2.36**, the long period part of the response will control if the period, T, is greater than the value where the short period and long period lines intersect, T_{int}.

$$T_{int} = \frac{(\mu^{\gamma}-1)}{(\mu-1)} T_o \tag{5.11}$$

A general expression for C_1 due to NF shaking can therefore be developed:

$$C_{1,NF} \begin{cases} = C_{1,FF}\, R^{1/\gamma-0.893}, & \text{for } T \geq T_{int} \\ = C_{1,FF}, & \text{for } T < T_{int} \end{cases} \tag{5.12}$$

A slightly more simple and more conservative method for assessment of NF demand would be to multiply $C_{1,FF}$ by $R^{1/\gamma-0.893}$ for structures of all periods.

5.5.3. Inelastic Demand in Multi-Element Structures

The FEMA356 (or FEMA273) LDP procedure has some limitations, and care must be made when using this procedure using the CM described above. This is because the mill type structures owned by PG&E are multi-degree of freedom (MDOF) multi-element structures and a method, based on the behavior of SDOF oscillators is used to estimate the inelastic behavior of the MDOF structures. Obviously, since this is an approximation, some aspects of the behavior will be lost. However, one particularly important aspect of the behavior may be lost which is described below (MacRae and Unocic, 2002). This is related to the difference between member and system ductility which is reflected in the *m*-factor approach in the FEMA356.

According to the FEMA356 member acceptance criteria the "component or element demand modifier to account for ductility", *m,* which represents the *member ductility capacity* must be greater than the "deformation-controlled design action due to gravity loads and earthquake loads", Q_{UD}, divided by the "knowledge factor", κ, and the "expected strength", Q_{CE}, as given in **Equation 5.13**. Here, κQ_{CE} can be regarded as the likely estimate of the component yield strength, and Q_{UD} represents the force that would produce the expected total deformation if the system remained elastic. This is a fictitious force. If we divide the force in the top and denominator by the stiffness of the element then the equation may be modified to that given in **Equation 5.13** where d_y is the member yield displacement. The value of d_u shown below is not the member displacement demand. It is $C_1C_2C_3$ multiplied by the displacement of the element if that element were assumes to remain elastic, d_{ec}, under the expected earthquake level shaking. This assumes that all elements of the structure have their elastic displacements enhanced by the same factor; $C_1C_2C_3$. However, once some elements start to yield, other elements (whether they be force or deformation controlled) do not yield since the force on them does not necessarily increase. The increase in deformation is therefore not shared equally by all the elements of a frame but it is concentrated in specific elements. The present FEMA356 approach is therefore unsafe in its application of inelastic design concepts to structures.

$$m > \frac{Q_{UD}}{\kappa Q_{CE}} = \frac{C_1C_2C_3\, d_{ec}}{d_{yc}} \qquad (5.13)$$

It is necessary for reasonable design that the *member* demand should be compared to the *member* capacity for consistent design. The present requirement, in which the *member ductility capacity*, *m,* is compared with $C_1C_2C_3d_{ec}/d_{yc}$ is unsafe.

The reason for the inconsistency of the FEMA356 method is related to the difference between member and system ductilities. This difference is (i) described below for a simple cantilever column on a soft foundation, then it is (ii) described in a way which will allow engineers to see the error in the FEMA356 method.

(a) Difference between Member and System Ductilities

Figure 5.18 shows that the yield displacement of the column-foundation system, d_{ys}, is equal to the sum of the displacement at the top of the column due to the elastic displacement of the

column at the ground surface, d_{fd}, the displacement at the top of the column due to the elastic rotation of the column at the ground surface, $d_{f\theta} = \theta_f L$, and the yield displacement of the column, d_{yc}, as given below. Here d_f, which is equal to $d_{fd} + d_{f\theta}$, is the elastic column displacement due to only foundation flexibility.

$$\begin{aligned} d_{ys} &= d_{fd} + \theta_f L + d_{yc} \\ &= d_{fd} + d_{f\theta} + d_{yc} \\ &= d_f + d_{yc} \end{aligned} \tag{5.14}$$

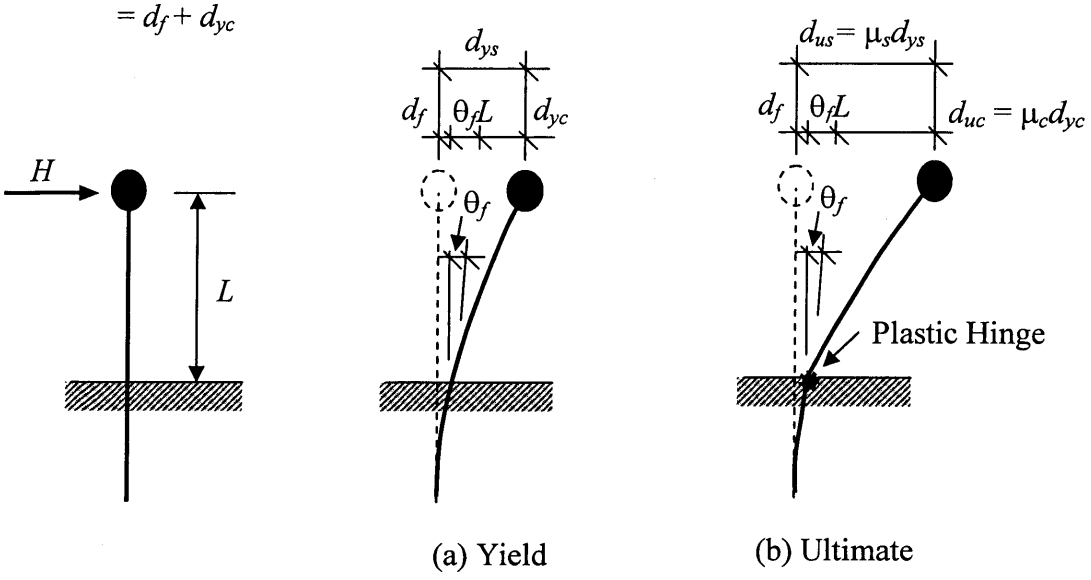

(a) Yield (b) Ultimate

Figure 5.18. Monotonic Behavior of Inelastic Column on Flexible Foundation

If the soil remains elastic and only the column deforms inelastically without strain hardening, then the total displacement, d_{us}, is due to the elastic displacement of the foundation, d_f, plus the inelastic displacement of the column, $\mu_c d_{yc}$, where μ_c is the column ductility demand as:

$$d_{us} = d_f + \mu_c d_{yc} \tag{5.15}$$

Since d_{us} may also be expressed in terms of the system displacement ductility, μ_s, as:

$$d_{us} = \mu_s d_{ys} \tag{5.16}$$

the system ductility, μ_s, may be related to the column displacement ductility demand, μ_c, as:

$$\begin{aligned} \mu_s &= d_{us}/d_{ys} \\ &= (d_f + \mu_c d_{yc})/d_{ys} \\ &= (d_f + d_{yc} + (\mu_c - 1)d_{yc})/d_{ys} \\ &= (d_{ys} + (\mu_c - 1)d_{yc})/d_{ys} \\ &= 1 + (\mu_c - 1).d_{yc}/d_{ys} \end{aligned} \tag{5.17}$$

Alternatively, this equation may be written to give μ_c as:

$$\mu_c = 1 + (\mu_s - 1).d_{ys}/d_{yc} \tag{5.18}$$

The column ductility demand, μ_c, for a yielding structure ($\mu_c > 1$) is greater or equal to the system displacement demand, μ_s, because the structure-foundation system yield displacement, d_{ys}, is always greater than the yield displacement of the column alone, d_{yc}.

For a 25m tall cantilever bridge column described in the 1990 Japanese bridge code (JRA, 1990), the displacement at the top of the column due to column and soil deformation, d_{ys}, when the yield force, H_y, was applied was 35.5mm (MacRae and Kawashima, 1993). The deflection of the column alone, d_{yc}, was 5.1mm. If the column is strong enough to resist a response acceleration, a_y, of $0.333g$ at the onset of yield, and the response acceleration for elastic response, a_e, is $1.0g$, then the columns have a lateral force reduction factor, $R = H_e/H_y = (ma_e)/(ma_y) = a_e/a_y$ of 3. The system ductility demand, μ_s, in this code is estimated by the equal energy method as $\mu_s = (R^2 + 1)/2 = (3^2 + 1)/2 = 5$. According to **Equation 5.18**, the column ductility demand, $\mu_c = 1 + (\mu_s - 1)d_{ys}/d_{yc} = 1 + (5 - 1)$ x 35.5mm/5.1mm = 28.8. This column displacement ductility demand, μ_c, of 28.8 is 5.8 times more than the system displacement ductility demand, μ_s, of 5. When the column is tested alone on a rigid foundation, it should perform well under a displacement of not $\mu_s d_{yc} = 5$ x 5.1mm = 25.5mm, but of $\mu_c d_{yc} = 28.8$ x 5.1mm = 147mm to ensure that it will behave well on its flexible foundation during the design level earthquake.

Conversely, if the same column has been subject to laboratory tests on a rigid foundation and has a displacement capacity of 25.5mm, then the column ductility capacity, μ_c, is 25.5mm/5.1mm = 5. According to **Equation 5.17**, the maximum system displacement ductility demand, μ_s, for such a column on the foundation described previously, μ_s, is 1 + (5 – 1) x 5.1mm/35.5mm = 1.57 and an appropriate lateral force reduction factor should be used for design.

The difference between system and member ductilities for structures on a flexible foundation, is not a new concept. The need for it to be included in design or testing methods has been described by many authors (Discussion Group 1980, Priestley and Park 1987, MacRae, Carr and Walpole 1990, MacRae and Kawashima 1990, Dodd 1992, Priestley et al. 1992, and MacRae and Kawashima 1993, Priestley et al. 1996). The New Zealand Bridge Manual (Transit 1994) requires that this difference in member and system ductilities be considered explicitly in design. However, a number of codes in which ductility concepts are used in design (AASHTO 1994, ATC-32 1996, JRA 1996 and ICC 2000) do not consider this difference. Recently, MacRae and Unocic (2001) have shown that foundation damping effects do not significantly change the large demands expected in these oscillators.

(b) Effect of Difference between Member and System Ductilities on FEMA356

FEMA356 requires that the member ultimate displacement capacity be estimated as an amplification factor multiplied by the elastic displacement of the member. To illustrate this effect we will use the bridge column described above.

According to the equal energy method, the ratio of inelastic system displacement to elastic system displacement is $d_u/d_e = \mu/R = 5/3 = 1.67$ in the example above. Therefore $C_1C_2C_3 = 1.67$. The displacement of the system if it were to remain elastic is $d_{es} = Rd_{ys} = 3$ x 35.5mm = 106.5mm. The displacement of the column alone if the system were to remain elastic is $d_{ec} = Rd_{yc}$ = 3 x 5.1mm = 15.3mm.

The expected system inelastic displacement, d_{us}, is given below. It is the same using basic kinematic principles or using the FEMA356 approach.

$$d_{us} = C_1C_2C_3.d_{es} = \mu/R.d_{es} = 1.667 \text{ x } 106.5\text{mm} = 177.5\text{mm}.$$

The actual member total displacement demand, d_{uc}, is

$$d_{uc} = \mu_c d_{yc} = 28.8 \text{ x } 5.1\text{mm} = 147\text{mm}$$

This member total displacement demand may also be computed as:

$$d_{uc} = d_{us} - d_f = 177.5\text{mm} - (35.5\text{mm} - 5.1\text{mm}) = 147\text{mm}$$

The FEMA356 estimate of system displacement is

$$d_{uc,FEMA} = C_1C_2C_3.d_{ec} = 1.667 \text{ x } 15.3\text{mm} = 25.5\text{mm}.$$

It is obvious that the FEMA356 LDP/LSP approach to estimate the ultimate deformation capacity of the system is flawed. In the case shown above, it estimates a displacement of $d_{uc,FEMA}/d_{uc}$ = 25.5mm/147mm = 17.3% of the total member displacement. In other words, the actual demand is 5.8 times greater than the FEMA356 demand. This is the same value as that given for the difference between member and system ductility demands in the example above.

The argument outlined above is as true for mill structures as it is for bridge columns. For example, if the maximum deflection of a mill-type structure occurs at the center of an out-of-plane wall then the side wall in-plane deformation, the roof in-plane deformation and the long wall out-of-plane deformation may contribute to the total deflection. When one element yields, the ductility of the yielding element may be found using **Figure 5.19**.

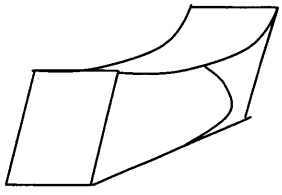

Figure 5.19. Contributions of Deformation in a Mill Structure

$$\mu_c = 1 + (\mu_s - 1)d_{ys}/d_{yc} \qquad (5.19)$$

5.5.4. Connection Strength

Connections are force controlled elements according to FEMA356. The connection between the wall and the roof and wall to columns should have sufficient strength to allow the yielding mechanism of the wall to be achieved since the connection displacement capacity is very small. It should be designed for the minimum of the elastic design force under the level of earthquake to be considered, or the maximum force that may be delivered from the wall.

If the wall has low flexural restraint at the top and bottom and one-way action is assumed, then the maximum uniformly distributed load is given below:

$$w = 8M_{max}/L^2 \tag{5.20}$$

where M_{max} is the maximum flexural capacity of the wall. The shear at the top and bottom of the wall is:

$$\begin{aligned} V_{max} &= wL/2 \\ &= 4M_{max}/L \end{aligned} \tag{5.21}$$

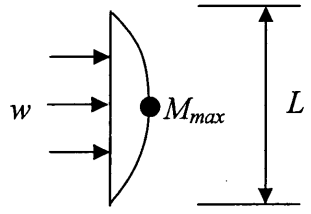

Figure 5.20. Loads on Yielding Wall with Little Restraint

The connection between the roof and wall must sustain this shear so the connection force, $F_{connection}$, is:

$$F_{connection} = \min \begin{cases} V_{max} \text{ due to wall yielding} \\ V_{elastic} \text{ from elastic LDP analysis} \end{cases} \tag{5.22}$$

FEMA273 also includes a modification factor, J, for the $V_{elastic}$ factor. This factor was the subject of much debate as described in the FEMA 273 commentary and it is believed that it should not be used in design.

FEMA356 Section 2.6.7.2 is different from FEMA273 and the wall and its connection to the structure is required to remain nominally elastic and the design strength of the wall is given as:

$$F_p = \chi S_{XS} W$$

5.5.5. Example of Assessment of Mill-Type Structures

A design example is beyond the scope of what was required for this project. However, it was felt that an example of the possible application of the methods developed in this report to mill-type structures would be useful.

The example given below is provided to illustrate how the design methods may be applied for NF shaking, how the difference between member and system ductility demand may be explicitly considered, and how the design force for connections may be obtained. In order to highlight these points a simplistic (and probably non-realistic) structure was chosen. This was carried out on purpose since real structures are complex and details of design for near fault shaking could easily become swamped in the other details. It is reemphasized that the example given below does not represent Berkeley F substation or any other structure owned by PG&E. Sizes of the walls, their strengths and their stiffnesses are also not necessarily realistic.

Also, the FEMA356 CM provisions are applied in a displacement format in the example below. Professional engineers are more likely to follow the "force format" for the CM in the FEMA356 code. The displacement format was used since it is believed that by looking at displacements a better understanding of the structural behavior is obtained. It is a more explicit "displacement-based design" than that required by FEMA356. Using displacements allows the difference between member and system ductility demands to be more easily obtained. Furthermore, it has already been noted that the "force format" formulation for estimation of inelastic demands in FEMA356 for multi-element structures may be non-conservative.

Problem: A mill type structure with a wall height of 30ft and a length in both directions of 60' is analyzed. The wall thickness is 4.25in on average. Some lightweight steel columns embedded in the wall help support the roof but their stiffness is negligible compared to that of the concrete. Walls are considered to span one-way between the foundation and the roof. Elastic spectra for the shaking is the 2in50 record representing the collapse prevention performance level of **Figure 2.14**. *(It should be noted that FEMA356 requires that the site-specific response acceleration parameters for the BSE-2 Earthquake Hazard Level shall be taken as the smaller of (a) the values of the parameters from mean probabilistic site-specific spectra at the 2%/50 year probability of exceedance, and (b) the values of the parameters from 150% of median deterministic site-specific spectra. In this case the median deterministic site-specific spectra was not available so the 2%/50 year probability of exceedance spectra was used).* It is considered that the structure was close to the fault but that it may be as far as 30km from the epicenter for evaluation of the inelastic demand.

Elastic Analysis Results: The FEMA356 LDP approach is followed and an elastic model is constructed using stiffnesses of the cracked members where appropriate. The effective fundamental natural period, $T = T_e$, is 0.2s. This mode corresponds to significant wall out of plane movement and some roof movement. If **Figure 2.14** is used, the spectral acceleration is approximately 2.4g. The peak displacement of the structure from the elastic modal analysis of the structure considering the modal mass participation occurs at the center of the wall and it is d_{es} = 0.94in. The roof above the wall moves 0.32in at this peak wall displacement so the wall mid-height deflection due to roof in-plane deformation is 0.16in and the elastic displacement of the wall if the system remains elastic, d_{ec}, is 0.94in-0.16in = 0.78in.

Assessment of Performance: Initial analysis indicates that the in-plane strength of the wall and the strength of the roof are sufficient to remain elastic under the expected excitations. Also, no sliding of the walls on the floor of the structure is expected since the connection strength is sufficient. The only part of the structure expected to sustain significant deformation is the wall due to its out-of-plane deformation. The yield displacement of the wall alone, considering its height and sparse reinforcing, and the cracked stiffness of the wall of $0.5E_cI_g$ according to FEMA356, is 0.30in.

The total displacement at the wall mid-height at wall yield is equal to the yield displacement of the wall itself plus the proportion of the displacement at the center of the wall associated with roof deformation at the level of shaking causing wall yield.

d_{ys} $= d_{yc} + d_f$ $= 0.30\text{in} + 0.16\text{in}$ (*0.30in/0.78in)
$= 0.30\text{in} + 0.061$ $= 0.361\text{in}$

Here, d_{ys} could also have been calculated as 0.94in*0.30in/0.78in.

a) The Wall Itself

The lateral force reduction factor for the system, R, is $F_e/F_y = d_{es}/d_{ys} = 0.94\text{in}/0.361\text{in} = 2.6$. According to FEMA356, $T = T_e = 0.2\text{s}$, and the characteristic period of the response spectrum, which is the transition from constant acceleration to constant velocity, is estimated as $T_s = 0.8\text{s}$ from **Figure 2.14**. The NSP C_1 factor, rather than the LSP or LDP C_1 factor should be used since the LSP or LDP C_1factor approaches do not converge to the correct value as R approaches unity.

$$C_1 = \frac{1+(R-1)\left(\frac{T_S}{T}\right)}{R} \geq 1$$

$$= \frac{1+(2.6-1)\left(\frac{0.8s}{0.2s}\right)}{2.6} = 2.84 \geq 1$$

It should be noted that this value of 2.84 is much greater than the artificial limit of $C_1 = 1.50$ in the FEMA356 LSP. The values of C_2 and C_3 are equal to 1.0 for the framing type used.

Since the period of the frame is less than 0.8s, no consideration for NF effects on the inelastic response are required. However, for the sake of illustration, it is assumed that it is not known whether NF shaking is going to change the inelastic response or not and the example is continued below.

For near fault shaking in the block 20-30km away from the epicenter, if the structural period is long, then using the value of $\gamma = 0.9$ from **Figure 4.6**,

$C_{1,NF}$ $= C_{1,FF} R^{1/\gamma - 0.893}$ $= C_{1,FF} R^{1/0.90 - 0.893}$
$= 2.84 \times 2.6^{1/0.90 - 0.893}$ $= 2.84 \times 1.23$
$= 3.5$

d_u $= C_1 C_2 C_3 d_e$ $= 3.5 \times 1.0 \times 1.0 \times 0.94\text{in}$ $= 3.29\text{in}$

The system ductility demand, μ_s (= $C_\mu R$ = 3.5 x 2.6) = d_u/d_y = 3.29in/0.361in = 9.1

$$T_o = 0.123\mu^{0.77} \quad (4.1b)$$
$$= 0.123 \times 9.1^{0.77}$$
$$= 0.674$$

$$T_{int} = \frac{(\mu^\gamma - 1)}{(\mu - 1)} T_o \quad (5.11)$$
$$= \frac{(9.1^{0.90} - 1)}{(9.1 - 1)} 0.674s$$
$$= 0.524\text{s}$$

Since the period of the structure, T (= 0.2s), is less than T_{int} (=0.524s), NF shaking effects do not need to be considered. It should be noted that the design method involves some conservatism since it is based on a bilinear *R-T* relationship. In general, NF shaking effects can be ignored on the inelastic demand if the fundamental period of the structure is less than 0.8s as shown in **Figure 4.17**.

$C_{1,NF}$ $= 2.84$

d_{us} $= C_1 C_2 C_3 d_{es}$ $= 2.84 \times 1.0 \times 1.0 \times 0.94\text{in}$ $= 2.67\text{in}$

The system ductility demand, μ_s = d_{us}/d_{ys} = 2.67in/0.361in = 7.40

The wall ductility demand from **Equation 5.18** is therefore:

$$\mu_c = 1 + (\mu_s - 1).d_{ys}/d_{yc} \quad (5.18)$$
$$= 1 + (7.40 - 1) \times 0.361/0.30 = 8.70$$

Alternatively, the ultimate displacement of the wall alone, d_{uc}, could be found as $d_{us} - d_f$ = 2.67in – 0.061in = 2.61in and the wall ductility, μ_c, is d_{uc}/d_{yc} = 2.61in/0.30in = 8.70 as given above.

Note: If the FEMA356 *force format* procedure were used, then the expected displacement demand of the structure, d_{uc}, would be computed as the amplification factor, $C_1C_2C_3$, multiplied by the response of the wall if it were to remain elastic which is $C_1C_2C_3d_{ec}$ = 2.84 x 0.78in = 2.21in which corresponds to a ductility demand of $C_1C_2C_3d_{ec}/d_{yc}$ = 2.21in/0.3in = 7.37. This is less than the actual displacement demand of 2.61in and the actual ductility demand of 8.70. In this case the difference is only 17% (which is also the difference between μ_c and μ_s), but if the roof displacement were a greater contribution of the total displacement at the center of the wall,

then the difference between these two values could be much greater as shown in the case of the bridge column. The FEMA 356 LDP does not rationally consider the difference between member and system ductility demands and as a result its estimate is unsafe.

The example above illustrates the effects of yielding of one element in any multi-element system. An example could have been written so that the in-plane walls yield, while the out-of-plane walls and roof remain elastic, and the same difference in system and member behavior would have been seen since the concepts are the same. This effect should be considered in design.

The performance of the wall is assessed two ways:

i) In FEMA 273, the wall can be assumed to be a "deformation controlled" element (Roeder and MacRae, 1999). In this case the ductility demand should be compared with an m value of 3 for the wall out-of-plane deformation using the value for columns controlled by flexure for collapse prevention (CP) performance. If the walls are non-load bearing, then use of $m = 4$ for beams controlled by flexure may be appropriate. In either case, since $\mu_c = 8.70 > m$, some strengthening and stiffening of this wall would be required to reduce the demand, μ_c, to below the collapse prevention level.

ii) In FEMA 356 Section 2.6.7.1, the wall is required to remain nominally elastic and the design strength of the wall is given as:

$$F_p = \chi S_{XS} W$$

where χ is a factor of 0.9 for flexible walls for the collapse prevention performance level. This provision requires that the wall behaves nearly elastically. In this case the uniformly distributed loading over the height of the wall, w_p, and the expected connection force, $F_{connection}$, are given below.

$$w_p = \chi S_{XS} W$$
$$\approx 0.9 \text{ x } 2.4\text{g x } 150 \text{ lb/ft}^3 * 4.25\text{in}/(12\text{in/ft}) = 115 \text{ lb/ft/ft width}$$

$$M_w = w_p l^2/8$$
$$= 115 \text{ lb/ft/ft width } x\ 30\text{ft}^2/8$$
$$= 12{,}900\text{lb-ft/ft width}$$
$$= 155 \text{ kip-in/ft width}$$

This required flexural strength is greater than the actual strength of 66.3 kip-in/ft width ($\approx S_{XS} W l^2/8/(d_{es}/d_{ys})$), this implies that the wall would need to be strengthened.

According to both methods, strengthening is required.

b) The Wall Connections

The required strength of the connection of the wall to the roof is also assessed using **Section 5.5.4** and by FEMA356.

i) According to **Section 5.5.4**, the connection strength must be greater than the minimum of the elastic force or the maximum strength demand. If the capacity of the wall itself were satisfactory, then:

$$F_{connection} = \min \begin{cases} V_{max} \text{ due to wall yielding} \\ V_{elastic} \text{ from elastic LDP analysis} \end{cases} \quad (5.22)$$

V_{max} due to wall yielding $= 4M_{max}/L$
$= 4 \times (66.3\text{kip-in/ft length of wall})/(30\text{ft}*12\text{in/ft})$
$= 736$ lb/ft length of wall
An over-strength factor for M_{max} could also be used if desired.

$V_{elastic}$ from elastic LDP analysis $\approx$ 1,900lb/ft length of wall ($=S_{XS}Wl/2$)

So $F_{connection}$ of 736 lb/ft length of wall must be provided to obtain satisfactory system performance. If this is not provided the wall will disconnect from the roof and the possibility of wall overturning and total structural collapse is increased.

ii) In FEMA 356 Section 2.6.7.2, the wall is required to remain nominally elastic and the design strength of the wall is given as:

$$F_p = \chi S_{XS} W$$

where χ is a factor of 0.9 for flexible walls for the collapse prevention performance level. This provision requires that the connection behave nearly elastically. In this case the uniformly distributed loading over the height of the wall, w_p, and the expected connection force, $F_{connection}$, be computed as:

$F_{connection} \approx 0.9\ S_{XS}Wl/2$
$\approx 0.9\ x$ 1,900lb/ft length of wall
$\approx$ 1,710lb/ft length of wall

The FEMA356 provisions are most conservative since they ignore the possibility of the wall yielding and limiting the demand on the connections.

Since walls of mill-type structures have seldom suffered damage in a real earthquake, and since they do possess some ductility capacity, it is possible that the newer FEMA356 provisions may be excessively conservative.

CHAPTER 6. CONCLUSIONS & RECOMMENDATIONS

In order to evaluate the effect of near-fault (NF) and far-fault (FF) shaking effects on structural response of mill-type buildings representative of many PG&E structures, analysis of a number of single-degree-of-freedom (SDOF) oscillators with bilinear hysteresis shapes were carried out to far-fault (FF) records as well as to near-fault (NF) records obtained at known locations relative to the epicenter and fault rupture surface. The Coefficient Method (CM) (FEMA273, FEMA356) and the Capacity Spectra Method (CSM) (ATC-40) relationships were calibrated to estimate the demands. It was found that:

1) For short period structures, such as PG&E mill type structures, with fundamental periods less than about 0.8s, directivity effects from NF shaking did not increase the demands above that found for FF shaking.

2) The following comparison of the CM and CSM methods were made:

(a) The CM is relatively simple to use, but it does not consider the influence of different types of damping or hysteretic loop shape easily, and results may be sensitive to the definition of yield displacement. The CSM is less sensitive to the definition of yield displacement and can take damping effects into account easily. However iteration is required to estimate the likely structural displacements, the method may require use of very long period response values which have dubious accuracy, three empirical relationships have to be assumed or calibrated, and an understanding of the structure's hysteretic shape is required to estimate the demand.

(b) Both the CM and CSM can be calibrated to estimate the exact response. For the CM a bilinear approximation of lateral force reduction factor, R, vs. fundamental period, T, for a specific ductility is reasonable. The CSM effective damping, ζ_{eff}, for a specific ductility, μ, as well as the spectral reduction, SR, for a specific damping, ζ, are dependent on period, T.

(c) Since oscillators with the same strength, stiffness and positive bilinear factor (excluding perfectly elastic oscillators or oscillators with strength degradation) have been shown to have approximately the same displacement demand irrespective of hysteretic loop shape, relationships for both the CM and CSM for bilinear structures are also applicable to reinforced concrete and timber structures with a bilinear backbone curve and pinched hysteresis loops.

(d) When both the CM and CSM are well calibrated, the scatter in displacement, Δ, for oscillators with an effective (secant) period, T_{eff}, less than about 3.0s is similar. For structures with T_{eff} greater than about 3.0s, the CSM has more scatter.

(e) When the CSM was calibrated according to ATC-40, ATC-40 significantly overestimated the average effective damping at periods greater than about 0.2s. ATC-40 non-conservatively estimated the median inelastic response over the majority of the period range from 0-3s and its estimation was as low as 60% of the median displacement for some periods. The CM calibrated according to FEMA356 conservatively estimated the median displacement over most of the period range. For some periods, FEMA356 estimated displacements more than 30% greater than the actual median displacements.

3) Oscillators with demands estimated by the CM, and with fundamental periods less than about 0.8s, were not affected significantly by near-fault shaking effects. For longer period oscillators, oscillator strengths may need to be increased by more than 60% to account for inelastic shaking effects from NF sites in the region of positive directivity compared to that for shaking from FF or NF near-epicenter sites for the same target displacement ductility. NF shaking did not cause significant trends in the displacement demands of oscillators evaluated by the CSM method. Modifications to the existing FEMA356 CM nonlinear static procedure (NSP) C_1 factor, accounting for NF shaking effects when appropriate, was developed for structures with fundamental periods in the range of 0-3s.

4) For design of PG&E structures, it was determined in conjunction with PG&E/PEER that the FEMA356 CM Linear Dynamic Procedure (LDP) should be used to evaluate the demands of PG&E mill-type structures. The estimation of inelastic response should be made using the C_1 factor from the FEMA356 Nonlinear Static Procedure (NSP). While the C_1 factor may be modified for NF shaking effects, this is only required for structures with periods greater than 0.8s. NF shaking effects therefore do not need to be considered on the inelastic response of the majority of PG&E mill-type structures since their fundamental periods are less than 0.8s. The difference between member and system ductility demands is not considered in the FEMA356 LDP often resulting in non-conservative demand estimates. A method to show how it can easily be accounted for in assessment and in design is provided. A design procedure and example for assessing NF shaking inelastic displacement demands on a mill type structure using the CM was provided.

It is believed that further understanding of the behavior of structures to near fault accelerations could be obtained using the following information:

1. More records from actual shaking at known locations relative to the fault are required to increase confidence in the values of γ and T_o.
2. Simple methods should be developed to determine pulse characteristics and to further understand the effect of pulses in records with high frequency shaking.
3. Analyses of SDOF oscillators with different hysteresis loops are required.
4. Effects of soil category on the response of structures to near-fault shaking should be investigated.
5. Statistical analyses are required to incorporate the risk of high severity and the low probability of near fault shaking in design.

REFERENCES

AASHTO., 1994, LRFD Bridge Design Specifications, First Edition, *American Association of State Highway Transportation Officials*, Washington, D.C.

Abrahamson N., 1998. Personal Correspondance.

AIJ 1993, "Recommendations for Loads on Buildings".

Ascheim M. A., 1999. "Yield Point Spectra, A Simple Alternative to the Capacity Spectrum Method", SEAOC Convention Proceedings.

ATC-32., 1996, Improved Seismic Design Criteria for California Bridges: Provisional Recommendations, *Applied Technology Council*, Redwood City, Ca.

ATC-40, 1996. "Seismic Evaluation and Retrofit of Concrete Buildings", Applied Technology Council, Redwood City.

Baez J. I. and Miranda E., 2000. "Amplification factors to estimate inelastic displacement demands for the design of structures in the near field", Proc. 12 World Conference on Earthquake Engineering.

Berrill J. B., Priestley M. J. N. And Chapman H. E., "Design Earthquake Loading and Ductility Demand", Bulletin of the NZ National Society for Earthquake Engineering, 13(3), September 1980, pp232-241.

Chai Y. H., Fajfar and Romstad K. M., "Formulation of Duration-Dependent Inelastic Seismic Design Spectrum", Journal of Structural Engineering, 124(8) August 1998.

Chopra, Anil K., *Dynamics of Structures - Theory and Applications to Earthquake Engineering*, Prentice-Hall, 1995.

Chopra, A. K. and Goel, R. K. (1999). *Capacity-Demand-Diagram Methods for Estimating Seismic Deformation of Inelastic Structures: SDF Systems*. Report No. PEER-1999/02, Pacific Earthquake Engineering Research Center, Richmond, CA, April.

Chopra, A. K. and Goel, R. K. (2000). Capacity-Demand-Diagram Methods based on Inelastic Design Spectrum, *2000 Structures Congress*, ASCE, Philadelphia, May 8-10, 2000.

Discussion Group, 1980, Discussion Group of the New Zealand National Society for Earthquake Engineering, Papers Resulting From the Deliberation of the Society's Discussion Group of the Seismic Response of Bridges, *Bulletin of the New Zealand National Society for Earthquake Engineering*, 13(3), 226-309.

Dodd, L. L., 1992, The Dynamic Behaviour of Reinforced Concrete Bridge Piers Subjected to New Zealand Seismicity, Research Report 92-04, Department of Civil Engineering, University of Canterbury.

Dunn, M., 1995. "Analysis of Bilinear Single Degree of Freedom Oscillators Subjected to Seismic Accelerations on Soft Soil Sites: Applications to Seismic Isolation", Master's Thesis, University of Washington.

Fajfar P., 1999. "Capacity Spectra Method Based on Inelastic Demand Spectra", Earthquake Engineering and Structural Dynamics, 28(9), 979-993.

Fajfar P., 2000. "A non-linear analysis method for performance based seismic design", Earthquake Spectra, 16(3), 573-592.

Fajfar P., 2000. "A Practical Nonlinear Method for Seismic Performance Evaluation", ASCE Structures Congress, Philadelphia.

FEMA273, 1997. "NEHRP Guidelines for the Seismic Rehabilitation of Buildings", Federal Emergency Management Agency, Washington D.C., 1996 Edition.

FEMA356, 2001. "NEHRP Guidelines for the Seismic Rehabilitation of Buildings", Federal Emergency Management Agency, Washington D.C., 2000 Edition.

Fenwick R. and Bull D. 2002. "What is the Stiffness of Reinforced Concrete Walls?", Response to Discussion from Priestley and Paulay, New Zealand Structural Engineering Society, SESOC, 15(1), pp35-41.

Freeman S. A. 1978. "Prediction of Response of Concrete Buildings to Severe Earthquake Motions", Douglas McHenry International Symposium on Concrete and Concrete Structures, SP-55, American Concrete Institute, Detroit, Michigan, pp589-605.

Gulkan P. and Sozen M. A., "Inelastic Response of Reinforced Concrete Structures to Earthquake Motions", American Concrete Institute Journal, December 1974.

Gulkan P. and Sozen M. A., "Inelastic Responses of Reinforced Concrete Structures to Earthquake Motions", in Reinforced Concrete Structures in Seismic Zones, N. M. Hawkins, Ed., ACI Publication SP-53, American Concrete Institute, Detroit, 1977, pp109-116.

ICBO, International Conference of Building Officials, "1997 Uniform Building Code", Whittier, CA, 1997.

ICC. 2000. "2000 International Building Code", *International Code Council.*

Iwan W. D. and Gates C. T., "The Shear Drift-Demand Spectrum: Implications for Earthquake-Resistant Design", ASCE Journal of Engineering Mechanics, EM9, 1979.

Iwan W. D., Huang C. T. and Guyader A. C., "Evaluation of Effects of Near-Fault Ground Motions", Report submitted to PG&E-PEER, September 1, 1998.

JRA 1996. "Design Specifications for Road Bridges, Part V Seismic Design", Japan Road Association, Tokyo, English Edition.

Judi H., Fenwick R. and Davidson B., "Influence of Hysteretic Form on the Basic Seismic Hazard Coefficients", New Zealand Structural Engineering Society, SESOC, 15(1), pp 7-12.

Kennedy R. P., Cornell C. A., Campbell R. D., Kaplan, S. and Perla, H. F., 1980. "Probabalistic Seismic Safety Study of an Existing Nuclear Power Plant", Nuclear Engineering and Design, 59, 1980, p 315-338.

Kircher C., "Review of PG&E-PEER Joint Research Program", CKA Project No. 438-010, PG&E Contract No. 4600008276, December 28, 1999.

Kowalsky M. J., Priestley M. J. N. and MacRae G. A., "Displacement-Based Design of RC Bridge Columns in Seismic Regions", *Earthquake Engineering and Structural Dynamics*, Vol. 24, 1995, pp. 1623-1643.

Krawinkler, H., "Near-Fault Shaking Effects on Structures", 6th ASCE Structures Congress, New Orleans, April 1999.

MacRae, G. A. and Kawashima K., 1990, Ductility Measurement for the Testing of Steel Bridge Piers, *Proceedings of the Annual Meeting of the Japan Society of Civil Engineering,* Niigata.

MacRae G. A. and Roeder C. W., "Near-Field Ground Motion Effects on Short Structures", Final Report to PG&E-PEER, October 1999.

MacRae G. A., Morrow D. and Roeder C. W., "Near-Fault Ground Motion Effects on Short Period Structures", *ASCE Journal of Structural Engineering*, September 2001.

MacRae, G. A., Carr, A. J. and Walpole W. R., 1990A. The Seismic Response of Steel Frames, *Research Report 90-6,* Department of Civil Engineering, University of Canterbury, New Zealand, March 1990.

MacRae G. A., Carr A. J. and Walpole W. R., 1990B. "The Dynamic Behaviour of Multistorey Steel Frames", *Eighth Japan Earthquake Engineering Symposium,* Tokyo, 12-14 December 1990, pp 1599-1604.

MacRae G. A., Priestley M. J. N. and Tao J., "*P*-Δ in Seismic Regions", *Structural Systems Research Project,* Report No. SSRP 93/05, Department of Applied Mechanics and Engineering Sciences, University of California, San Diego, May 1993, 115pp.

MacRae G. A., Unocic F., and Kramer S., "Seismic Demands of Columns on Flexible Foundations", Earthquake Spectra. (Submitted 2001)

MacRae G. A. and Kawashima K., "Estimation of the Deformation Capacity of Steel Bridge Piers", *in Stability and Ductility of Steel Structures under Cyclic Loading,* Edited by Fukumoto Y. and Lee G., CRC Press Inc., 1992, pp. 335-347.

MacRae, G. A. and Kawashima K., 1993, The Seismic Response of Bilinear Oscillators Using Japanese Earthquake Records, *Journal of Research of the Public Works Research Institute,* Vol. 30, Ministry of Construction, Japan.

MathWorks Inc., "MATLAB", Version 5.1.0.421, May 25, 1997.

Miranda E. and Bertero V. V., "Evaluation of Strength Reduction Factors for Earthquake-Resistant Design", Earthquake Spectra, 10(2), 1994.

Miranda E., "Estimation of Inelastic Deformation Demands of SDOF Systems", Journal of Structural Engineering, 127(9), September 2001.

Miranda E., "Inelastic Displacement Ratios for Structures on Firm Sites", Journal of Structural Engineering, 126(10), 1150-1159.

Newmark N. M. and Hall W. J., Procedures and Criteria for Earthquake-Resistant Design, Building Science Series 46, National Bureau of Standards, 1973.

Nishiyama M., 2000. "Response Prediction of Precast Concrete Buildings against Earthquake Excitations by the Capacity Spectra Method", Proc. 12 World Conference on Earthquake Engineering, Auckland, NZ.

National Geophysical Data Center, 1996. Earthquake Strong Motion, 3 CD collection, Bolder, Colorado.

Priestley, M. J. N. and Park, R., 1987, Strength and Ductility of Concrete Bridge Columns Under Seismic Loading, *ACI Struct. Journal*, 84(1), p61-76.

Priestley M. J. N., "Performance Based Design", Keynote Lecture, 12 World Conference on Earthquake Engineering, Auckland, NZ, 2000.

Priestley M. J. N., Seible F. and Chai Y. H., 1992, Design Guidelines for Assessment Retrofit and Repair of Bridges for Seismic Performance, Structural Systems Research Project 92/01, Department of Applied Mechanics and Engineering Sciences, University of California, San Diego.

Priestley M. J. N., Seible F. and Calvi G. M., 1996, *Seismic Design and Retrofit of Bridges*, John Wiley and Sons, Inc., p135, 282-285.

Reinhorn A., "Inelastic Analysis Techniques in Seismic Evaluations", Seismic Design Methodologies for the Next Generation of Codes, edited by Fajfar and Krawinkler, Balkema, Rotterdam, ISBN 90 54 10 928 9, 1997.

Roeder C. W. and MacRae G. A., "Seismic Behavior of Concrete-Filled Steel Frame Substations", Final Report, *PGE-PEER*, April 1999.

SANZ, 1984. "NZS3101:1984, Design of RC Building Structures", Standards Association of New Zealand.

Smith N., Private Correspondance, 1998.

Somerville, P., Smith N., Graves R. W. and Abrahamson N., "Modification of Empirical Strong Motion Attenuation Relations to Include the Amplitude and Duration Effects of Rupture Directivity", Seismological Research Letters, 68(1), January/February, 1997.

Transit, 1994, Bridge Manual, *Transit New Zealand*, Wellington, New Zealand. (Plus amendment No. 1, June 1995).

Tsopelas, P., Constantinou, M. C., Kircher, C. A., and Whittaker, A. S. (1997). Evaluation of simplified methods of analysis of yielding structures, Technical Report NCEER-97-0012, National Center for Earthquake Engineering Research, State University of New York, Buffalo, Oct.

Vidic T., Fajfar P. and Fischinger M., "Consistent Inelastic Design Spectra; Strength and Displacement", Earthquake Engineering and Structural Dynamics, 23, p507-521, 1994.

APPENDIX A1.

IMPULSE SHAKING

IMPULSE SHAKING AND THE CSM

(by Hiroyuki Tagawa)

An impulsive motion is shown in Figure 1. The area enclosed by time and force, $\int m\ddot{u}_g dt$ is 1, however the time duration, *dt*, is infinitely small. Inelastic SDOF oscillator with ductility μ, and initial stiffness *k*, as well as the substitute elastic SDOF oscillator with constant stiffness k_{eff}, $(=k_o/\mu)$, and effective damping ration ζ_{eff}, are subject to the impulsive motion. The effective damping ratio which gives the same maximum displacements to both oscillators is calculated. The maximum displacements are calculated as follows:

a) Maximum displacement of Inelastic SDOF oscillators

For simplicity, the case of stiffness ratio r = 0.0, is first considered. Since the EEM is satisfied for impulsive motion, the absorbed energies in inelastic structures and elastic structures of like mass are the same. This considered, the maximum displacement, Δ_{max}, of inelastic SDOF oscillators with r = 0.0 and ductility of μ for an impulsive motion can be calculated as follows:

$$\Delta_{\max} = \frac{1}{2} \cdot \left\{ \left(\frac{1}{m\omega_o \Delta_y} \right)^2 + 1 \right\} \cdot \Delta_y$$

Here ω_o is the natural frequency and Δ_y is the yield displacement.

Since $\Delta_{\max} = \mu\Delta_y$, the equation can be simplified to:

$$\Delta_{\max} = \frac{\mu}{\sqrt{2\mu - 1} \cdot m\omega_o} \qquad \text{(A1)}$$

Equation A1 can also be obtained by solving the equations of equilibrium of motion in the elastic and inelastic parts (Shibata, 1981).

b) Maximum displacement of substitute elastic SDOF oscillators

The effective frequency, ω_{eff}, is

$$\omega_{eff} = \frac{\omega_o}{\sqrt{\mu}}$$

The displacement history of the substitute structure Δ_s, for impulse is given by Duhamel's integral as follows:

$$\Delta^s(t) = \frac{1}{m\omega'} \cdot e^{(-\zeta_{eff}\omega_{eff}t)} \cdot \sin(\omega_{eff} \cdot t)$$

Here: $\omega' = \sqrt{1-\zeta_{eff}^{\ 2}}\,\omega$

The maximum displacement Δ^s_{max}, will occur close to $\omega_{eff}t = \pi/2$. So, the maximum displacement Δ^s_{max}, if it is assumed that $\omega_{eff} = \omega'$.

$$\Delta^s_{\max} = \frac{1}{m\omega_{eff}} \cdot e^{-\zeta_{eff}(\pi/2)} \qquad \text{(A2)}$$

a) Damping due to Ductility

Maximum displacements of inelastic oscillators and substitute elastic oscillators should be same. From **Equations A1 and A2**, the effective damping, ζ_{eff}, is calculated as

$$\zeta_{eff} = \frac{2}{\pi} \cdot \ln\sqrt{2-\frac{1}{\mu}}$$

By generalizing for bilinear factor and adding the initial damping it is possible to show that:

$$\zeta_{eff} = \frac{2}{\pi} \cdot \ln\sqrt{1-\frac{1}{\mu}+\frac{1}{1+\mu r-r}} + \zeta_o \qquad \text{(A3)}$$

Equation A3 provides a good estimate of the effective damping for mediate- and long-period structures, and a conservative estimate for short-period structures.

b) SR due to Damping

Displacement reduction factor, *SR*, due to damping for impulsive motion is calculated by dividing **Equation A2** by the value of **Equation A2** at $\zeta_{eff} = 0$. Therefore, *SR* due to effective damping can be expressed as follows:

$$SR(\zeta_{eff}) = e^{\left(-\zeta_{eff} \cdot \frac{\pi}{2}\right)} \qquad \text{(A4)}$$

Equation A4 is conservative compared to values obtained for actual ground-motions.

c) SR due to Inelasticity

SR due to inelastic behavior for impulsive loading is obtained by combining **Equation A1** and **Equation A4**. It can be expressed as follows:

$$SR = \frac{1}{\sqrt{1 - \frac{1}{\mu} + \frac{1}{\mu r - r + 1}}} \qquad \textbf{(A5)}$$

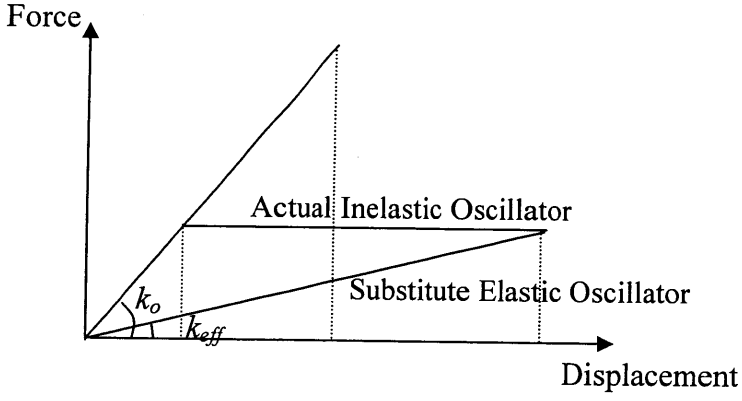

Figure 1. Inelastic and Substitute Structures

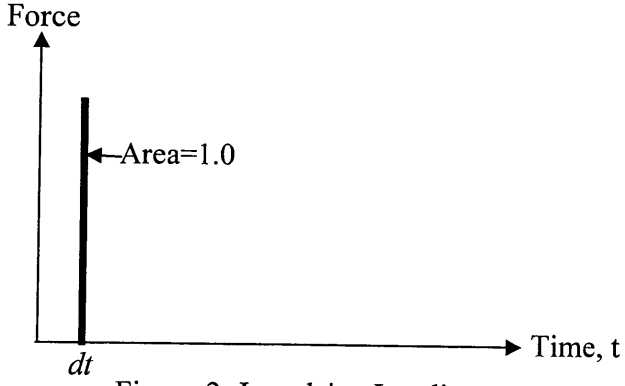

Figure 2. Impulsive Loading

APPENDIX A2.

TURKEY AND TAIWAN RECORDS

APPENDIX A2. ANALYSES PERFORMED USING TAIWAN AND TURKEY RECORDS

Chi-Chi		r_rup	s (km)	Area	Mu	SN	SP
	ALS	15.3	14	22	(2,4,6,8)	x	
	CHY002	26.8	14	32	(2,4,6,8)	x	
	CHY004	50.9	14	42	(2,4,6,8)	x	
	CHY006	14.9	14	22	(2,4,6,8)	x	
	CHY008	45.3	14	42	(2,4,6,8)	x	
	CHY010	25.4	14	32	(2,4,6,8)	x	
	CHY012	64.2	14	42	(2,4,6,8)	x	
	CHY014	41.5	14	42	(2,4,6,8)	x	
	CHY015	43.5	14	42	(2,4,6,8)	x	
	CHY017	64.4	14	42	(2,4,6,8)	x	
	CHY019	57.1	14	42	(2,4,6,8)	x	
	CHY024	9.1	14	12	(2,4,6,8)	x	x
	CHY025	18.8	14	22	(2,4,6,8)	x	
	CHY026	29.3	14	32	(2,4,6,8)	x	
	CHY027	44.1	14	42	(2,4,6,8)	x	
	CHY028	7.3	14	12	(2,4,6,8)	x	x
	CHY029	15.3	14	22	(2,4,6,8)	x	
	CHY032	39.3	14	42	(2,4,6,8)	x	
	CHY033	48.2	14	42	(2,4,6,8)	x	
	CHY034	20.2	14	32	(2,4,6,8)	x	
	CHY035	18.1	14	22	(2,4,6,8)	x	
	CHY036	20.4	14	32	(2,4,6,8)	x	
	CHY039	36.7	14	42	(2,4,6,8)	x	
	CHY041	26	14	32	(2,4,6,8)	x	
	CHY042	34.9	14	42	(2,4,6,8)	x	
	CHY044	60.2	14	42	(2,4,6,8)	x	
	CHY046	29.5	14	32	(2,4,6,8)	x	
	CHY047	29.4	14	32	(2,4,6,8)	x	
	CHY050	50.1	14	42	(2,4,6,8)	x	
	CHY052	45	14	42	(2,4,6,8)	x	
	CHY054	53.8	14	42	(2,4,6,8)	x	
	CHY055	59.7	14	42	(2,4,6,8)	x	
	CHY057	62.8	14	42	(2,4,6,8)	x	
	CHY058	65.1	14	42	(2,4,6,8)	x	
	CHY061	66.9	14	42	(2,4,6,8)	x	
	CHY062	64.1	14	42	(2,4,6,8)	x	
	CHY076	45.7	14	42	(2,4,6,8)	x	
	CHY079	55	14	42	(2,4,6,8)	x	
	CHY080	7	14	12	(2,4,6,8)	x	x
	CHY081	47.7	14	42	(2,4,6,8)	x	
	CHY082	38.3	14	42	(2,4,6,8)	x	
	CHY086	35.4	14	42	(2,4,6,8)	x	
	CHY087	34.5	14	42	(2,4,6,8)	x	
	CHY088	42.8	14	42	(2,4,6,8)	x	
	CHY090	63.8	14	42	(2,4,6,8)	x	
	CHY092	22.5	14	32	(2,4,6,8)	x	
	CHY093	53.2	14	42	(2,4,6,8)	x	
	CHY094	38	14	42	(2,4,6,8)	x	
	CHY100	58.8	14	42	(2,4,6,8)	x	
	CHY101	11.1	14	22	(2,4,6,8)	x	
	CHY102	46.2	14	42	(2,4,6,8)	x	
	CHY104	20.7	14	32	(2,4,6,8)	x	
	CHY107	55.9	14	42	(2,4,6,8)	x	

CHY109	47.8	14	42	(2,4,6,8)	x	
CHY110	47.8	14	42	(2,4,6,8)	x	
ESL	44.9	14	42	(2,4,6,8)	x	
HWA	58.8	14	42	(2,4,6,8)	x	
HWA002	53.9	14	42	(2,4,6,8)	x	
HWA003	56.1	14	42	(2,4,6,8)	x	
HWA005	43.9	14	42	(2,4,6,8)	x	
HWA006	44	14	42	(2,4,6,8)	x	
HWA007	59.8	14	42	(2,4,6,8)	x	
HWA009	59.7	14	42	(2,4,6,8)	x	
HWA011	56.7	14	42	(2,4,6,8)	x	
HWA012	60.3	14	42	(2,4,6,8)	x	
HWA013	57.4	14	42	(2,4,6,8)	x	
HWA014	58.3	14	42	(2,4,6,8)	x	
HWA015	54.9	14	42	(2,4,6,8)	x	
HWA016	54.7	14	42	(2,4,6,8)	x	
HWA017	53.9	14	42	(2,4,6,8)	x	
HWA019	58.8	14	42	(2,4,6,8)	x	
HWA020	44.9	14	42	(2,4,6,8)	x	
HWA023	57.1	14	42	(2,4,6,8)	x	
HWA024	44.3	14	42	(2,4,6,8)	x	
HWA025	61.5	14	42	(2,4,6,8)	x	
HWA026	58.8	14	42	(2,4,6,8)	x	
HWA027	56.8	14	42	(2,4,6,8)	x	
HWA028	57.9	14	42	(2,4,6,8)	x	
HWA029	56.3	14	42	(2,4,6,8)	x	
HWA030	46.4	14	42	(2,4,6,8)	x	
HWA031	50.4	14	42	(2,4,6,8)	x	
HWA032	43.2	14	42	(2,4,6,8)	x	
HWA033	49	14	42	(2,4,6,8)	x	
HWA034	42	14	42	(2,4,6,8)	x	
HWA035	45.9	14	42	(2,4,6,8)	x	
HWA036	43.6	14	42	(2,4,6,8)	x	
HWA037	46.6	14	42	(2,4,6,8)	x	
HWA038	42.9	14	42	(2,4,6,8)	x	
HWA039	46.7	14	42	(2,4,6,8)	x	
HWA041	50	14	42	(2,4,6,8)	x	
HWA043	54.9	14	42	(2,4,6,8)	x	
HWA044	54.5	14	42	(2,4,6,8)	x	
HWA046	59.3	14	42	(2,4,6,8)	x	
HWA048	55.3	14	42	(2,4,6,8)	x	
HWA049	54	14	42	(2,4,6,8)	x	
HWA050	56.7	14	42	(2,4,6,8)	x	
HWA051	55.8	14	42	(2,4,6,8)	x	
HWA054	43.6	14	42	(2,4,6,8)	x	
HWA055	48.7	14	42	(2,4,6,8)	x	
HWA056	48.8	14	42	(2,4,6,8)	x	
HWA057	58.2	14	42	(2,4,6,8)	x	
HWA058	48.5	14	42	(2,4,6,8)	x	
HWA059	52	14	42	(2,4,6,8)	x	
HWA060	60.6	14	42	(2,4,6,8)	x	
HWA2	58.8	14	42	(2,4,6,8)	x	
ILA067	48.7	14	42	(2,4,6,8)	x	
KAU001	54.6	14	42	(2,4,6,8)	x	
KAU047	64.5	14	42	(2,4,6,8)	x	
KAU050	52.1	14	42	(2,4,6,8)	x	
KAU054	40.5	14	42	(2,4,6,8)	x	

	NST	37	14	42	(2,4,6,8)	x	
	NSY000	9.7	14	12	(2,4,6,8)	x	x
	STY	52.1	14	42	(2,4,6,8)	x	
	TCU	5.7	14	12	(2,4,6,8)	x	x
	TCU033	38.2	14	42	(2,4,6,8)	x	
	TCU034	33	14	42	(2,4,6,8)	x	
	TCU036	16.7	14	22	(2,4,6,8)	x	
	TCU038	22.4	14	32	(2,4,6,8)	x	
	TCU039	16.7	14	22	(2,4,6,8)	x	
	TCU040	21	14	32	(2,4,6,8)	x	
	TCU042	23.3	14	32	(2,4,6,8)	x	
	TCU045	24.1	14	32	(2,4,6,8)	x	
	TCU046	14.3	14	22	(2,4,6,8)	x	
	TCU047	33	14	42	(2,4,6,8)	x	
	TCU048	14.4	14	22	(2,4,6,8)	x	
	TCU049	4.5	14	12	(2,4,6,8)	x	x
	TCU050	10.3	14	22	(2,4,6,8)	x	
	TCU051	8.3	14	12	(2,4,6,8)	x	x
	TCU052	0.2	14	12	(2,4,6,8)	x	x
	TCU053	6.7	14	12	(2,4,6,8)	x	x
	TCU054	5.9	14	12	(2,4,6,8)	x	x
	TCU055	6.9	14	12	(2,4,6,8)	x	x
	TCU056	11.1	14	22	(2,4,6,8)	x	
	TCU057	12.6	14	22	(2,4,6,8)	x	
	TCU059	17.8	14	22	(2,4,6,8)	x	
	TCU060	9.5	14	12	(2,4,6,8)	x	x
	TCU061	17.8	14	22	(2,4,6,8)	x	
	TCU063	10.4	14	22	(2,4,6,8)	x	
	TCU064	15.1	14	22	(2,4,6,8)	x	
	TCU065	1	14	12	(2,4,6,8)	x	x
	TCU067	0.3	14	12	(2,4,6,8)	x	x
	TCU068	1.1	14	12	(2,4,6,8)	x	x
	TCU070	19.1	14	22	(2,4,6,8)	x	
	TCU071	4.9	14	12	(2,4,6,8)	x	x
	TCU072	7.4	14	12	(2,4,6,8)	x	x
	TCU074	13.7	14	22	(2,4,6,8)	x	
	TCU075	1.5	14	12	(2,4,6,8)	x	x
	TCU076	2	14	12	(2,4,6,8)	x	x
	TCU078	7.5	14	12	(2,4,6,8)	x	x
	TCU079	10	14	12	(2,4,6,8)	x	x
	TCU082	5.7	14	12	(2,4,6,8)	x	x
	TCU084	10.4	14	22	(2,4,6,8)	x	
	TCU087	3.2	14	12	(2,4,6,8)	x	x
	TCU089	8.2	14	12	(2,4,6,8)	x	x
	TCU095	43.4	14	42	(2,4,6,8)	x	
	TCU098	45	14	42	(2,4,6,8)	x	
	TCU100	12.1	14	22	(2,4,6,8)	x	
	TCU101	2.9	14	12	(2,4,6,8)	x	x
	TCU102	1.8	14	12	(2,4,6,8)	x	x
	TCU103	4	14	12	(2,4,6,8)	x	x
	TCU104	13.6	14	22	(2,4,6,8)	x	
	TCU105	18.1	14	22	(2,4,6,8)	x	
	TCU106	15.2	14	22	(2,4,6,8)	x	
	TCU107	20.4	14	32	(2,4,6,8)	x	
	TCU109	13.1	14	22	(2,4,6,8)	x	
	TCU110	12.6	14	22	(2,4,6,8)	x	
	TCU111	22.2	14	32	(2,4,6,8)	x	
	TCU112	27.2	14	32	(2,4,6,8)	x	

	TCU113	31.5	14	42	(2,4,6,8)	x	
	TCU115	22.8	14	32	(2,4,6,8)	x	
	TCU116	11.9	14	22	(2,4,6,8)	x	
	TCU117	25.6	14	32	(2,4,6,8)	x	
	TCU119	39	14	42	(2,4,6,8)	x	
	TCU120	8.1	14	12	(2,4,6,8)	x	x
	TCU122	9	14	12	(2,4,6,8)	x	x
	TCU123	15.1	14	22	(2,4,6,8)	x	
	TCU128	9.7	14	12	(2,4,6,8)	x	x
	TCU129	1.2	14	12	(2,4,6,8)	x	x
	TCU136	9	14	12	(2,4,6,8)	x	x
	TCU138	10.1	14	22	(2,4,6,8)	x	
	TCU140	34	14	42	(2,4,6,8)	x	
	TCU141	23.8	14	32	(2,4,6,8)	x	
	TCU145	36.3	14	42	(2,4,6,8)	x	
	TTN001	57.6	14	42	(2,4,6,8)	x	
	TTN020	57.7	14	42	(2,4,6,8)	x	
	TTN022	60.6	14	42	(2,4,6,8)	x	
	TTN023	63.3	14	42	(2,4,6,8)	x	
	TTN031	57	14	42	(2,4,6,8)	x	
	TTN032	59.1	14	42	(2,4,6,8)	x	
	WGK	11.1	14	22	(2,4,6,8)	x	
	WNT	1.2	14	12	(2,4,6,8)	x	x
Kocaeli	Sakarya	43.7	3.4	15	(2,4,6,8)	x	
	Yarimca	8.2	4.4	11	(2,4,6,8)	x	
	Izmit	4.8	5	11	(2,4,6,8)	x	
	Duzce	100	12.5		(2,4,6,8)	x	
	Gebze	25	13.5	23	(2,4,6,8)	x	
	Arcelik	25	21.6	32	(2,4,6,8)	x	
	Goynuk	78	35.5		(2,4,6,8)	x	
	Iznik	9.5	8.4	11	(2,4,6,8)	x	
	Meciditekoy	25	62.3	42	(2,4,6,8)	x	
Duzce	Duzce	2.5	8.2	11	(2,4,6,8)	x	
	Bolu	75	17.6		(2,4,6,8)	x	
	Sakarya	15.5	49.9	42	(2,4,6,8)	x	
	Mudurnu	1	33.6	41	(2,4,6,8)	x	

APPENDIX A3.

FAR FAULT RECORDS

Table A3. Far Field Record Set

Date	Earthquake	Station	filename	Comp	Epicentral Distance (km)	Mag	A_g max (cm/s^2)	Vmax (cm/s)	Dmax (cm)
651026	Japanese	Kushiro Central Wharf, Ground	JAP03.034	NS	125	6	105.60	4.90	0.60
680518	Japanese	Ofunato Harbor, Ground	JAP03.099	NS	145	7	85.30	13.80	2.20
680612	Japanese	Miyako Harbor Works, Ground	JAP03.103	NS	103	6	190.20	5.90	1.20
680612	Japanese	Miyako Harbor Works, Ground	JAP03.104	EW	103	6	163.50	5.10	0.60
710802	Erimo-Misaki Prefecture	Kushiro Central Wharf, Ground	JAP03.145	NS	202	7	89.70	7.00	1.40
710802	Erimo-Misaki Prefecture	Kushiro Central Wharf, Ground	JAP03.146	EW	202	7	76.10	6.80	1.20
720229	Hachijojima	Yamashita Wharf Substation	JAP03.149	NS	293	7	79.80	3.70	0.90
720229	Hachijojima	Yamashita Wharf Substation	JAP03.150	EW	293	7	58.40	3.30	0.80
730617	Nemuro Penninsula	Kushiro Central Wharf, Ground	JAP03.153	NS	129	7	200.90	27.50	6.40
730617	Nemuro Penninsula	Kushiro Central Wharf, Ground	JAP03.154	EW	129	7	126.80	15.70	4.60
780612	Miyagi Prefecture	Ofunato Harbor, Jetty	JAP03.172	N41E	103	6	206.70	12.80	2.20
780612	Miyagi Prefecture	Ofunato Harbor, Jetty	JAP03.173	E41S	103	6	222.10	14.10	5.10
850919	Michoacan, Mexico City	C. De Abastos Oficina	MEX02.014	N90E	386	8	68.90	41.86	21.67
850919	Michoacan, Mexico City	Secretaria Comunicacion & Tran	MEX02.050	N90W	381	8	158.40	57.42	21.94
850919	Michoacan, Mexico City	Tlahuac Bombas	MEX02.083	N00E	390	8	104.20	64.10	34.61
850919	Michoacan, Mexico City	Tlahuac Bombas	MEX02.086	N90W	390	8	106.70	44.50	39.29
850919	Michoacan, Mexico City	Tlahuac Deportivo	MEX02.092	N00E	388	8	117.70	34.73	16.80
850919	Michoacan, Mexico City	Aeropuerto	MEX03.076	N90W	131	8	161.80	18.34	4.62
560209	El Alamo, Baja	Imperial Valley Irrigation Dist., El Centro	USACA01.031	S00W	121	7	32.40	3.97	2.45
560209	El Alamo, Baja	Imperial Valley Irrigation Dist., El Centro	USACA01.032	S90W	121	7	50.10	6.96	4.09
680409	Borrego Mountain	Light And Power Bldg,San Diego	USACA01.058	S00W	107	6	29.50	5.97	4.44
410209	Northwest California	City Hall, Ferndale	USACA01.079	N45E	102	7	61.30	3.51	1.99
410209	Northwest California	City Hall, Ferndale	USACA01.080	S45E	102	7	38.40	3.44	2.15
680409	Borrego Mountain	Nuclear Power Plant, San Onofre	USACA01.118	N33E	134	6	40.00	3.67	1.65
680409	Borrego Mountain	Nuclear Power Plant, San Onofre	USACA01.119	N57W	134	6	45.50	4.20	2.88
660807	Gulf Of California	Imperial Valley Irrigation Dist., El Centro	USACA02.181	NORTH	148	6	13.50	2.44	2.03

Date	Earthquake	Station	filename	Comp	Epicentral Distance (km)	Mag	A_g max (cm/s^2)	Vmax (cm/s)	Dmax (cm)
660807	Gulf Of California	Imperial Valley Irrigation Dist., El Centro	USACA02.182	EAST	148	6	14.80	2.40	1.67
660912	Northern California	Pacific T&T Bldg., Sacramento	USACA02.298	SOUTH	152	6	14.50	1.57	0.74
660912	Northern California	Pacific T&T Bldg., Sacramento	USACA02.299	EAST	152	6	12.50	1.75	0.74
680409	Borrego Mountain	Jet Propulsion Lab, Caltech, Pasadena	USACA02.343	S82E	222	6	30.50	4.42	2.16
680409	Borrego Mountain	Hollywood Storage Building, Los Angeles	USACA02.364	SOUTH	128	6	30.10	11.10	8.78
680409	Borrego Mountain	Hollywood Storage Building, Los Angeles	USACA02.365	WEST	128	6	35.00	5.12	3.40

APPENDIX A4.

US NEAR FAULT RECORDS

Table A4. Rupture Directivity Record Set

Earthquake	Station / Description	file	Rupture Distance (km)	Site Code	X	θ	Y	ϕ	Fault Length (km)	M_w
Kobe, 1/17/95	Kobe, 17 Jan 95 – Abeno	abn	28.39	s3	0.62	37.87	0.69	64.40	40	7.2
Imperial Valley, 10/15/79	Aeropuerto Mexicali	aero	0.40	s3	0.03	19.89	0.88	2.38	40	6.5
Loma Prieta, 10/17/89	Eqk,10/17/89, Agnew - Agnews State Hospital	agnw	24.30	s3	0.50	42.87	0.83	35.21	40	7
Imperial Valley, 10/15/79	Agrarias	agra	0.80	s3	0.08	13.26	0.88	4.12	40	6.5
Whittier Narrows, 10/1/87	Oct 87,7:42 PDT, Alhambra, Fremont School	alhc	13.36	s3	0.56	9.83	0.55	55.47	12	6
Whittier Narrows, 10/1/87	Whitter, 1 Oct 87,7:42 PDT, Alhambra, 900 S. Fremont,basement	alhu	14.36	s4	0.59	25.34	0.50	47.11	12	6
Whittier Narrows, 10/1/87	Whittier 1 Oct 87,7:42 PDT, Altadena, Eaton Canyon Park	alta	19.50	s3	0.32	74.42	0.50	16.81	12	6
Kobe, 1/17/95	Jan 96 – Amagasaki	ama	14.81	s3	0.59	23.11	0.74	46.74	40	7.2
Loma Prieta, 10/17/89	Loma Prieta Eqk,10/17/89, Anderson Dam, Downstream	and2	19.60	s3	0.22	70.13	0.83	32.23	40	7
Morgan Hill, 4/24/84	Anderson Dam, Downstream	andd	4.50	s3	0.57	7.00	0.70	14.69	20	6.2
Imperial Valley, 10/15/79	2317 UTC, El Centro Array 1, Borchard Ranch	ar01	22.00	s3	0.70	38.21	0.88	64.44	40	6.5
Imperial Valley, 10/15/79	Imperial Valley, 2317 UTC, El Centro Array 2, Keystone Road	ar02	15.60	s3	0.68	29.79	0.88	55.97	40	6.5
Imperial Valley, 10/15/79	2317 UTC, El Centro Array 3, Pine Union School	ar03	10.80	s3	0.56	25.72	0.88	45.80	40	6.5
Imperial Valley, 10/15/79	El Centro ARY 4, Anderson Rd.	ar04	7.10	s3	0.63	15.63	0.88	33.91	40	6.5
Imperial Valley, 10/15/79	El Centro ARY 5, James Rd.	ar05	4.10	s3	0.69	8.43	0.88	21.21	40	6.5
Imperial Valley, 10/15/79	El Centro ARY 6, Hudson Rd.	ar06	1.20	s3	0.67	2.65	0.88	6.75	40	6.5
Imperial Valley, 10/15/79	El Centro ARY 7, Imperial Valley Coll.	ar07	0.20	s3	0.66	0.37	0.88	0.94	40	6.5
Imperial Valley, 10/15/79	El Centro ARY 8, Cruickshank Rd.	ar08	3.80	s3	0.66	8.07	0.88	19.66	40	6.5
Imperial Valley, 10/15/79	El Centro ARY 10, Hospital	ar10	8.00	s3	0.64	17.42	0.88	37.30	40	6.5
Imperial Valley, 10/15/79	Imperial Valley, 2317 UTC, El Centro Array 11, McCabe School	ar11	12.30	s3	0.61	26.52	0.88	49.39	40	6.5
Imperial Valley, 10/15/79	Imperial Valley, 2317 UTC, El Centro Array 12, Brockman Road	ar12	18.00	s3	0.62	36.05	0.88	59.74	40	6.5
Imperial Valley, 10/15/79	Imperial Valley, 2317 UTC, El Centro Array 13, Strobel Residence	ar13	21.70	s3	0.65	39.67	0.88	64.13	40	6.5
Whittier Narrows, 10/1/87	Whittier 1 Oct 87,7:42 PDT, Long Beach, Baldwin Hills	bald	22.95	s4	0.63	19.73	0.50	28.75	12	6
Imperial Valley, 10/15/79	Bonds Corner, El Centro	bond	2.40	s3	0.13	25.53	0.88	13.08	40	6.5
Tabas, 9/16/78	Tabas,16 Sep 78; Boshrooyeh Station	bos	25.00	s3	0.62	37.52	0.26	32.57	95	7.4
Imperial Valley, 10/15/79	Imperial Valley, 2317 UTC, Brawley, Municipal Airport	braw	13.10	s3	0.81	13.34	0.88	42.97	40	6.5

Earthquake	Station / Description	file	Rupture Distance (km)	Site Code	X	θ	Y	ϕ	Fault Length (km)	M_w
Whittier Narrows, 10/1/87	Whitter, 1 Oct 87,14:42 GMT,Brea Dam,Downstream (951)	bred	20.04	s2	0.38	41.10	0.50	14.21	12	6
Whittier Narrows, 10/1/87	Whitter, 1 Oct 87,7:42 PDT, Los Angeles, Bulk Mail Facility	bulk	12.93	s3	0.50	52.01	0.50	32.07	12	6
North Palm Springs, 7/8/86	Cabazon, Post Office	caba	8.40	s3	0.57	45.86	0.64	6.48	22	6
Santa Barbara, 8/13/78	Santa Barbara, 13 Aug 78,Cachuma Dam, Toe (106)	cach	28.00	s3	1.00	12.50	1.00	27.97	10	6
Imperial Valley, 10/15/79	Imperial Valley, 2317 UTC, Calipatria Fire Station- #5061	cali	28.40	s3	0.81	18.76	0.88	60.30	40	6.5
Imperial Valley, 10/15/79	Fire Station, Calexico	calx	10.10	s3	0.30	40.61	0.88	43.97	40	6.5
Loma Prieta, 10/17/89	Eqk, 17 Oct 89, Capitola, Fire Station	cap	15.10	s3	0.02	86.50	0.73	47.00	40	7
Imperial Valley, 10/15/79	Mexicali Casa, Flores	casa	9.72	s3	0.11	66.27	0.88	42.77	40	6.5
San Fernando, 2/9/71	710209, Castaic Old Ridge Route (110)	cast	21.50	s3	0.29	74.52	0.97	88.11	16	6.6
Coalinga, 5/2/83	Coalinga, 2 May 83, Cantua Creek School (46314)	ccsc	29.59	s3	0.50	57.36	0.74	84.54	10	6.4
Imperial Valley, 10/15/79	79, 2316 GMT, IV Mainshock, Station 6604, Cerro Prieto	cerr	18.40	s1	0.19	31.03	0.88	50.17	40	6.5
Imperial Valley, 10/15/79	79, 2316 GMT, IV Mainshock, Station 6604, Chihuahua	chih	12.00	s3	0.19	11.44	0.88	19.91	40	6.5
Loma Prieta, 10/17/89	Loma Prieta,17 Oct 89,Coyote Lk Dam-Down Strm,(5750	cldd	20.50	s3	0.43	55.87	0.83	33.23	40	7
Morgan Hill, 4/24/84	Coyote Lake Dam, San Martin	clyd	0.10	s2	0.82	6.33	0.70	18.80	20	6.2
Imperial Valley, 10/15/79	Compuertas	comp	4.47	s3	0.15	37.00	0.88	23.07	40	6.5
Landers, 6/28/92	28 Jun 92, Coolwater	cool	26.00	s3	0.47	12.12	0.47	48.28	70	7.3
Loma Prieta, 10/17/89	Corralitos	cor	3.40	s3	0.12	44.03	0.83	5.85	40	7
Santa Barbara, 8/13/78	Santa Barbara, 13 Aug 78,Santa Barbara Courthouse (283)	cour	11.20	s3	0.26	25.34	1.00	54.14	10	6
San Fernando, 2/9/71	9 Feb 71, Century Park E (425)	cpke	26.00	s3	0.50	75.65	0.77	30.90	16	6.6
North Palm Springs, 7/8/86	Palm Springs Eqk, 8 Jul 86,0920 GMT,Cranston Forest Station	cran	27.50	xx	0.56	69.93	0.64	27.97	22	6
Parkfield, 6/27/66	Chalome, Shandon, CA ARY 5	cs05	3.73	s3	0.67	7.93	0.77	20.49	35	6.1
Parkfield, 6/27/66	Chalome, Shandon, CA ARY 8	cs08	8.04	s3	0.68	16.48	0.77	38.85	35	6.1
Parkfield, 6/27/66	66,Cholame Shandon Array 12 (016)	cs12	13.54	s3	0.69	26.30	0.77	53.57	35	6.1
Tabas, 9/16/78	78; Dayhook Station	day	14.00	s2	0.01	86.92	0.65	41.44	95	7.4
North Palm Springs, 7/8/86	Desert Hot Springs	dhsp	6.7	s3	0.43	7.57	0.58	37.27	22	7.3
Landers, 6/28/92	28 Jun 92,Desert Hot Springs,(12149)	dhsp	18.6	s3	0.13	15.71	0.47	69.53	22	6
Imperial Valley, 10/15/79	El Centro Differetial Array 1	dif1	5.50	s3	0.65	11.18	0.88	26.19	40	6.5
Imperial Valley, 10/15/79	El Centro Differetial Array 2	dif2	5.50	s3	0.65	11.18	0.88	26.19	40	6.5

Earthquake	Station / Description	file	Rupture Distance (km)	Site Code	X	θ	Y	ϕ	Fault Length (km)	M_w
Imperial Valley, 10/15/79	El Centro Differetial Array 3	dif3	5.40	s3	0.65	11.18	0.88	26.19	40	6.5
Imperial Valley, 10/15/79	El Centro Differetial Array 4	dif4	5.20	s3	0.65	11.18	0.88	26.19	40	6.5
Imperial Valley, 10/15/79	El Centro Differetial Array 5	dif5	5.10	s3	0.65	11.18	0.88	26.19	40	6.5
Imperial Valley, 10/15/79	Differential Array, Dogwood Rd.	diff	5.20	s3	0.65	11.18	0.88	26.19	40	6.5
Whittier Narrows, 10/1/87	Oct 87,7:42 PDT, Downey, County Maintenance Building	down	16.65	s3	0.45	70.22	0.50	14.10	12	6
North Palm Springs, 7/8/86	Devers Hill Substation	dvhl	4.05	s3	0.21	52.60	0.64	14.95	22	6
Superstition Hills B, 11/24/87	Superstition Hills, 24 Nov 87 El Centro-Imperial Cn	elcn	14.20	s3	0.90	6.30	0.74	23.42	20	6.6
Erzincan, Turkey, 3/13/92	Erzincan, Turkey	erzi			0.33	9.65	0.84	3.00	55	
Kobe, 1/17/95	Kobe, 17 Jan 96 – Fukushima	fks	21.75	s3	0.63	30.01	0.72	57.03	40	7.2
Santa Barbara, 8/13/78	13 Aug 78, Freitas Building,Station 302	frei	11.00	s3	0.44	9.75	1.00	56.38	10	6
North Palm Springs, 7/8/86	Eqk, 8 Jul 86,0920 GMT,Fun Valley, Reservoir 351	funv	11.00	s3	0.43	5.20	0.61	33.88	22	6
Whittier Narrows, 10/1/87	Whitter, 1 Oct 87,7:42 PDT, Garvey Reservoir, Control Bldg	garv	12.84	s1	0.22	8.35	0.50	58.47	12	6
Loma Prieta, 10/17/89	Gavilon College Phys. Sci. Bldg.	gav	9.50	s3	0.50	23.21	0.83	10.79	40	7
Morgan Hill, 4/24/84	24 Apr 84 Gavilan College 47006	gav	16.00	s2	0.50	23.21	0.50	58.47	40	6.2
Loma Prieta, 10/17/89	Gilroy #1, Gavilon Water Tower	gil1	16.00	s2	0.94	9.75	0.83	10.30	20	6.2
Morgan Hill, 4/24/84	24 Apr 84 Gilroy 1 47379	gil1	9.17	s2	0.50	23.02	0.70	38.62	40	7
Loma Prieta, 10/17/89	Eqk,10/17/89, Gilroy Ary 2,Hwy 101/Bolsa Road Motel	gil2	10.60	s3	0.50	25.62	0.83	13.90	40	7
Loma Prieta, 10/17/89	Eqk,10/17/89, Gilroy Ary 3,Gilroy Sewage Plant	gil3	12.40	s3	0.50	27.33	0.83	16.98	40	7
Morgan Hill, 4/24/84	Morgan Hill, 24 Apr 84 Gilroy 4 57382	gil4	14.1	s3	0.94	1.85	0.70	8.27	40	7
Loma Prieta, 10/17/89	Eqk,10/17/89, Gilroy Ary 4,San Ysidro School	gil4	13.00	s3	0.50	31.25	0.83	21.22	40	6.2
Morgan Hill, 4/24/84	Morgan Hill, 24 Apr 84 Gilroy 6 57383	gil6	18	s3	0.94	4.29	0.70	18.38	40	7
Loma Prieta, 10/17/89	Eqk,10/17/89, Gilroy Ary 6,San Ysidro	gil6	12.00	s2	0.50	35.68	0.70	18.38	40	6.2
Morgan Hill, 4/24/84	Morgan Hill, 24 Apr 84 Gilroy 7 57245	gil7	22.4	s3	0.94	10.44	0.83	31.56	40	7
Loma Prieta, 10/17/89	Eqk,10/17/89, Gilroy Ary 7,Mantelli Ranch	gil7	13.00	s3	0.50	37.09	0.70	40.14	40	6.2
Loma Prieta, 10/17/89	Eqk,10/17/89, Gilroy - 2 story Hist Comm. Bldg	gilb	10.6	s3	0.50	31.12	0.83	17.18	40	7
San Fernando, 2/9/71	San Fernando, 9 Feb 71, Glendale, Muni Bldg (122)	glen	18.80	s3	0.50	48.28	0.77	21.89	16	6.6
Whittier Narrows, 10/1/87	Oct 87,14:42 GMT,Griffith Park Obs (141)	grif	21.23	s1	0.63	11.27	0.50	43.82	12	6
Morgan Hill, 4/24/84	Halls Valley	hall	2.50	s3	0.06	9.35	0.70	2.68	20	6.2

Earthquake	Station / Description	file	Rupture Distance (km)	Site Code	X	θ	Y	ϕ	Fault Length (km)	M_w
Loma Prieta, 10/17/89	Eqk, 17 Oct 89, Hollister, South St. & Pine Dr.	hol	27.60	s3	0.50	11.86	0.83	7.43	40	7
San Fernando, 2/9/71	710209, Hollywood Stor Bldg Bsmt(135)	holb	21.00	s3	0.50	64.30	0.77	24.48	16	6.6
Loma Prieta, 10/17/89	Eqk,10/17/89, Hollister City Hall Annex,Bsmt	holc	27.00	s3	0.50	11.98	0.83	7.40	40	7
Morgan Hill, 4/24/84	Morgan Hill,24 Apr 84,Hollister Diff Ary (1656)	hold	24.5	s3	0.94	1.94	0.70	12.19	40	7
Loma Prieta, 10/17/89	Eqk,10/17/89, Hollister Airport Diff Ary SMA1	hold	28.00	s3	0.50	16.13	0.83	13.26	40	6.2
Imperial Valley, 10/15/79	Post Office, Holtville	holt	7.50	s3	0.45	22.52	0.88	35.38	40	6.5
Whittier Narrows, 10/1/87	Oct 87,7:42 PDT, Los Angeles, Hollywood Storage FF	hsbf	22.43	s3	0.63	0.80	0.50	58.67	12	6
Imperial Valley, 10/15/79	Imperial County FF	imco	7.43	s3	0.67	15.45	0.88	35.27	40	6.5
Whittier Narrows, 10/1/87	Whittier 1 Oct 87,7:42 PDT, Inglewood, Union Oil Yard	ingl	21.54	s2	0.63	51.12	0.50	7.65	12	6
Imperial Valley, 5/19/40	Imperial Valley Irrig. Dist., El Centro	ivir	10.00	s3	0.15	19.17	0.53	19.24	N/A	6.9
Northridge, 1/17/94	Jensen Filtration Plant Gen. BL GND.	jens	6.24	s3	0.13	79.11	0.85	16.02	15	6.7
Landers, 6/28/92	Joshua Tree, Fire Station	josh	25.10	s3	0.13	5.32	0.47	37.09	22	6
North Palm Springs, 7/8/86	Springs Eqk, 8 Jul 86, Joshua Tree - Fire Station	josh	7.40	s3	0.43	45.59	0.64	72.65	22	7.3
Northridge, 1/17/94	Pacoima, Kagel Canyon	kagc	8.17	s1	0.19	61.09	0.85	8.64	15	6.7
Gazli, USSR, 5/17/76	Karakyr Point, USSR	kara	3.00	s2	0.16	5.08	0.66	48.86	58	6.8
Kobe, 1/17/95	Kobe University (Ceorka)	kbu	3.77	s1	0.41	9.74	0.79	19.00	40	7.2
Kobe, 1/17/95	Kobe (Ceorka)	kobc	6.18	s1	0.46	13.84	0.78	26.71	40	7.2
Kobe, 1/17/95	Kobe (JMA)	kobj	3.37	s3	0.30	11.28	0.79	16.84	40	7.2
Koyna, India, 12/10/67	Koyna Dam	koyn	3.00	s1	0.11	0.00	0.30	23.00	N/A	6.3
Kobe, 1/17/95	Kobe Port Island, Surface	kpi1	6.58	s4	0.31	20.18	0.79	26.71	40	7.2
Whittier Narrows, 10/1/87	Oct 87,7:42 PDT, Century City, LA Country Club, North	lacn	27.80	s3	0.63	7.11	0.50	45.21	12	6
Whittier Narrows, 10/1/87	Oct 87,7:42 PDT, Century City, LA Country Club, South	lacs	27.62	s3	0.63	7.30	0.50	44.92	12	6
Whittier Narrows, 10/1/87	Whittier 1 Oct 87,7:42 PDT, Lancaster, Medical Office Bldg FF	lanc	68.11	s3	0.63	74.46	0.50	42.02	12	6
Whittier Narrows, 10/1/87	Oct 87,7:42 PDT, Long Beach, Rancho Los Cerritos	lbrc	24.17	s3	0.52	75.74	0.50	0.61	12	6
Whittier Narrows, 10/1/87	Oct 87,7:42 PDT, Long Beach, Recreation Park	lbrp	29.30	s3	0.04	89.09	0.50	4.40	12	6
Long Beach, 3/10/33	Long Beach,33/03/10,Long Beach Public Utilites Bldg	lbub	15.79	s3	1.00	13.93	0.70	13.87	16	6.5
Loma Prieta, 10/17/89	Lexington Dam, Left Abutment	lex1	6.30	s2	0.40	33.24	0.83	8.79	40	7
Loma Prieta, 10/17/89	Los Gatos Presentation Ctr.	lgpc	3.50	s1	0.45	13.88	0.83	6.72	40	7

Earthquake	Station / Description	file	Rupture Distance (km)	Site Code	X	θ	Y	ϕ	Fault Length (km)	M_w
Landers, 6/28/92	Lucerne Valley	lucr	1.10	s3	0.60	3.40	0.47	0.63	70	7.3
North Palm Springs, 7/8/86	Eqk, 8 Jul 86,0920 GMT,Morongo Valley, Fire Station	moro	11.90	s3	0.04	80.77	0.64	15.46	22	6
Whittier Narrows, 10/1/87	Oct 87,7:42 PDT, Mt.Wilson, Caltech Seismic Station	mtwi	22.94	s1	0.10	86.51	0.50	6.87	12	6
Northridge, 1/17/94	Newhall, LA County Fire Station	newh	7.10	s1	0.54	59.89	0.85	6.01	15	6
Northridge, 1/17/94	Arleta, Nordhoff fire Station	nord	9.23	s3	0.19	47.74	0.81	26.58	15	6.7
Santa Barbara, 8/13/78	Santa Barbara, 13 Aug 78, UCSB, North Hall,Ground/Core	nort	10.70	s3	1.00	20.90	1.00	35.02	10	6
Whittier Narrows, 10/1/87	Whitter,7:42 PDT,Norwalk, 12400 Imperial Hwy,S.Grnd1O	norw	15.92	s3	0.29	75.94	0.50	16.31	12	6
North Palm Springs, 7/8/86	North Palm Springs Post Office	nplm	4	s3	0.36	37.99	0.64	14.41	22	6
Whittier Narrows, 10/1/87	Whittier 1 Oct 87,7:42 PDT, Los Angeles, Obregon Park	obre	12.66	s3	0.63	18.64	0.50	48.78	12	6
Kobe, 1/17/95	Kobe, 17 Jan 95 - H1170546.OSA:135.52 2E, 34.6783 N	osaj	26.02	s3	0.67	32.27	0.70	61.27	40	7.2
Northridge, 1/17/94	Pacoima Dam, Downstream	pacd	7.95	s1	0.19	77.27	0.85	3.03	15	6.7
San Fernando, 2/9/71	Pacoima Dam	paco	3.3	s1	0.17	69.62	0.67	10.71	16	6.6
Imperial Valley, 10/15/79	Imperial Valley,Parachute Test Facility USGS 5051	para	16.50	s3	0.81	10.20	0.88	38.65	40	6.5
Loma Prieta, 10/17/89	Eqk,10/17/89, Palo Alto VA Hosp, Bldg 1, Basement	pavb	26.10	s3	0.50	22.10	0.83	22.45	40	7
North Palm Springs, 7/8/86	Palm Springs Airport	plma	9.60	s3	0.43	45.72	0.64	10.08	22	6
Whittier Narrows, 10/1/87	Whittier 1 Oct 87,7:42 PDT, Pomona, 4th & Locust FF	pomo	28.80	s3	0.38	11.48	0.50	37.26	12	6
Northridge, 1/17/94	Rinaldi Receiving Station, FF	rrs	7.13	s3	0.06	83.54	0.85	20.61	15	6.7
Whittier Narrows, 10/1/87	Whittier 1 Oct 87,7:42 PDT, Los Angeles, 116th Street School	schl	19.04	s4	0.63	48.85	0.50	12.38	12	6
Northridge, 1/17/94	Sylmar Converter Station FF	scs	6.19	s3	0.12	79.31	0.85	16.23	15	6.7
Northridge, 1/17/94	Sylmar Converter Station E FF	scse	6.08	s3	0.08	83.09	0.85	14.94	15	6.7
North Palm Springs, 7/8/86	Springs Eqk, 8 Jul 86, Silent Valley – Poppet Fla	sile	17.70	s2	0.57	52.75	0.64	19.77	22	6
Loma Prieta, 10/17/89	Hills Instr.#57563 Free Field TRIG: 00:04 18.3	snj	14.40	s3	0.16	71.86	0.83	25.18	40	7
Whittier Narrows, 10/1/87	Oct 87,7:42 PDT, San Marino, Southwestern Academy	snmr	15.84	s3	0.48	48.19	0.50	36.35	12	6
North Palm Springs, 7/8/86	North Palm Springs Eqk, 8 Jul 86, San Jacinto - Soboba	sobo	23.90	s3	0.57	58.40	0.64	25.11	22	6
Loma Prieta, 10/17/89	Eqk,10/17/89, Stanford Pkg Garage, grnd level	spg	26.10	s3	0.50	22.10	0.83	22.45	40	7
Northridge, 1/17/94	Sepulveda VA Hospital	spva	8.94	s3	0.17	66.34	0.79	28.62	15	6.7
Loma Prieta, 10/17/89	Saratoga, Aloha Ave.	srtg	8.30	s3	0.50	22.76	0.83	9.18	40	7
NW Territories, 12/23/85	Iverson, NW Territories, Sta. 1	sta1	9.62	s1	0.04	75.59	0.45	25.29	33	6.8

Earthquake	Station / Description	file	Rupture Distance (km)	Site Code	X	θ	Y	ϕ	Fault Length (km)	M_w
NW Territories, 12/23/85	Slide Mountain, Sta. 2	sta2	6.05	s1	0.09	44.22	0.33	38.24	33	6.8
NW Territories, 12/23/85	NW Territories, Sta. 3, 23 Dec 85, 0516 GMT	sta3	18.48	s1	0.18	67.81	0.68	3.90	33	6.8
Loma Prieta, 10/17/89	Loma Prieta Eqk,10/17/89, Sunnyvale – Colton Avenue	sunc	24.10	s4	0.50	34.42	0.83	31.47	40	7
Imperial Valley, 10/15/79	Imperial Valley, Superstition Mountain USGS 286	supr	27.80	s1	0.81	16.14	0.88	56.70	40	6.5
Northridge, 1/17/94	Sylmar, Olive View FF	sylm	6.35	s3	0.05	87.02	0.85	8.38	15	6.7
Tabas, 9/16/78	Tabas	tab	1.15	s2	0.59	11.46	0.26	3.01	95	7.4
Kobe, 1/17/95	Takatori (JR)	tato	4.30	s3	0.20	19.14	0.79	18.95	95	7.2
Parkfield, 6/27/66	Temblor, CA, Station 2	temb	4.43	s1	0.66	9.47	0.77	23.89	35	6.1
Santa Barbara, 8/13/78	Santa Barbara, 13 Aug 78, UCSB, Goleta, FF	ucsb	10.60	s3	1.00	16.54	1.00	40.23	10	6
Whittier Narrows, 10/1/87	Whitter, 1 Oct 87,7:42 PDT, Vernon, CMD Terminal,Basement	vern	13.38	s3	0.63	36.42	0.50	33.46	12	6
Loma Prieta, 10/17/89	Eqk,17 Oct 89, 36 58.2N, 121 59.70W,UCSC Station	waho	17.70	s3	0.09	74.73	0.68	53.20	40	7
Loma Prieta, 10/17/89	Eqk,10/17/89, Watsonville-4 story building,Chan.13	wats	10.30	s4	0.44	14.64	0.83	6.38	40	7
Whittier Narrows, 10/1/87	Whitter, 1 Oct 87,7:42 PDT, Whittier Narrows Dam Upstream	wdup	12.56	s3	0.27	26.79	0.50	53.71	12	6
Superstition Hills B, 11/24/87	Superstition Hills, 24 Nov 87 Westmoreland FF 11369	wes2	17.80	s3	0.72	44.61	0.74	57.69	20	6.6
Imperial Valley, 10/15/79	Imperial Valley, 2317 UTC, Westmoreland Temp FF,#7901	west	19.80	s3	0.81	4.98	0.88	23.25	40	6.5
Whittier Narrows, 10/1/87	Whitter, 1 Oct 87,7:42 PDT, Whittier, 7215 Bright Ave, Basement	whit	12.78	s3	0.38	52.59	0.50	33.84	12	6
North Palm Springs, 7/8/86	Whitewater Canyon Trout Farm	wwtf	5.90	s3	0.18	30.76	0.63	31.78	22	6
Landers, 6/28/92	28 Jun 92,Yermo Fire Station,(22074)	yerm	25.00	s3	0.52	3.71	0.47	20.52	70	7.3